COMPARISON OF PRECISION ORBIT DERIVED DENSITY ESTIMATES FOR CHAMP AND GRACE SATELLITES

BY

Eric Dale Fattig

Submitted to the graduate degree program in Aerospace Engineering and the Graduate Faculty of the University of Kansas in partial fulfillment of the requirements for the degree of Master's of Science.

Chairperson: Dr. Craig McLaughlin

Committee members

Dr. Saeed Farokhi

Dr. Shahriar Keshmiri

Date defended: _____

The Thesis Committee for Eric Dale Fattig certifies that this is the approved Version of the following thesis:

COMPARISON OF PRECISION ORBIT DERIVED DENSITY ESTIMATES FOR CHAMP AND GRACE SATELLITES

Committee:

Chairperson: Dr. Craig McLaughlin

Dr. Saeed Farokhi

Dr. Shahriar Keshmiri

Date approved:

ABSTRACT

Current atmospheric density models cannot adequately represent the density variations observed by satellites in Low Earth Orbit (LEO). Using an optimal orbit determination process, precision orbit ephemerides (POE) are used as measurement data to generate corrections to density values obtained from existing atmospheric models. Densities obtained using these corrections are then compared to density data derived from the onboard accelerometers of satellites, specifically the CHAMP and GRACE satellites. This comparison takes two forms, cross correlation analysis and root mean square analysis. The densities obtained from the POE method are nearly always superior to the empirical models, both in matching the trends observed by the accelerometer (cross correlation), and the magnitudes of the accelerometer derived density (root mean square). In addition, this method consistently produces better results than those achieved by the High Accuracy Satellite Drag Model (HASDM).

For satellites orbiting Earth that pass through Earth's upper atmosphere, drag is the primary source of uncertainty in orbit determination and prediction. Variations in density, which are often not modeled or are inaccurately modeled, cause difficulty in properly calculating the drag acting on a satellite. These density variations are the result of many factors; however, the Sun is the main driver in upper atmospheric density changes. The Sun influences the densities in Earth's atmosphere through solar heating of the atmosphere, as well as through geomagnetic heating resulting from the solar wind.

Data are examined for fourteen hour time spans between November 2004 and July 2009 for both the CHAMP and GRACE satellites. This data spans all available levels of solar and geomagnetic activity, which does not include data in the elevated and high solar

activity bins due to the nature of the solar cycle. Density solutions are generated from corrections to five different baseline atmospheric models, as well as nine combinations of density and ballistic coefficient correlated half-lives. These half-lives are varied among values of 1.8, 18, and 180 minutes. A total of forty-five sets of results emerge from the orbit determination process for all combinations of baseline density model and half-lives. Each time period is examined for both CHAMP and GRACE-A, and the results are analyzed. Results are averaged from all solutions periods for 2004-2007. In addition, results are averaged after binning according to solar and geomagnetic activity levels. For any given day in this period, a ballistic coefficient correlated half-life of 1.8 minutes yields the best correlation and root mean square values for both CHAMP and GRACE. For CHAMP, a density correlated half-life of 18 minutes is best for higher levels of solar and geomagnetic activity, while for lower levels 180 minutes is usually superior. For GRACE, 180 minutes is nearly always best. The three Jacchia-based atmospheric models yield very similar results. The CIRA 1972 or Jacchia 1971 models as baseline consistently produce the best results for both satellites, though results obtained for Jacchia-Roberts are very similar to the other Jacchia-based models.

Data are examined in a similar manner for the extended solar minimum period during 2008 and 2009, albeit with a much smaller sampling of data. With the exception of some atypical results, similar combinations of half-lives and baseline atmospheric model produce the best results. A greater sampling of data will aid in characterizing density in a period of especially low solar activity.

In general, cross correlation values for CHAMP and GRACE revealed that the POE method matched trends observed by the accelerometers very well. However, one period of time deviated from this trend for the GRACE-A satellite. Between late October 2005 and

January 2006, correlations for GRACE-A were very low. Special examination of the surrounding months revealed the extent of time this period covered. Half-life and baseline model combinations that produced the best results during this time were similar to those during normal periods. Plotting these periods revealed very short period density variations in the accelerometer that could not be reproduced by the empirical models, HASDM, or the POE method.

Finally, densities produced using precision orbit data for the GRACE-B satellite were shown to be nearly indistinguishable from those produced by GRACE-A. Plots of the densities produced for both satellites during the same time periods revealed this fact. Multiple days were examined covering all possible ranges of solar and geomagnetic activity. In addition, the period in which GRACE-A correlations were low was studied. No significant differences existed between GRACE-A and GRACE-B for all of the days examined.

ACKNOWLEDGEMENTS

I am very thankful to Dr. McLaughlin for allowing me to perform this research. I have learned much as a result of his teaching and advisement. I am also very appreciative of Dr. Farokhi and Dr. Keshmiri for their time and effort in serving as members of my thesis committee.

This research is made possible by the support of the National Science Foundation under Grant No. 0832900. Special thanks to Jens Ramrath, Jim Wright, Jim Woodburn, and John Seago for help with this research and with Orbit Determination Tool Kit, as well as David Vallado for his help with data conversion and ODTK. Thanks to Bruce Bowman for HASDM CHAMP and GRACE data, and to Sean Bruinsma, Jeff Forbes, and Eric Sutton for access to accelerometer derived densities for CHAMP and GRACE.

I would also like to thank my research predecessors, Andrew Hiatt, Travis Lechtenberg, and Steve Mance. They were a great help to me in my learning and understanding of the subjects. Much of their work was necessary for my research to be successful. In addition, thanks to Travis, Steve, Piyush Mehta, Travis Locke, Dhaval Krishna, and Anoop Kumar for their company and entertaining conversation.

TABLE OF CONTENTS

NOMENCLATURE

Symbol	Definition	Units
$\vec{a}_{drag}$	acceleration vector due to atmospheric drag	m/s^2
a_p	geomagnetic 3-hourly planetary equivalent amplitude index	gamma, Telsa, or kg s m^{-1}
A	satellite cross-sectional area	m^2
A_p	geomagnetic daily planetary amplitude index	gamma, Telsa, or kg s m^{-1}
$\Delta B/B$	estimated ballistic coefficient correction	~
BC	ballistic coefficient	m^2/kg
c_D	satellite drag coefficient	~
d	cross correlation delay	
$F_{10.7}$	daily solar radio flux measured at 10.7 cm wavelength	SFU
$\bar{F}_{10.7}$	$F_{10.7}$ running 81-day centered smoothed data set	SFU
$\bar{F}_S$	Jacchia-Bowman 2008 new solar index	SFU
g_o	gravitational acceleration	m/s^2
Δh	altitude change	m
K_p	geomagnetic planetary index	~
$M_{10.7}$	solar proxy for far ultra-violet radiation	SFU
$\bar{M}_{10.7}$	$M_{10.7}$ running 81-day centered smoothed data set	SFU
m	satellite mass	kg
M	mean molecular mass	amu

N	number of elements	
Δp	atmospheric pressure change	N/m^2
p_o	absolute pressure	N/m^2
$\hat{P}$	filter covariance matrix	
$\tilde{P}$	smoother covariance matrix	
$\bar{P}$	differenced covariance matrix	
$\vec{r}$	satellite position vector	m
R	universal gas constant	$J\ K^{-1}\ mol^{-1}$
$\vec{R}$	McReynold's consistency test ratio	
$S_{10.7}$	solar extreme ultra-violet radiation at 26-34 nm wavelength	SFU
$\bar{S}_{10.7}$	$S_{10.7}$ running 81-day centered smoothed data set	SFU
t	time	S
T	temperature	K
v_{rel}	satellite velocity magnitude relative to Earth's atmosphere	m/s
$\vec{v}_{rel}$	satellite velocity vector relative to Earth's atmosphere	m/s
$w\ t$	Gaussian white random variable	
x	x component of satellite position vector	m
x	Gauss-Markov process dynamic scalar random variable	
x	cross correlation series	
ΔX	state error	
$\Delta\hat{X}$	optimal state error estimate	

$\boldsymbol{X}$	satellite state vector	
$\bar{\bar{X}}$	difference state vector	
$\vec{\bar{X}}_{filter}$	filter state estimate	
$\vec{\bar{X}}_{smoother}$	smoother state estimate	
Δy	measurement residual	
y	y component of satellite position vector	m
y	cross correlation series	
Y_{10}	mixed solar index	SFU
z	z component of satellite position vector	m

Greek Letters	**Definition**	**Units**
α	Gauss-Markov process variable	
β	Solar Beta Angle	deg
$\Delta\rho/\rho$	estimated atmospheric density correction	~
ρ	atmospheric density	kg/m^3
$\vec{\sigma}$	denominator for McReynold's consistency test ratio	
σ_w^2	variance of Gaussian white random variable	
τ	user defined correlated half-life	
ω_{Earth}	Earth's angular velocity magnitude	rad/s
$\vec{\omega}_{Earth}$	Earth's angular velocity vector	rad/s
Φ	transition function	

Abbreviations	Definition
CHAMP	Challenging Minisatellite Payload
CIRA	COSPAR International Reference Atmosphere
COSPAR	Committee on Space Research
CNES	Centre National d'Études Spatiales
DCA	Dynamic Calibration of the Atmosphere
DORIS	Doppler Orbitography by Radiopositioning Integrated on Satellite
Dst	Disturbance Storm Time index
DTM	Drag Temperature Model
ESA	European Space Agency
EUV	Extreme Ultra-Violet
FUV	Far Ultra-Violet
GEOSAT	Geodetic Satellite
GFO	GEOSAT Follow-On
GOES	Geostationary Operational Environmental Satellites
GPS	Global Positioning System
GRACE	Gravity Recovery And Climate Experiment
GSFC	Goddard Space Flight Center
HASDM	High Accuracy Satellite Drag Model
ICESat	Ice, Cloud, and Land Elevation Satellite
MSISE	Mass Spectrometer Incoherent Scatter Extending from ground to space

MUV	Middle Ultra-Violet
NASA	National Aeronautics and Space Administration
NOAA	National Oceanic and Atmospheric Administration
NORAD	North American Aerospace Defense Command
NRLMSISE	Naval Research Laboratory Mass Spectrometer Incoherent Scatter Extending from ground to space
ODTK	Orbit Determination Tool Kit
POE	Precision Orbit Ephemerides
PSO	Precision Science Orbit
RSO	Rapid Science Orbit
SBUV	Solar Backscatter Ultraviolet
SEE	Solar Extreme ultraviolet Experiment
SEM	Solar Extreme-ultraviolet Monitor
SETA	Satellite Electrostatic Triaxial Accelerometer
SFU	Solar Flux Units
SLR	Satellite Laser Ranging
SOHO	Solar and Heliospheric Observatory
SOLSTICE	Solar/Stellar Irradiance Comparison Experiment
SORCE	Solar Radiation and Climate Experiment
STAR	Spatial Triaxial Accelerometer for Research
TAD	Traveling Atmospheric Disturbance
TIMED	Thermosphere Ionosphere Mesosphere Energetics and Dynamics

TLE	Two Line Element
UARS	Upper Atmosphere Research Satellite
XRS	X-Ray Spectrometer

LIST OF FIGURES

LIST OF TABLES

1 INTRODUCTION

1.1 Objective

The goal of this research is to generate corrections to atmospheric models using precision orbit ephemerides from multiple satellites and to compare the results. These corrections provide more accurate density estimates that will allow for improved atmospheric drag calculations, better orbit determination and prediction, and insight into density variations in the upper atmosphere, specifically the thermosphere and exosphere. The ability of precision orbit ephemerides to model short period density variations will be examined.

1.2 Motivation

Measurements of extreme upper atmospheric density have shown that current models fail to model the variability in this region. Satellite orbits passing through the thermosphere and exosphere rely on these models, and consequently, orbit determination and prediction is subject to weaknesses in these models. Improved knowledge of upper atmospheric density will allow for improved orbit determination which will help prevent collisions, as well as improve prediction of satellite life-spans. Operations of some satellites orbiting at these altitudes require precise position and velocity information, which will be improved through better atmospheric modeling.

Atmospheric density is one of the most significant uncertainties in modeling dynamics of Low Earth Orbiting (LEO) satellites, as it is directly related to

atmospheric drag encountered by these satellites. Atmospheric drag effects on an orbiting body increase with lower mass, higher cross-sectional area, and higher velocity, which is a function of orbit altitude.

Two of the main effects with a major impact on the Earth's upper atmospheric density, specifically in the thermosphere and exosphere, are solar heating and geomagnetic heating. Both of these effects result from variations in solar output. Extreme ultraviolet (EUV) wavelength radiation directly heats the upper atmosphere. Charged particles ejected by the Sun interact with Earth's magnetic field and cause geomagnetic heating of the atmosphere. Unfortunately, data for magnetic field and solar flux used in the atmospheric density models are only available as averaged three hour or daily global values.

Corrections to the current atmospheric density models will allow more accurate orbit determination and prediction. These corrections will also provide a better understanding of thermospheric and exospheric densities and their variations. Density corrections can be obtained through the use of a precision orbit determination scheme. This is done for multiple baseline atmospheric density models and combinations of density and ballistic coefficient correlated exponential Gauss-Markov half-lives, which will be discussed at length in subsequent sections. The corrected density estimates can then be compared with densities derived from accelerometers onboard the CHAMP and GRACE satellites. Densities obtained from accelerometer data were derived by Sean Bruinsma of the Centre National d'Etudes Spatiales (CNES) in References 1-4. Densities obtained through the corrections are

also compared to the work of Bruce Bowman at the U.S. Air Force Space Command using the High Accuracy Satellite Drag Model (HASDM) in Reference 5.

The equations used to model drag acting on satellites in LEO can then be updated with the improved density estimates obtained from these corrections. Improvement in the density models correlates to a direct improvement in drag modeling. Drag is one of the most significant perturbation forces acting on bodies orbiting in LEO, and, consequently, orbit determination and prediction will be enhanced. This in turn will provide better information for prediction of the satellite's future state, operational lifetime of the satellite, and reentry time. Better density modeling will also allow for improved study of the effects of space weather on Earth's atmosphere.

1.3 Satellite Drag

Satellites are affected by perturbations such as solar radiation pressure, Earth infrared, Earth albedo, third body effects, geopotential, and atmospheric drag. For satellites in LEO, Earth oblateness and drag are the dominant perturbations. The significance of drag on a satellite's orbit is a function of altitude. At higher altitudes, drag may be negligible; however, at low altitudes drag is extremely important. In some instances, drag can be advantageous. Drag can be used for aerobraking of the satellite, or can be used to correct the attitude of the satellite through the use of satellite tethers. Due to the importance of atmospheric drag on satellites, upper atmospheric modeling is an area of ongoing research. The study of drag is divided into three main areas by Vallado (Ref. 6): determination of satellite orbits affected by

drag, estimating lifetimes of satellites, and determining the physical properties of the atmosphere.

Drag occurs when atmospheric particles transfer momentum to the satellite, changing the satellite's velocity. Drag is considered a non-conservative force as the total energy of the satellite is not conserved during passage through the atmosphere. Drag decreases the semi-major axis and eccentricity of the satellite's orbit. The effect over time is circularization of the orbit. Periodic effects in other orbital elements also occur as a result of drag (Ref. 6).

According to Ref. 6, the ability to completely model perturbations due to the atmosphere requires knowledge of a wide range of fields including molecular chemistry, thermodynamics, aerodynamics, hypersonics, meteorology, electromagnetic, planetary sciences, and orbital mechanics. Awareness of atmospheric properties is necessary to study drag on satellites, as the study of astrodynamics in the atmosphere is a very complicated task. By examining the acceleration in the along-track direction of the satellite's motion, it is possible to infer the drag experienced by a satellite. The familiar aerodynamics equation for drag is adapted to find the acceleration due to drag induced by the atmosphere:

$$\vec{a}_{drag} = -\frac{1}{2}\frac{c_D A}{m}\rho v_{rel}^2 \frac{\vec{v}_{rel}}{|\vec{v}_{rel}|}$$

The drag coefficient, c_D, is a non-dimensional parameter that characterizes the relative influence of drag on an aerodynamic body. A high value of c_D indicates the body is highly affected by drag, and vice versa. Currently, satellite drag coefficients

are approximated using either a flat plate or spherical model. For flat plate models, the drag coefficient is about 2.2, and for spherical models it is approximately 2.0 to 2.1 (Ref. 6). The cross-sectional area of the satellite perpendicular to the velocity vector is denoted by *A*. For many satellites, the cross-sectional area may have fairly large uncertainty as it is a function of the satellite attitude, a parameter which changes over time, due to asymmetrical geometry. In order to have an accurate representation of *A* as a function of time during the orbit, accurate spacecraft geometry and attitude knowledge as a function of time are required. The mass of the satellite is represented by *m*. The mass of the satellite can change over its lifetime due to the expenditure of fuel for maneuvers. The local atmospheric density is denoted by ρ. Density is difficult to calculate and is often found from measured non-conservative accelerations. The vector $\vec{v}_{rel}$ is the velocity of the satellite relative to Earth's rotating atmosphere. This relative velocity in the absence of winds is given by the equation (Ref. 6):

$$\vec{v}_{rel} = \frac{d\vec{r}}{dt} - \vec{\omega}_{Earth} x \vec{r} = \begin{bmatrix} \frac{dx}{dt} + \omega_{Earth} y & \frac{dy}{dt} - \omega_{Earth} x & \frac{dz}{dt} \end{bmatrix}^T$$

Earth's atmosphere rotates with the Earth; however, the rotational speed of the atmosphere is highest closest to Earth's surface and decreases with altitude. Satellites are subjected to this motion as well as atmospheric winds. The relative velocity of the atmosphere due to the rotational speed and winds encountered by the spacecraft cause aerodynamic lift, side, and drag forces. The drag forces act along the velocity vector of the satellite in the opposite direction of the velocity.

The ballistic coefficient, *B*, is also frequently used as a measure of drag on an object. The historic definition for ballistic coefficient is given by the following equation:

Traditional Definition of Ballistic Coefficient

$$B = \frac{m}{c_D A}$$

In this work, the ballistic coefficient will be defined as the inverse of this definition, or:

Definition of Ballistic Coefficient in this Document (Inverse BC)

$$B = \frac{c_D A}{m}$$

Nominal ballistic coefficients provided by Bruce Bowman and the values used in Orbit Determination Tool Kit (ODTK) are consistent with the definition used in this document, which will be called the inverse ballistic coefficient. With this definition, higher inverse ballistic coefficient corresponds to higher drag, and vice versa.

Pressure and density changes in the atmosphere are modeled by two main relationships: the ideal gas law and the hydrostatic pressure equation. The ideal gas law for density is:

$$\rho = \frac{p_0 M}{g_0 R T}$$

Density, ρ, is calculated from its relation to absolute pressure, p_0, mean molecular weight of the atmosphere, M, acceleration due to gravity, g_0, the universal gas constant, R, and the local static temperature, T. Atmospheric temperature is very

important as Earth is exposed to solar heating as it rotates on its axis. The effect of solar heating on the atmospheric density is the main cause of difficulty in modeling density.

The hydrostatic pressure equation is:

$$\Delta p = -\rho g \Delta h$$

This relationship states that the change in pressure, Δp, is a function of atmospheric density, ρ, gravitational acceleration, g, and a change in altitude, Δh. The hydrostatic pressure equation and the ideal gas law are the basis for modeling drag for satellites passing through the atmosphere. The complexity and variability of the atmosphere make determination of drag an extremely difficult problem (Ref. 6).

1.4 Neutral Atmosphere

References 6-10 contain information about atmospheric density, specifically the neutral atmosphere, time-varying effects on density, density variation drivers, and the space environment as it pertains to Earth's atmosphere.

1.4.1 Neutral Atmosphere Structure

Earth's neutral atmosphere is subdivided into five sections according to temperature profiles. Boundaries between these layers are not necessarily easily definable and can vary on the order of tens of kilometers. The lowest layer beginning at the surface of the Earth is the troposphere. The temperature in the troposphere decreases with altitude and terminates at about 12 km. The stratosphere has a profile in which temperature increases from 12 to 50 km. This results from ozone absorbing

radiation in the ultraviolet wavelengths. The mesosphere ranges from approximately 50 to 80 km. In the mesosphere temperature again decreases as altitude increases. The troposphere, stratosphere, and mesosphere together form the lower atmosphere. Study of the lower atmosphere is not typically involved in orbit determination, except for the importance of upper

and lower atmospheric coupling, as lower atmospheric disturbances may propagate into the upper atmosphere.

The upper atmosphere consists of the thermosphere and exosphere. Above the mesosphere is the thermosphere. The thermosphere ranges from approximately 85 to 600 km. In this region the temperature increases with altitude. Some descriptions of the upper atmosphere define everything above 85 km as the thermosphere. In the thermosphere the composition of the atmosphere changes from being primarily composed of nitrogen to mostly atomic oxygen. Temperature increase in this region is mainly due to absorption of UV radiation. A great number of spacecraft operate in the thermosphere. The outermost layer of Earth's atmosphere is the exosphere. It is defined as the atmosphere above approximately 600 km. Here the temperature profile is essentially constant with altitude. Due to the extremely low density in the exosphere, particles in this region do not interact or collide as they do in lower portions of the atmosphere. Therefore, these particles display trajectories which are mainly affected by Earth's gravity. The atmosphere is no longer considered a fluid in the upper thermosphere and the exosphere, but is described by individual particles with corresponding trajectories.

1.4.2 Variations Affecting Static Atmospheric Models

Static atmospheric models assume no temporal variations. In reality, latitudinal and longitudinal variations are essential for orbit determination purposes. A satellite passing near the equatorial plane will effectively experience a decrease in altitude due to Earth's oblateness. This decrease in effective altitude causes the satellite to pass through a region of higher density and consequently, higher drag. Longitudinal variations are more often examined in time-varying models because of diurnal or daily effects. Earth's terrain features such as oceans or mountains also affect atmospheric density. Differences in atmosphere at lower altitudes due to these features can propagate upwards, affecting thermospheric and exospheric densities.

1.4.3 Time-Varying Effects on Thermospheric and Exospheric Density

The Earth's upper atmospheric density is influenced by multiple factors, but the Sun is the most important. The Sun affects density through direct heating in the extreme ultraviolet (EUV) region of the electromagnetic spectrum. The Sun also ejects charged particles that interact with Earth's magnetic field causing variations in density. Other variations impacting atmospheric density include:

- Solar rotation
- Solar cycle
- Variation of the solar cycle
- Differences in solar cycles
- Seasonal and semi-annual variations
- Rotation of the atmosphere
- Magnetic storms

- Winds
- Tides
- Gravity waves
- Irregular short-periodic variations

Solar Rotation

The Sun completes a rotation every 27 days. This means that any active locations on the surface of the Sun will be facing the Earth every 27 days. Irregularities in flux are due to changes in the active solar regions on the surface of the Sun. The $F_{10.7}$ index, which will be presented later, is a measure of solar flux affecting atmospheric density and reflects these variations due to solar rotation.

Solar Cycle

The Sun's magnetic field reverses polarity approximately every 11 years. During this 11 year period, solar activity will undergo one complete period. An increased number of sunspots and solar flares, greater solar flux, and a greater number of ejected charged particles are characteristic of solar maximum. This increases Earth's atmospheric density while causing it to be more variable. Solar minimum is characterized by minimal sunspots and solar flares, decreased emission of charged particles, and less flux. Earth's upper atmosphere contracts and becomes less dense as a result.

Variation of the Solar Cycle

There is also a secondary solar cycle which lags the primary solar cycle. The cause of this cycle is currently unknown; however, it is thought to be related to the sunspot cycle.

Differences in Solar Cycles

The 11 year solar cycles are not uniform in magnitude. Some cycles have greater or lesser activity at various points in the cycle than others. Interestingly, the most recent cycle has displayed a prolonged and especially quiet solar minimum (Ref. 11).

Seasonal and Semi-Annual Variations

The distance between the Sun and the Earth changes throughout the year as a result of the eccentricity of Earth's orbit. This causes minor variations in density. In addition, the declination of the Sun varies with the seasons and causes variations in density according to the latitude and time of year.

Rotation of the Atmosphere

Earth's atmosphere rotates as Earth rotates to some degree. Friction causes a velocity profile associated with the rotation of the atmosphere. At lower altitudes the velocity is greater than the velocity at higher altitudes.

Magnetic Storms

Any fluctuation of Earth's magnetic field can produce variations in atmospheric density. At higher levels of geomagnetic activity these variations become more pronounced. Magnetic storms occur as a result of solar wind variability, which often accompanies coronal mass ejections or solar flares. Magnetic substorms are significant changes in the magnetosphere of Earth which result in energy deposition in the atmosphere near the poles. These substorms usually produce auroras. An increase in density near the poles results from the substorms, and the disturbance propagates to lower latitudes moving in the direction of the opposite pole.

Winds

As at lower altitudes, winds occur in the upper atmosphere as well. These winds can be a result of the magnetic storms and substorms mentioned above. Winds in the thermosphere and exosphere impact orbiting satellites and therefore are of importance for orbit determination. These winds can be difficult to predict, but some generalities can be made. On the lit side of the Earth winds flow from the equator towards the poles, and on the night side they flow in the opposite direction. Winds travel from the summer hemisphere to the winter hemisphere, and winds travel west after local sunrise and east near local sunset, which becomes especially pronounced during periods around the equinoxes.

Tides

Gravitational forces are responsible for tides. These tides occur in the ocean and also the atmosphere. These tides have a minor effect on atmospheric density. However, solar tides or diurnal tides due to solar heating are significant in the upper atmosphere. EUV absorption increases temperature and density at high altitudes causing these tides.

Gravity Waves

When a fluid is disturbed from its equilibrium position, gravity can act as a restoring force to return it to its original position. The fluid may then overshoot the equilibrium point, and then be sent in the opposite direction by other forces. This is similar to a spring; however, gravity is the acting force in this case.

Gravity waves can affect satellites in the upper atmosphere as disturbances in the lower atmosphere may generate upward traveling waves altering density. Atmospheric gravity waves can transfer energy from lower altitudes into the lower levels of the thermosphere. As the waves travel upwards they are dissipated as a result of viscous damping.

Irregular Short-Periodic Variations

Unpredictable occurrences such as short-term changes in geomagnetic activity, random solar flares, or hydrogen currents in Earth's upper atmosphere can cause minor changes known as irregular short-periodic variations.

1.5 Atmospheric Density Models

According to Reference 6, there are two basic types of atmospheric models. The first method is to produce a physical model from theory using conservation laws and models of the atmospheric constituents. Corrections are then made based on additional input parameters. The second method is to use satellite tracking data and in-situ measurements supplemented by simplified concepts from the physical theory. Different models are often better suited to different applications.

Models also fall into static or time-varying categories. In some cases, the simpler static model may be adequate for the given problem. The time-varying models are significantly more accurate but require more computational resources and accurate input parameters as a function of time. The best model for a given situation depends on the user's particular needs.

In this research multiple atmospheric models are examined. Jacchia family models used include Jacchia 1971 (Ref. 12), Jacchia-Roberts (Ref. 13), and the Committee on Space Research (COSPAR) International Reference Atmosphere, CIRA 1972 (Ref. 14). Also utilized are two Mass Spectrometer Incoherent Scatter – Extended models. These are the MSISE 1990 model (Ref. 15) and the Naval Research Laboratory MSISE model (NRLMSISE 2000) (Ref. 16). The Jacchia-Bowman atmospheric model is also discussed (Ref. 17).

1.5.1 Solar and Geomagnetic Indices

Solar activity and geomagnetic activity are responsible for most of the variability in density in Earth's upper atmosphere. Solar activity can significantly

affect satellites in the upper atmosphere. During periods of low activity variations are slight; however, during periods of solar maximum variations in density, and subsequently drag, can be very large. Accordingly, orbit predictability suffers during periods of high solar activity.

The atmosphere is heated as it absorbs EUV radiation emitted by the Sun. In order to measure the amount of radiation received at the surface of the Earth, a proxy index is used. This is necessary since nearly all EUV radiation is absorbed by the atmosphere before reaching the Earth's surface. Some current satellites can measure EUV flux directly. Unfortunately, most atmospheric models are not formulated to use EUV data. Radiation of 10.7 cm wavelength and EUV radiation are both produced in the same layers of the Sun's chromosphere and corona. Therefore, 10.7 cm wavelength can be measured at the surface and translated into knowledge of EUV flux. This index, known as $F_{10.7}$, is widely used and has been recorded since around 1940 for scientific purposes. $F_{10.7}$ is measured in Solar Flux Units (SFU), and 1 SFU is equivalent to 10^{-22} $W \cdot m^{-2} \cdot Hz^{-1}$.

$F_{10.7}$ values generally fall somewhere in the 70 to 300 SFU range. The National Oceanic and Atmospheric Administration releases daily measurement values of $F_{10.7}$. Historically, these values have been measured at two sites. From 1947 until 1991 measurements were obtained at the Algonquin Radio Observatory in Ottawa, Ontario, Canada daily at 1700 UT. After 1991, values are obtained from the Dominion Radio Astrophysical Observatory in Penticton, British Columbia, Canada at 2000 UT. This $F_{10.7}$ data is available from Reference 18. This data is available as

daily observed, daily adjusted, and 81 day averaged values. The daily adjusted values are adjusted to a distance of 1 AU, as the Sun to Earth distance changes throughout the year. The 81 day averaged values take into account the solar rotation period, i. e., the 81 day averaged values are averages of values over three solar rotations. For many applications a daily value of $F_{10.7}$ may not provide enough temporal resolution as the flux is often changing on a much shorter time scale than a day. Other solar indices exist and some of them will be discussed in a subsequent section on the Jacchia-Bowman 2008 atmospheric model.

The Sun impacts the density of Earth's atmosphere not only through direct interaction of radiation, but also through indirect effects of charged particles interacting with Earth's magnetic field. Ionization occurring in the upper atmosphere causes geomagnetic heating, altering atmospheric density, which in turn changes the drag experienced by satellites in the upper atmosphere. To model geomagnetic heating in atmospheric models, K_p is used as a measure of geomagnetic activity. K_p is a geomagnetic planetary index which is a worldwide average of geomagnetic activity in non-auroral zones. This geomagnetic planetary index is quasi-logarithmic because it ranges from 0.0 to 9.0. K_p is averaged from measurements taken from twelve sites every three hours. These measurements are corrected for the latitude of the site.

The geomagnetic planetary amplitude, a_p, is a linear equivalent to the geomagnetic planetary index K_p. This index is provided every three hours, and is averaged to create a daily planetary amplitude, A_p. These values fall in the range of 0

to 400, rarely exceeding 100 and averaging around 10 to 20. The units for planetary amplitude are gamma. One gamma is equivalent to 10^{-9} Tesla or 10^{-9} $kg \cdot s \cdot m^{-1}$. Geomagnetic activity mirrors the 11-year solar cycle as well as having a secondary cycle. This cycle is semi-annual, dependent on the alignment of the solar wind and Earth's magnetic field. This cycle is more variable and less predictable than the main cycle. Data for geomagnetic planetary amplitude and geomagnetic planetary index are found in Reference 19. Table 1.1 displays the bins of solar and geomagnetic activity used in this research and set forth in Reference 16, and the historic distributions of time in these activity bins, the distributions for the lifetimes of the satellites examined, and the distributions for the data sets examined in this research.

Table 1.1: Solar and Geomagnetic Activity Level Bins and Distributions

Bin	1957-2010	CHAMP Available Data	GRACE Available Data	Data Examined 2004-2007	Data Examined 2008-2009
Low Solar Activity $F_{10.7}$ (SFU) < 75	19.18%	30.71%	51.97%	36.84%	100%
Moderate Solar Activity $75 \leq F_{10.7} < 150$	51.27%	48.42%	48.03%	63.16%	0%
Elevated Solar Activity $150 \leq F_{10.7} < 190$	15.52%	12.44%	0.00%	0.00%	0%
High Solar Activity $F_{10.7} \geq 190$	14.02%	8.43%	0.00%	0.00%	0%
Quiet Geomagnetic Activity A_p (gamma) ≤ 10	60.70%	69.56%	78.76%	32.63%	43.75%
Moderate Geomagnetic Activity $10 < A_p < 50$	35.72%	28.02%	20.08%	28.42%	56.25%
Active Geomagnetic Activity $A_p \geq 50$	3.59%	2.42%	1.16%	38.95%	0.00%

1.5.2 Jacchia 1971 Atmospheric Model

The Jacchia 1970 model was updated to create the Jacchia 1971 atmospheric model. This model assumes a fixed boundary condition in the atmosphere at 90 km. The assumption is also made that mixing occurs between 90 and 100 km and diffusive equilibrium occurs above 100 km. Observational data of EUV absorption and mass spectrometer data had indicated that the ratio of atomic oxygen to diatomic oxygen (O/O_2) was much higher than previous models produced. The Jacchia 1971 model attempted to rectify this new information. The model uses diffusion to model the temperature profile between 120 and 125 km, and above 125 km a temperature profile which asymptotically approaches the temperature of the exosphere is used (Ref. 12). An 81 day average for solar and geomagnetic activity is used to smooth any variations caused by the 27 day rotation of the Sun.

1.5.3 Jacchia-Roberts Atmospheric Model

Another Jacchia family model is the Jacchia-Roberts atmospheric model. This model is also an improvement to the Jacchia 1970 model. Roberts modified the Jacchia model to integrate partial fractions to achieve densities between 90 and 125 km, as opposed to using tabulated atmospheric densities. Above 125 km, an asymptotic function approaching the exospheric temperature is used which differs from the asymptotic function used by Jacchia in his 1971 model. In addition, exospheric temperature is calculated analytically as a function of position, time, solar activity, and geomagnetic activity. The Jacchia-Roberts model produces values very close to Jacchia models (Ref. 13).

1.5.4 CIRA 1972 Atmospheric Model

The Committee on Space Research (COSPAR) releases atmospheric models periodically with the first being in 1961. In 1972, COSPAR released an updated model utilizing the Jacchia 1971 atmospheric model (Ref. 14). For altitudes in the 25-500 km range, mean values are used. CIRA 1972 is semi-theoretical, also containing free variables which utilize some ground-based measurements as well as satellite drag data.

1.5.5 MSISE 1990 and NRLMSISE 2000 Atmospheric Models

Mass spectrometer data from satellites is used in conjunction with incoherent scatter radar obtained from ground-based locations to create a model of the atmosphere. The Drag Temperature Model (DTM), based on airglow temperatures, also provides data which is used in the formulation of the MSISE models (Ref. 16). These models are extended - denoted by the last letter in the acronym - meaning they model the entire atmosphere from sea level through the exosphere. The MSISE models are more accurate for some applications as they can access more data than earlier models. However, in some instances older models such as those in the Jacchia family of models are superior. NRLMSISE 2000 is an updated version of MSISE 1990 released by the Naval Research Laboratory. Improvements upon the previous edition include extensive use of drag and accelerometer data (Ref. 16).

1.5.6 Jacchia-Bowman Atmospheric Models

Perhaps the most current atmospheric model builds off of Jacchia's diffusion equations and is known as the Jacchia-Bowman model. The most recent edition of this model is Jacchia-Bowman 2008. Exospheric temperatures in this model are calculated using both satellite data gathered on-orbit and ground-based observations. Jacchia-Bowman takes new solar proxies and indices into account, along with a geomagnetic index algorithm and a new function modeling semiannual density variation. Reference 17 contains all the information regarding the Jacchia-Bowman 2008 atmospheric model.

Unlike some atmospheric models which may use one measure of solar activity, the Jacchia-Bowman model utilizes four different solar indices. The first index used is the proxy $F_{10.7}$, sometimes denoted as F_{10}, which was previously discussed in the last subsection, and is an indicator of EUV radiation flux in the upper atmosphere. A centered 81 day running average is used in this model and others, denoted as $\overline{F}_{10.7}$.

Because the $F_{10.7}$ index does not fully reflect the amount of solar energy deposited in the upper atmosphere, other indices are also used. A NASA/ESA satellite called the Solar and Heliospheric Observatory (SOHO) can directly measure solar EUV radiation using an onboard instrument called the Solar Extreme-ultraviolet Monitor (SEM). Radiation measured by the SEM is in the 26 to 34 nm wavelength range. This instrument provides data reported in SFU for an index known as S_{10}. Similar to $F_{10.7}$, an 81 day centered average, $\overline{S}_{10}$, is also produced.

Another solar index incorporated by the Jacchia-Bowman models is M_{10}. M_{10} is an index of middle ultraviolet wavelength radiation. A number of satellites launched by the NOAA have Solar Backscatter Ultraviolet (SBUV) spectrometers onboard. These spectrometers, after some manipulation of data, can produce a measure of chromospheric and photospheric solar active region activity (Ref. 17). M_{10} serves as a proxy for far ultraviolet radiation (FUV) in Jacchia-Bowman. $\overline{M}_{10}$, or the 81 day averaged value, is also available.

Lastly, the Y_{10} solar index is used in Jacchia-Bowman models. NOAA possesses a series of satellites known as the Geostationary Operational Environmental Satellites (GOES) which feature X-ray spectrometers (XRS). The XRS observes X-rays in the 0.1 to 0.8 nm range. During periods of high solar activity X-rays at these wavelengths deposit a great deal of energy in the mesosphere and lower thermosphere. X_{10} is an index of these X-rays. Lyman-α emission also greatly affect this part of the atmosphere; however, they are the primary driver during periods of low to moderate solar activity. NASA's Solar Radiation and Climate Experiment (SORCE) satellites and Upper Atmosphere Research Satellites (UARS) use an instrument called the Solar Stellar Comparison Experiment (SOLSTICE) to measure Lyman-α emission. The Solar Extreme Ultraviolet Experiment (SEE) on the NASA Thermosphere Ionosphere Mesosphere Energetics and Dynamics (TIMED) satellite also measures this. The Y_{10} solar index is a mixed index which weights the results from X_{10} more heavily during periods of higher solar activity and Lyman-α emissions more heavily during periods of lower activity.

The $\overline{F}_{10.7}$ index is superior overall to the other indices presented (Ref. 17), but in the Jacchia-Bowman models the shortcomings of this index are somewhat overcome by augmenting $\overline{F}_{10.7}$ with $\overline{S}_{10}$ during periods of solar minimum. A new index $\overline{F}_S$ is created which is a weighted combination of these two indices. This new index and the other solar indices are used to calculate a new nighttime minimum exospheric temperature, which is used to generate atmospheric densities. Jacchia-Bowman 2008 differs from the 2006 version in that it introduces the Y_{10} solar index.

The Jacchia-Bowman models also use an index called the Disturbance Storm Time (Dst) which is an evaluation of geomagnetic storm strength. This index is obtained from four sites on the equator which takes measurements of the magnetosphere. Jacchia-Bowman models incorporate Dst into the calculation of exospheric temperature, and subsequently atmospheric density, as a function of time during magnetic storms. Dst is a more accurate manner of modeling deposition of energy in the upper atmosphere during geomagnetic storms than the three-hourly geomagnetic planetary amplitude. During periods where the three-hourly geomagnetic planetary amplitude is very high but there is no geomagnetic storm according to the Disturbance Storm Time technique, errors can occur in modeling. However, the Jacchia-Bowman models minimize these errors through use of an algorithm implemented in calculation of density.

1.6 Previous Research on Atmospheric Density Model Corrections

In previous research there have been two primary methods of modeling atmospheric density for satellite drag analysis. Dynamic calibration of the atmosphere (DCA) is one method, and the other is the use of onboard accelerometers which measure non-conservative accelerations such as drag.

1.6.1 Dynamic Calibration of the Atmosphere

Dynamic calibration of the atmosphere (DCA) is a method by which density values obtained from existing atmospheric models are improved or corrected. Density variations and their associated statistics are provided by this technique. DCA started with the work of Nazarenko and others in the early 1980's, (Ref. 6) and continues today. Observation data or two-line element set data are used to generate orbital elements and satellite drag data. At the same time, an atmospheric variation model is created from accumulated data. These two items are combined to create a solution (Ref. 6).

DCA determines corrections to density every three hours, with the use of radar observations, or once daily for two line element sets, from "calibration" satellites. Some more recent DCA schemes only generate a density correction once daily. A "true" ballistic coefficient is needed as an input to an atmospheric density model such as one of the Jacchia or MSISE family models previously discussed. The "true" ballistic coefficient is the method by which densities are changed from an existing model. References 20 through 29 detail some recent DCA analyses.

In Reference 20, Storz et al. utilize 75 inactive payloads and debris to solve for a global correction to density that changes dynamically in the thermosphere and exosphere. This technique is called the High Accuracy Satellite Drag Model (HASDM). Corrections are made every three hours. In addition, HASDM predicts density in advance using a model which predicts EUV radiation and geomagnetic activity in advance. HASDM decreased atmospheric density model errors for satellites orbiting at less than 600 km (Ref. 20).

In Reference 21, Bowman examines the semiannual thermospheric density variation from 1970 to 2002 over the altitude range of 200 to 1100 km using a HASDM modified Jacchia 1970 model. Special orbit perturbations on 13 different satellites over this altitude range are used to process observational data from radar. This study found that the semiannual density variation may change considerably from one year to the next, up to 100%.

Two line element (TLE) sets are used to create density corrections by Yurasov et al. in Reference 22. The data is taken from observations of several hundred inactive objects in LEO perturbed by drag. The density corrections were generated as a linear function of altitude. An orbit determination and prediction process was performed on the satellites using the original densities and the densities with the calculated corrections. These results were compared to assess the feasibility of the methods used.

An earlier study which uses TLE data was performed by Cefola et al. (Ref. 23). This study created corrections to the Russian GOST model. This method creates

corrections as a linear function of altitude, but also incorporates a bias term to the corrections. Hundreds of satellites in LEO are examined from April 2002 to January 2003. Density corrections are made for a one day grid using the TLE data as well as solar and geomagnetic activity data as inputs.

Yurasov et al. attempt to improve estimates of spacecraft reentry time through the use of DCA techniques and density corrections in Reference 24. The NRLMSISE 2000 model is corrected in this procedure using data from several hundred drag-perturbed objects in LEO. Both spherical and non-spherical space objects are examined. The result is improved reentry time predictions for all space objects, with spherical objects' reentry times showing more improvement as a result of constant ballistic coefficients as opposed to time-varying ballistic coefficients of non-spherical objects.

In Reference 25, the authors seek to improve DCA techniques introduced by Nazarenko and Yurasov. They create successive refinements using a series of vanishing coefficients when determining corrections to the atmospheric density. Each refinement uses the previous corrections as the starting point for the next refinement. The authors also introduce a new formulation in an effort to remove bias in the solution set. Orbit observation residual error is reduced in this study by an order of magnitude using the theory of successive refinements.

The same authors examine corrections to the NRLMSISE 2000 model using dynamic calibration of the atmosphere in References 26 and 27. In Reference 26, they discuss the difficulty in applying corrections to an existing model. Subtleties in generating these

corrections can significantly impact orbit determination and prediction. This study states that the model used to generate density corrections at a given point in the orbit must be the exact same as the underlying model. In Reference 27, the authors seek to independently validate the work of Yurasov and Nazarenko. For the periods of November 1999 to November 2003 and January 1995 to June 2000, DCA is used to generate corrections to the NRLMSISE 2000 model. These results are compared to the Russian DCA results. The ability to determine corrections is dependent on solar and geomagnetic activity. The authors conclude that the original Russian DCA method is valid, and that DCA is a worthwhile method, but that more extensive investigation is required.

Recent research using DCA has been performed using GEODYN, the NASA Goddard Space Flight Center Precision Orbit Determination and Geodetic Parameter Estimation Program (Ref. 28). Results obtained from creating density corrections to the NRLMSISE model for GEODYN were applied to the GEOSAT Follow-On (GFO) mission. Results from GEODYN were compared with results using the MSIS 1986 model up to 600 km for a variety of solar and geomagnetic activity levels. The authors found that no significant improvements in ballistic coefficient estimation were made. However, the orbit of GFO is approximately 800 km, higher than the applicable range for this method.

In Reference 29, Doornbos, Klinkrad, and Visser use TLE data to calibrate the neutral density of the thermosphere. This method generates daily adjustment of density model calibration parameters. The authors utilized and compared results from two separate methods of calibration on approximately 50 objects during 2000. The first uses height-dependent scale factors, and the second corrects the CIRA 1972 model. Using a single daily parameter improvements were made in error from around 30% for the base models to around 15% with the calibration technique.

Unfortunately, DCA approaches have several disadvantages (Ref. 30). DCA is internal to a particular scheme. Hence, outside users of the scheme must rely on that system to update its density corrections. In addition, access to density corrections at all times may be necessary. Another shortcoming of DCA is its inability to improve on temporal and spatial resolution of existing atmospheric models. These approaches are limited temporally by the use of daily solar flux or averaged geomagnetic indices. Shorter period variations cannot be captured by this method. DCA also models the atmosphere discretely based on the intervals of input data. This results in continuous solutions over these intervals, but causes discontinuities between intervals. Finally, the use of TLE data by most DCA schemes limits the accuracy of the results.

1.6.2 Accelerometers

Select spacecraft orbiting in the upper atmosphere feature onboard accelerometers, which can measure accelerations due to non-conservative forces. The data from these accelerometers can be used to estimate atmospheric density. During orbital maneuvers such as station keeping or attitude change maneuvers, additional accelerations occur which may render the data obtained from accelerometers inaccurate. There are several non-conservative forces experienced by spacecraft in LEO. Solar radiation pressure, Earth infrared radiation pressure, and Earth albedo pressure all contribute along with atmospheric drag. Since radiation pressures from these sources are known to a good degree of accuracy, drag can be isolated from accelerometer data. Unfortunately, not many satellites possess these onboard accelerometers. Current satellites equipped with accelerometers capable of measuring drag perturbations are CHAMP, which has now reentered, and the

GRACE satellites. Past satellites have featured sufficiently accurate accelerometers, such as the Satellite Electrostatic Triaxial Accelerometer (SETA) mission (Ref. 31). Operating at around 200 km, this satellite provided meaningful data on the traveling atmospheric disturbances created by density propagation from energy deposition at high latitudes due to magnetic storms.

Density estimation derived from CHAMP accelerometer data was first performed by Bruinsma and Biancale in Reference 1 and by Konig and Neumayer in Reference 32. Further publications ensued setting forth methods for obtaining atmospheric densities from the accelerometer data in References 2 through 4.

Major changes in the thermosphere caused by coronal mass ejections or other large events can be detected by accelerometers as evidenced in Reference 32. The authors show that accelerometer data can be used instead of modeling non-conservative forces in orbit determination schemes. The authors suggest the use of SLR data to verify the calibration of the accelerometer is correct to ensure that there are truly improvements as a result of using this data.

In Reference 1, the total atmospheric density is computed from STAR accelerometer readings and compared with the DTM2000 model. The authors state that a systematic bias may exist due to uncertainties in the modeling of drag coefficient. The magnitude of winds encountered by CHAMP, along with calibration of the instrument affects the accuracy of the results. Accelerometer data looks to be very useful as a greater amount of data becomes available from the onboard accelerometer.

Bruinsma and Biancale set forth the procedure by which they derive atmospheric densities from accelerometer data (Ref. 2). Due to the nature of its orbit, CHAMP provides good coverage, both in altitude and geography, for the duration of its lifetime. Accelerometer data began in 2001, and CHAMP recently terminated its mission through reentry in September 2010. Accelerometer measurements are corrected for items such as bias and orbital maneuvers. Aerodynamic coefficients are estimated based on a 15 plate model of the satellite. Uncertainties exist in calibration of the accelerometer and the drag coefficient as well as the effect of geomagnetic activity.

Reference 3 sets forth the accuracy achievable by CHAMP's onboard accelerometer and some of its associated limitations. CHAMP features GPS and SLR tracking systems, allowing very accurate readings of position and velocity over time. Data is examined over a 21 month range, providing time periods of differing solar and geomagnetic activities. This reference also contains a great deal of information on CHAMP, its mission, and the STAR accelerometer.

Further discussion of the STAR accelerometer is found in Reference 4. In addition to its accelerometer, CHAMP also possesses a GPS receiver. This receiver allows modeling of the accelerometer bias and scale factors as a function of time. Since the densities derived from this method assume insignificant winds, the accuracy of the output is largely dependent on uncertainty in calibration and the existence of winds in the upper atmosphere, which are usually a result of geomagnetic activity. Three periods of time associated with geomagnetic storms are examined. The authors

conclude that winds during periods such as these may degrade the accuracy of the results by around 10%.

Schlegel et al. use the CHAMP accelerometer to characterize thermospheric density structures in polar regions in Reference 33. Density variations occurred around the magnetic cusp, as predicted by some models. However, models predict these density structures to occur lower than 300 km. CHAMP detected these structures above 400 km. The cause of these thermospheric density structures is the collision of energetic solar particles in Earth's magnetic field interacting with the upper atmosphere. The short-term nature of these occurrences may be undetectable by other methods, but the accelerometer is able to record the density variations.

Collaboration between the Centre National d'Études Spatiales (CNES) and the University of Colorado researchers produced several publications using accelerometer data from CHAMP and GRACE (Ref. 34-39). Specifically, these papers address the impact of solar and geomagnetic events on upper atmospheric densities. Existing models often cannot characterize density variations which occur very quickly, as discussed with the polar magnetic variations. The accelerometer, however, measures these variations and the accompanying density waves that propagate towards the opposite poles. An advantage the accelerometer density method possesses over predictions made by empirical or analytical models is the coverage provided by the nearly 90° inclination orbits of the CHAMP and GRACE satellites.

Reference 40 sets forth the procedure used in obtaining density values from the accelerometer data available from the GRACE satellites. Once again, calibration

issues, maneuvers, accurate force modeling, and all the items discussed with the CHAMP accelerometer apply to the GRACE satellites. However, the GRACE satellites operate at a higher altitude for most of the duration with available data.

Bruinsma and Forbes further examine the use of the STAR accelerometer aboard CHAMP to identify density variability (Ref. 41). In this paper, use of accelerometer data is used to show that waves are generated as a result of density variations at high latitudes which propagate towards the lower latitudes. When geomagnetic activity is lower, the waves usually dissipate at mid-latitudes, while higher geomagnetic activity and lower solar activity produce waves which dissipate in equatorial latitudes. Traveling atmospheric disturbances (TAD) are also detectable by the STAR accelerometer (Ref. 42). The size and speed of these TADs can be observed through use of the CHAMP accelerometer. Zhou et al. discuss global density distributions and their variations during major geomagnetic storms (Ref. 43). The NRLMSISE 2000 model is corrected using the readings obtained from the accelerometer during these storms.

CHAMP and both GRACE satellites have onboard accelerometers which provide invaluable information characterizing density variations in the upper atmosphere. A weakness of the accelerometer density method is the low number of spacecraft and limited altitude ranges and spatial coverage. DCA on the other hand, possesses many satellites and a great deal of data but is not nearly as accurate.

1.6.3 Additional Approaches

In addition to the use of accelerometers or DCA to estimate density corrections to existing models, effort has been made to use precision orbit determination for satellites which feature precise measurement systems. Satellites with these measurement systems include ICESat, Envisat, CryoSat, CHAMP, GRACE, and Gravity field and steady-state Ocean Circulation Explorer (GOCE) (Ref. 44). In Reference 44, the authors use dynamic calibration of the atmosphere techniques on satellites with precision orbit data. Due to the inability of current models to properly incorporate space weather data, errors are introduced in orbit determination and prediction. Corrections to existing density models based on data from precision orbit ephemerides obtained using SLR or GPS increases accuracy of the density estimates. Calibration of density models using TLE data in conjunction with precise orbit data and accelerometer data will greatly increase accuracy and resolution, both temporally and spatially.

Non-conservative accelerations can be estimated through a technique known as GPS accelerometry as well. In References 45 through 47, van den IJssel et al. utilize this approach. Reference 45 shows the feasibility of measuring non-conservative accelerations using GPS satellite-to-satellite tracking (SST) data from CHAMP. This method requires a very accurate gravity field model; fortunately, the GRACE mission has provided this. The best results are obtained in the along-track direction of the orbit. In Reference 46, van den IJssel and Visser examine the performance of this GPS accelerometry for both CHAMP and GRACE. Temporal

resolution of 20 minutes is achievable for this method. High frequency accelerations, such as those caused by density variations due to geomagnetic activity, are only somewhat detectable, however. This approach may have more possibility of application, as many future missions will feature GPS receivers.

In Reference 48, both batch filter and extended Kalman filter methods are utilized in the examination of empirical accelerations experienced by the GRACE-B satellite. The orbit accuracy is known to between 4 and 7 cm using GPS data. The Kalman filter/smoother technique and the standard batch technique are compared for orbit determination using this data. The Kalman filter was more desirable from an efficiency of computing perspective, while the batch least-squares method produced smoother trajectories and was more robust. Similar results were obtained from both methods; however, the amplitudes differed by a factor of approximately 1.5. The results were highly accurate, even considering the high solar activity due to a large solar storm experienced during the time period examined.

Another approach to atmospheric density correction is through the use of Doppler Orbitography and Radio positioning Integrated by Satellite (DORIS) and SLR data. In Reference 49, the authors study satellites orbiting in LEO during periods of very active geomagnetic activity. Multiple satellites at differing altitudes, between 800 and 1400 km, are included. Orbit analysis with multiple atmospheric models reveals errors in the output products using the DORIS data. However, improved data processing strategies significantly improved results, essentially to the

same quality as results from normal geomagnetic activity periods. This proves to be another feasible method for generating corrections to atmospheric density models.

1.7 Current Research on Atmospheric Density Model Corrections

In this research, improving knowledge of upper atmospheric density is achieved through the use of data obtained from orbiting spacecraft. Currently, many satellites possess GPS receivers which can provide precision orbit data. When these precision orbit ephemerides (POE) are applied as observations to an optimal orbit determination scheme, accuracies of a few centimeters are achievable. Accuracy is greatly improved for this method compared with TLE data. Densities obtained through this orbit determination procedure can be compared to densities derived from the onboard accelerometers of satellites, namely CHAMP and GRACE. This work builds upon previous work by studying results from both CHAMP and GRACE, increasing the time periods covered, and looking at data obtained during the relatively recent extended solar minimum. Results can then be compared between CHAMP and GRACE satellites to assess differences.

McLaughlin and Bieber began work on estimating density corrections to baseline models using orbit determination and precision orbit data for CHAMP in Reference 30. Density estimates found using corrections to multiple atmospheric density models were consistent within approximately 10%. In addition, overlapping orbit solutions were found to be consistent within about 10%. In Reference 50, results obtained using these methods are compared to data derived from CHAMP accelerometer data. Reference 51 continues this research, seeking to find the best inputs of various orbit determination parameters such as baseline density model and Gauss-Markov process half-lives. The authors found that this method outperformed the Jacchia 1971 empirical model and usually outperformed HASDM.

Periods of high solar activity were also examined using these techniques in Reference 52. Multiple days which had varying levels of solar and geomagnetic activity were also examined. Comparison with accelerometer derived densities is then performed. Input parameters in the orbit determination process were varied so that the effects on density estimation could be monitored. Results are binned according to solar and geomagnetic activity levels, as well as examining overall averages. Cross correlation between densities obtained from POE data and accelerometer data provide a quantitative basis for comparison. In Reference 53, Hiatt furthers this research with a greater range of time periods examined, as well as examining additional considerations such as sensitivity to ballistic coefficient or solution fit span length. In Reference 54, Lechtenberg again furthers this research with addition of GRACE and TerraSAR-X solutions, study of the ability of this method to observe traveling atmospheric disturbances, and brief examination of time periods in which the CHAMP and GRACE satellites were coplanar.

Reference 55 examines the CHAMP, GRACE, and TerraSAR-X satellites over the same time periods. Conclusions drawn from comparison of CHAMP and GRACE POE derived densities with their accelerometers are applied to TerraSAR-X. Densities are generated for all three satellites during the same time period. Further examination of the CHAMP and GRACE coplanar periods is performed. In Reference 56, the authors compare density estimation for CHAMP and GRACE for the same time periods. Results are compared to the accelerometers during periods spanning all available solar and geomagnetic activity levels.

1.8 Gauss-Markov Process

A concept used in orbit determination is that of the Gauss-Markov process. A Gauss-Markov process possesses the characteristics of both Gaussian and Markovian processes. A Gaussian process is one featuring Gaussian, or normal, probability distribution. Markovian processes display the Markov property, which essentially states that the future state of the process depends only on the current state and not on any previous states. Reference 57 contains more information about the Gauss-Markov process and its mathematical formulation. First-order Gauss-Markov processes are introduced in orbit determination schemes as dynamic model compensation to address inaccurately modeled or unmodeled accelerations experienced by the satellite.

1.9 Estimating Density and Ballistic Coefficient Separately

As discussed above, acceleration due to drag acting on a satellite is a function of both atmospheric density and ballistic coefficient. Estimation of density and ballistic coefficient simultaneously in an orbit determination process is very difficult, as two unknowns are in one equation. Wright sets forth a method for estimating both ballistic coefficient and density simultaneously in References 58 and 59.

In the past, errors in the ballistic coefficient model, the atmospheric density model, and possibly even gravity field model were absorbed in the estimation of the ballistic coefficient. Current methods which allow simultaneous estimation of both parameters utilize two significantly differing exponential half-lives. In the Gauss-Markov model, one half-life is for the ballistic coefficient and one is for the density.

These half-lives determine to what extent the previous state affects the calculation of the current state. In this research, Orbit Determination Tool Kit (ODTK) is used. ODTK is software which allows user input of density correlated half-life and ballistic coefficient correlated half-life for the orbit determination scheme. These correlated half-lives are the amount of time each parameter takes to decay to half the initial value in the absence of update measurements. Through this method, density and ballistic coefficient can be separated and observed, as will be more fully explained in the next chapter.

1.10 Satellites Examined

1.10.1 CHAMP Satellite

The Challenging Minisatellite Payload (CHAMP) mission was launched in July 2000. Originally slated for a 5 year mission, CHAMP provided data until its reentry in September 2010. CHAMP provides data on Earth's magnetic field as well as generating gravity field measurements. In addition, CHAMP possesses the Spatial Triaxial Accelerometer for Research (STAR) which is used in the study of non-conservative accelerations such as drag due to atmospheric density (Ref. 60). An artist's rendering of CHAMP is seen in Figure 1.1.

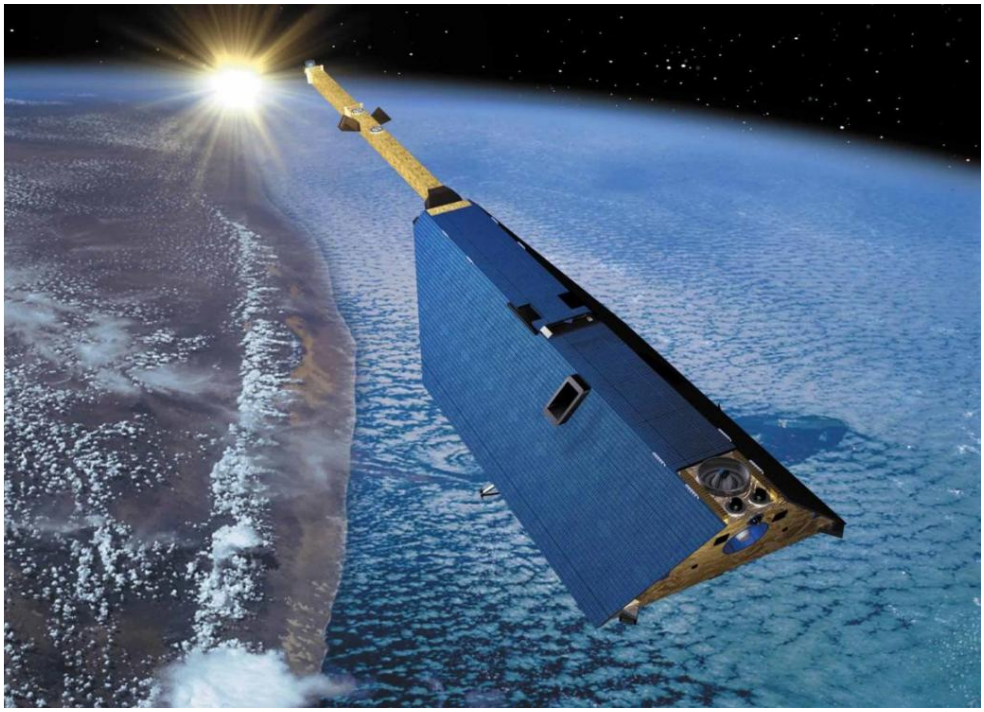

Figure 1.1: Rendering of CHAMP Satellite (Ref. 60).

1.10.2 GRACE Satellites

The Gravity Recovery and Climate Experiment (GRACE) consists of twin satellites, GRACE-A and GRACE-B, launched in March 2002. The main purpose of this mission is to measure the gravitational field of Earth to a very high level of precision. A GPS and microwave ranging system accurately measures the distance between the two satellites (Ref. 61). Spatial variations in mass density of the Earth will cause acceleration or deceleration, changing the distance between the satellites. The gravity field can be inferred from these measurements. These satellites also feature onboard accelerometers used in generating atmospheric density corrections in this work. Data from both GRACE-A and GRACE-B are examined. Figure 1.2 shows a depiction of the GRACE satellites in orbit.

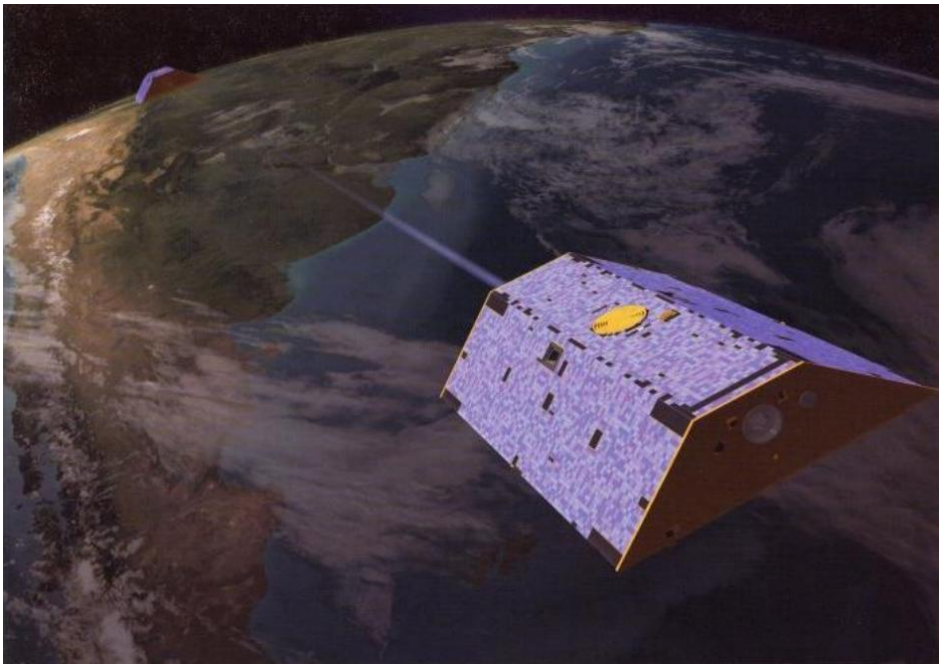

Figure 1.2: Rendering of GRACE Satellites (Ref. 61).

2 METHODOLOGY

This section discusses the methods used to generate results. Position and velocity data for many time periods are obtained for the CHAMP and GRACE satellites and are used as observations in an optimal orbit determination scheme. Ballistic coefficient and density are estimated as a result of this process. Using densities derived from accelerometer data from these satellites as truth for comparison purposes, variations in the orbit determination scheme were performed by changing inputs such as density correlated half-life, ballistic coefficient correlated half-life, and baseline atmospheric density model.

2.1 Precision Orbit Ephemerides

Precision orbit ephemerides (POE) are available in two forms from the Helmholtz Centre Potsdam website: http://isdc.gfz-potsdam.de. POE data can be obtained as Precision Science Orbits (PSO) or Rapid Science Orbits (RSO). PSO data are not available for the GRACE satellites. Published accuracies of the RSO data are 5 to 10 cm for most of the duration of the missions; however, very early in the mission accuracies were as low as 25 cm. All data used in this research is obtained in the form of RSO data. Information on POE can be found in References 62 through 65.

2.2 Optimal Orbit Determination

Information on orbit determination is taken from Reference 57, as well as References 62 through 66. Orbit determination is the estimation of the trajectory of a

body in orbit, including spacecraft or natural satellites. Adequate measurements of the body are required to perform orbit determination. Artificial satellites possess characteristics such as size and mass which make nongravitational forces of great importance in determination and prediction of their orbits. Pressure forces such as solar radiation pressure, Earth albedo, and pressure due to atmospheric drag significantly affect the orbits of these spacecraft.

Six independent measurements are needed for the unique determination of an orbit. These six parameters can be the three-dimensional position and velocity vectors or six orbital elements. The state vector for a particular problem which includes the six elements mentioned as well as possible additional parameters to be estimated by the orbit determination process. The state vector is denoted as $\mathbf{X}(t)$, and the state vector can be determined at any point in time for the orbit given an initial state vector and governing equations for the forces experienced by the satellite. The equations of motion can be integrated to give the state of the spacecraft at any time. However, uncertainties exist in the initial state as well as the dynamical models governing the spacecraft's motion, and corresponding errors are produced in the actual trajectory from the predicted trajectory. As the orbit is propagated these errors will increase over time. Updates in the form of observations will greatly increase the accuracy of the state vector. The locations of these ground stations must be known very accurately to produce observations which are useful to improving the orbit determination. Even with these update measurements, however, the predicted orbit will deviate from the actual orbit due to systematic and random errors in the process.

Observations are often nonlinear functions of the state variables. These variables include range, range rate, azimuth, elevation, or other observable parameters.

Precision orbit ephemerides are used in this research as observations in the optimal orbit determination process. Position and velocity from these POE data are very accurate measurements and are used for the Kalman filter/smoother which makes use of Gauss-Markov processes. Kalman filtering and Gauss-Markov processes will be elaborated on later in this document. Observations taken from the POE data are used to update the state estimate at each time step throughout the orbit determination process.

The "best" state estimate is a somewhat subjective notion. In optimal orbit determination the optimal solution can be defined in various ways. Some methods are less accurate but considerably faster. Sequential and batch methods can be used, and the user must choose whether to minimize errors in the orbit or residuals. If the user chooses to linearize the problem, the choice of the best linearization method is another important one. A definition for optimal provided by Wright (Ref. 67) will be used in this work, and is set forth in the following items:

1. *"Sequential processing is used to account for force modeling errors and measurement information in the time order in which they are realized.*
2. *The optimal state error estimate* $\Delta\hat{X}$ *is the expectation of the state error* ΔX *given the measurement residual* Δy. *That is* $\Delta\hat{X} = E\{\Delta X \mid \Delta y\}$. *This is Sherman's Theorem.*

3. *Linearization of state estimate time transition and state to measurement representation is local in time, not global.*
4. *The state estimate structure is complete.*
5. *All state estimate models and state estimate error model approximations are derived from appropriate force modeling physics, and measurement sensor performance.*
6. *All measurement models and measurement error model approximations are derived from appropriate sensor hardware definition and associated physics, and measurement sensor performance.*
7. *Necessary conditions for real data:*
    - *Measurement residuals approximate Gaussian white noise.*
    - *McReynolds' filter-smoother consistency test is satisfied with probability 0.99.*
8. *Sufficient conditions for simulated data: The state estimate errors agree with the state estimate error covariance function.*

The first six requirements defined standards for optimal algorithm design, and the creation of a realistic state estimate error covariance function. The last two requirements enable validation: They define realizable test criteria for optimality. The last requirement implies the development and use of a physically realistic measurement simulator."

2.3 Gauss-Markov Process Half-Lives

Orbit Determination Tool Kit (ODTK) uses two variables called the density correlated half-life and the ballistic coefficient correlated half-life. These variables define Gauss-Markov processes, as discussed earlier. These values can be altered by the user to affect estimated density and ballistic coefficient. The baseline atmospheric model chosen generates a density, ρ, as well as an inverse ballistic coefficient, B. Corrections to the density, Δρ/ρ, and corrections to the inverse ballistic coefficient, ΔB/B, are generated from the estimation process. The half-lives represent the amount of time required for the estimated correction to decay to half its value without measurement data updates.

In References 68 and 69, ODTK documentation discusses these half-lives. Given $x = x(t)$ is a dynamic scalar random variable, which in this case is either density or ballistic coefficient, the following equation is satisfied for an exponential Gauss-Markov sequence:

$$x(t_{k+1}) = \Phi(t_k, t_{k+1})x(t_k) + \sqrt{1-\Phi^2(t_{k+1}, t_k)}w(t_k)$$

In this equation, $w(t)$ is a Gaussian variable possessing zero mean and constant standard deviation. This white noise function is also dependent only on the previous measurement, and thus is a Markovian process as well. The initial value of the Gaussian white noise variable is equal to the initial value of the dynamic scalar random variable. The following equations define the transition function:

$$\Phi(t_{k+1}, t_k) = e^{\alpha|t_{k+1}-t_k|}$$

$$\alpha = \frac{\ln(1/2)}{\tau}$$

The half-life, τ, is the half-life input by the user (Ref. 68).

2.4 Filter-Smoother Description

A sequential filter is used by ODTK in the process of orbit determination. This filter uses precision orbit ephemerides as observations. The output is a state vector as a function of time. The state vector includes three-dimensional position and velocity in Cartesian coordinates, relative atmospheric density, relative ballistic coefficient, and other parameters such as station biases, additional forces, measurements, and model parameters. The POE measurements are processed by the filter when integrating the equations of motion and determining the state at the next time step. A converged state and covariance result from this procedure, which are used in subsequent steps of the filter.

The smoothing process starts at the final output step and works sequentially backwards in time. Only data produced in the filtering process is used by the smoother. The output of the smoother is again a state estimate; however, this output is superior to only filtering, as all measurement data is taken into account (Ref. 57). Further information on filtering and smoothing schemes can be found in Reference 57, in addition to References 6, 66, 67, and 69.

2.5 McReynolds' Filter-Smoother Consistency Test

A consistency test used to validate the filter and smoother estimates is called the McReynolds' Filter-Smoother consistency test. The estimates output from the

filter and the smoother are compared to one another. A dimensionless ratio is created, denoted $\vec{R}$. The numerator of the ratio is the difference of the state estimates from the filter and smoother at each time point. The denominator of this ratio is formed by taking the square roots of the main diagonal elements of a matrix which is the difference of the covariance matrices from the filter and smoother at each time point. The test is considered a pass if 99% of the ratios for all time points in the period examined are less than or equal to 3. Reference 67 contains more information about the McReynolds' consistency test. The following equations show this test:

$$\vec{R} = \left| \frac{\vec{\bar{X}}_{i,\,filter} - \vec{\bar{X}}_{i,smoother}}{\sigma_i} \right| \leq 3$$

$$\sigma_i = \sqrt{\bar{P}_{i,\,filter} - \bar{P}_{i,smoother}}$$

2.6 Using Orbit Determination to Estimate Atmospheric Density

In this optimal orbit determination scheme, optimality is in the minimum variance or least-squares sense. Corrections to baseline atmospheric models and a baseline ballistic coefficient are estimated by ODTK in the sequential filtering and smoothing procedure. In addition, state variables are calculated, position and velocity consistency tests are performed, and residuals are found. ODTK can generate corrections to multiple atmospheric models, including the Jacchia 1971, CIRA 1972, Jacchia-Roberts, MSISE 1990, and NRLMSISE 2000 atmospheric models. An extremely accurate gravity model is used by ODTK, which uses data from the GRACE satellites in addition to Earth-based gravity information. This is the GRACE

Gravity Model GGM02C (Ref. 70). Accuracy is further increased through the use of force models for drag, radiation pressure effects, lunar and solar gravitational effects, ocean and solid Earth tides, and general relativity.

Estimation of atmospheric density in ODTK results from corrections to one of five baseline atmospheric models, the Jacchia 1971, CIRA 1972, Jacchia-Roberts, MSISE 1990, or NRLMSISE 2000 atmospheric model. Since the Jacchia 1971, CIRA 1972, and Jacchia-Roberts are all based on the Jacchia 1970 model, results from these models should not differ greatly from one another. Similarly, the MSISE1990 and NRLMSISE 2000 results will likely produce results that differ little from one another.

There are two types of corrections which are applied to the baseline atmospheric model in ODTK. The first type of correction is derived from historical solar and geomagnetic activity, specifically from the $F_{10.7}$ index and a_p, and also incorporates the perigee height of the satellite. The corrections of this type are propagated forward in time from the epoch of the time period examined using Gauss-Markov processes. A transformation is then used which relates corrections determined at perigee to every time point at which these corrections are applied to the baseline density. A second type of correction uses the observations as well as current conditions to create a dynamic correction. Since the method used is a sequential one, as opposed to a batch approach, corrections can be estimated at each time step. These corrections also use the user input of density correlated half-life and ballistic coefficient correlated half-life.

A nominal value for ballistic coefficient of the satellite being examined is input into ODTK. Reference 71 provides nominal values for CHAMP of 0.00444 m^2/kg in 2002-2003 and 0.00436 m^2/kg for 2004-2006. Changes in nominal ballistic coefficient are due to orbit decay as well as mass changes resulting from maneuvers and station keeping. During examined periods after 2006, nominal ballistic coefficient was extrapolated based on knowledge of the mass of CHAMP (Ref. 53). GRACE has a nominal ballistic coefficient of 0.00687 m^2/kg (Ref. 71). This number remains the same as no orbit raising maneuvers are performed.

Atmospheric density is examined in light of different parameters. These parameters are baseline atmospheric density model used, density correlated half-life, ballistic coefficient correlated half-life, solar activity level, and geomagnetic activity level.

2.6.1 Varying Baseline Density Model

Five different baseline atmospheric density models are used by ODTK to estimate density. These are the previously mentioned Jacchia 1971, CIRA 1972, Jacchia-Roberts, MSISE 1990, and NRLMSISE 2000 atmospheric models. Further discussion about these is found in Section 1.5. Seeking the best atmospheric density model for given situations is a major goal of this research, and is begun in References 53 and 54.

2.6.2 Varying Density and Ballistic Coefficient Correlated Half-Lives

The ballistic coefficient and density exponential Gauss-Markov process half-lives are varied by orders of magnitude. Examined in this research are half-lives of 1.8 minutes, 18 minutes, and 180 minutes. All nine possible combinations of these values for both density and ballistic coefficient half-lives are used for each baseline atmospheric density model, resulting in forty-five total sets of results for each time period. In Reference 53, Hiatt studied the results of using Gauss-Markov process half-lives of 1,800 minutes, 18,000 minutes, and 180,000 minutes and determined that these higher values always produced worse results. Consequently, this work only examines the three half-life values mentioned.

The following tables contain all the dates examined for CHAMP and GRACE. The broadest range possible of solar and geomagnetic activity levels was used; however, due to the time periods of GRACE data available, no periods of elevated solar activity or high solar activity are examined in this work. Table 2.1 shows the time periods examined for both CHAMP and GRACE, the initial time of the period examined in UTC time, and the corresponding A_p and $F_{10.7}$ activity levels for 2004. All time spans are 14 hours. Tables 2.2 through 2.6 display the same information for the years 2005-2009.

Table 2.1: Dates Examined for CHAMP and GRACE Satellites with Corresponding Geomagnetic and Solar Activity for 2004.

Year	Month	Day	t_i	A_p	$F_{10.7}$
2004	Nov	6	22	50	129.6
2004	Nov	7	10	140	129.6
2004	Nov	7	22	140	129.6
2004	Nov	8	10	140	140.9
2004	Nov	8	22	140	140.9
2004	Nov	9	10	161	140.9
2004	Nov	9	22	161	140.9

Table 2.2: Dates Examined for CHAMP and GRACE Satellites with Corresponding Geomagnetic and Solar Activity for 2005.

Year	Month	Day	t_i	A_p	$F_{10.7}$
2005	Jan	16	22	58	144.5
2005	Jan	17	10	84	137.5
2005	Jan	17	22	84	137.5
2005	Jan	18	10	84	132.5
2005	Jan	18	22	84	132.5
2005	Jan	19	10	60	132.5
2005	Jan	20	22	66	122.7
2005	Jan	21	10	66	113.5
2005	Mar	11	10	5	110.1
2005	Mar	11	22	5	110.1
2005	Mar	12	10	5	113.8
2005	Mar	12	22	5	113.8
2005	Mar	13	10	19	113.8
2005	Mar	13	22	19	113.8
2005	Mar	14	10	19	111.5
2005	Mar	17	10	13	101.4
2005	Mar	17	22	13	101.4
2005	Mar	18	10	11	96.5
2005	Mar	18	22	11	96.5
2005	Apr	4	22	50	88.3
2005	Apr	5	10	50	88.3
2005	May	7	22	91	101.3
2005	May	8	10	91	110.0
2005	May	8	22	91	110.0
2005	May	9	10	10	119.2
2005	May	9	22	10	119.2
2005	May	10	10	12	125.3
2005	May	10	22	12	125.3
2005	May	11	10	14	125.3
2005	May	11	22	14	125.3
2005	May	12	10	21	125.9
2005	May	12	22	21	125.9

Year	Month	Day	t_i	A_p	$F_{10.7}$
2005	May	13	10	21	125.9
2005	May	13	22	21	125.9
2005	May	15	10	87	103.0
2005	May	29	22	90	94.9
2005	May	30	10	90	96.3
2005	Jun	11	22	54	108.0
2005	Jun	12	10	54	103.0
2005	Jun	22	22	50	79.5
2005	Jun	23	10	50	77.5
2005	Jul	9	22	57	106.6
2005	Jul	10	10	57	101.8
2005	Aug	23	22	102	106.9
2005	Aug	24	10	102	98.6
2005	Sep	10	22	101	116.0
2005	Sep	11	10	101	118.0
2005	Sep	11	22	101	118.0
2005	Sep	12	10	75	118.0
2005	Sep	14	22	52	119.4
2005	Sep	15	10	52	119.4
2005	Oct	23	10	4	74.2
2005	Oct	23	22	4	74.2
2005	Oct	24	10	21	73.4
2005	Oct	24	22	21	73.4
2005	Oct	25	10	21	73.0
2005	Oct	25	22	21	73.0
2005	Oct	26	10	11	72.0
2005	Oct	26	22	11	72.0
2005	Oct	27	10	8	73.1
2005	Oct	27	22	8	73.1
2005	Oct	28	10	5	74.1
2005	Oct	28	22	5	74.1
2005	Oct	29	10	5	75.6

Table 2.3: Dates Examined for CHAMP and GRACE Satellites with Corresponding Geomagnetic and Solar Activity for 2006.

Year	Month	Day	t_i	A_p	$F_{10.7}$
2006	Aug	1	22	12	72.8
2006	Aug	2	10	9	72.1
2006	Aug	2	22	9	72.1
2006	Aug	3	10	5	71.3
2006	Aug	3	22	5	71.3
2006	Dec	22	10	18	73.2
2006	Dec	22	22	18	73.2
2006	Dec	23	10	16	73.5
2006	Dec	23	22	16	73.5
2006	Dec	24	10	12	76.4

Table 2.4: Dates Examined for CHAMP and GRACE Satellites with Corresponding Geomagnetic and Solar Activity for 2007.

Year	Month	Day	t_i	A_p	$F_{10.7}$
2007	Mar	8	10	4	72.5
2007	Mar	8	22	4	72.5
2007	Mar	9	22	4	71.6
2007	May	11	10	2	71.5
2007	May	11	22	2	71.5
2007	May	12	22	2	73.5
2007	Jul	24	10	2	68.6
2007	Jul	24	22	2	68.6
2007	Jul	25	10	9	68.6
2007	Jul	25	22	9	68.6
2007	Jul	26	10	9	68.7
2007	Jul	26	22	9	68.7
2007	Jul	27	10	7	69.9
2007	Jul	27	22	7	69.9

Table 2.5: Dates Examined for CHAMP and GRACE Satellites with Corresponding Geomagnetic and Solar Activity for 2008.

Year	Month	Day	t_i	A_p	$F_{10.7}$
2008	Feb	1	10	19	71.8
2008	Feb	1	22	19	71.8
2008	Feb	2	10	19	71.8
2008	Feb	2	22	19	71.8
2008	Feb	3	10	17	71.3
2008	Feb	3	22	17	71.3
2008	Feb	4	10	8	71.3
2008	Feb	4	22	8	71.3
2008	Mar	10	10	19	70.3
2008	Mar	10	22	19	70.3
2008	Mar	11	10	15	70.2
2008	Mar	11	22	15	70.2
2008	Mar	12	10	14	69.5
2008	Mar	12	22	14	69.5
2008	Mar	13	10	16	69.9
2008	Mar	13	22	16	69.9

Table 2.6: Dates Examined for CHAMP and GRACE Satellites with Corresponding Geomagnetic and Solar Activity for 2009.

Year	Month	Day	t_i	A_p	$F_{10.7}$
2009	Feb	1	10	3	69.5
2009	Feb	1	22	3	69.5
2009	Feb	2	10	4	69.3
2009	Feb	2	22	4	69.3
2009	Feb	3	10	14	69.5
2009	Feb	3	22	14	69.5
2009	Feb	4	10	14	70.1
2009	Feb	4	22	14	70.1
2009	Jul	10	10	7	68.2
2009	Jul	10	22	7	68.2
2009	Jul	11	10	3	68.2
2009	Jul	11	22	3	68.2
2009	Jul	12	10	8	68.0
2009	Jul	12	22	8	68.0
2009	Jul	13	10	8	67.2
2009	Jul	13	22	8	67.2

2.6.3 Solar and Geomagnetic Activity Level Bins

The solar and geomagnetic activity level bins defined previously are used to sort the density results obtained through the optimal orbit determination procedure for all of the time periods studied. This allows analysis of the results produced according to differing levels of solar and geomagnetic activity. Of particular interest is the effect of increased levels of activity on the results, as higher levels cause more density variability in the upper atmosphere.

2.7 Validation of the Estimated Atmospheric Density

Densities obtained through the use of POE data as observations in the filter/smoother scheme used in ODTK are compared to the accelerometer derived densities produced by Bruinsma et al. in References 1 through 4. Both sets of results produce a density estimate every 10 seconds. Unfortunately, the time stamps for these densities are not the same. Therefore, the POE densities are linearly interpolated to the time stamps found in the accelerometer derived density files. This is due to the fact that the accelerometer derived densities are taken as truth, so the POE derived densities are interpolated instead. The POE densities are also compared to densities produced by the HASDM model previously discussed (Ref. 5).

2.8 Cross Correlation

The cross correlation coefficient is a number between -1 and 1 which indicates the degree to which two series of numbers correlate, and is a measure of precision. A cross correlation coefficient of 1 indicates a perfect correlation, -1 indicates a perfect

negative correlation, and 0 indicates no correlation at all. In this case, the cross correlation coefficient is calculated for two series of densities which are each a function of time. Reference 72 provides the method for determining cross correlation of two series of time-varying density values. The cross correlation coefficient, *CC*, for time-varying data sets *X* and *Y*, with means denoted by $\overline{X}$ and $\overline{Y}$, and a given delay, *D*, is given by the equation:

$$CC(D) = \frac{\sum[(X_i - \overline{X})(Y_{i-d} - \overline{Y})]}{\sqrt{\sum(X_i - \overline{X})^2}\sqrt{\sum(Y_{i-d} - \overline{Y})^2}}$$

Since direct comparison of the densities obtained by various methods is desired, only the zero-delay cross correlation coefficient is examined in this work. Cross correlation is calculated for all forty-five cases of each time period to determine the best combination of baseline atmospheric density model, density correlated half-life, and ballistic coefficient correlated half-life.

2.9 Root Mean Square Values

Another measure used to determine the best combination of these factors is the Root Mean Square (RMS) technique. The same data sets can be examined to find the average difference between one data set $\overline{X}$, and another data set $\overline{Y}$, with *n* timestamps from the following equation:

$$RMS = \sum_{i=1}^{n}\sqrt{\frac{(X_i - Y)^2}{n}}$$

RMS values in this research are reported in units of the quantity in question, atmospheric density. Therefore, RMS values will have units of 10^{-12} kg/m^3. RMS

values are used in conjunction with cross correlation values to determine which inputs produce results closest to the assumed "truth" densities obtained from the accelerometers.

3 VARYING SELECT ORBIT DETERMINATION PARAMETERS FOR CHAMP AND GRACE SATELLITES

Varying certain parameters in the orbit determination process affects the results produced. The overall effects of varying the baseline atmospheric density model and the density and ballistic coefficient correlated half-lives are examined in this chapter, as well as examining results binned according to solar and geomagnetic activity levels. The baseline atmospheric density model is used to create density values at each step in the orbit determination. These values are then updated using corrections generated though the orbit determination process. Cross Correlation (CC) and Root Mean Square (RMS) values are calculated for zero-delay for every combination of baseline atmospheric density model and all three values of density and ballistic coefficient correlated half-lives. Cross correlation of densities with the HASDM model and the Jacchia 1971 model are also computed. HASDM uses CHAMP in its calibration, and the accelerometer derived densities use HASDM. Biases may exist due to nominal ballistic coefficient estimate errors. Cross correlation is a more effective measure of atmospheric density variations.

3.1 Overall Averages

CC and RMS are averaged over all solution sets between 2004 and 2007 are examined and presented in this section. Data from the extended solar minimum of 2008-2009 will be examined in the next chapter. Time periods which possess atypically poor results are examined separately in Chapter 5.

Table 3.1: Zero Delay Cross Correlation Coefficients Time Averaged over all Solution Periods for CHAMP. *The columns represent the baseline model used in calculating POE derived densities. Correlation with HASDM and the Jacchia 1971 empirical model are included. Yellow (light gray) highlighting indicates the best value for the baseline model. Orange (darker gray) indicates the best value of all possible combinations.*

		A_p Avg	$F_{10.7}$ Avg	HASDM	Jacchia 1971
		43.3	101.8	0.867	0.813
BC-Density Half-Lives	CIRA 1972	Jacchia 1971	Jacchia-Roberts	MSISE 1990	NRLMSISE 2000
1.8-1.8	0.872	0.871	0.870	0.845	0.846
18-1.8	0.863	0.862	0.862	0.842	0.842
180-1.8	0.854	0.853	0.853	0.838	0.839
1.8-18	0.883	0.883	0.883	0.852	0.855
18-18	0.879	0.878	0.878	0.849	0.851
180-18	0.867	0.867	0.867	0.841	0.844
1.8-180	0.880	0.880	0.880	0.852	0.852
18-180	0.872	0.872	0.872	0.845	0.845
180-180	0.854	0.854	0.854	0.833	0.833

Table 3.1 displays the cross correlation coefficients for the CHAMP satellite obtained for the POE estimated densities with the accelerometer derived densities for all possible combinations of baseline atmospheric density model and ballistic coefficient and density half-lives averaged over all the time periods examined. The Jacchia family of atmospheric models, namely CIRA 1972, Jacchia 1971, and Jacchia-Roberts, all exhibit results which differ very little. Similarly, the MSISE 1990 and NRLMSISE 2000 models have similar results. This is expected as the Jacchia-based models stem from a common previous model, and the MSIS models are also based on an earlier model from the same heritage. This similarity between two sets of atmospheric models will be seen for all levels of solar and geomagnetic activity as presented later in this chapter.

Another clear trend is the higher correlations obtained from using a Jacchia-based atmospheric model as the baseline versus an MSIS-based model. A ballistic coefficient correlated half-life of 1.8 minutes and a density correlated half-life of 18 minutes yield the

best correlation for all baseline atmospheric models. CIRA 1972 produces the best correlation; however, Jacchia 1971 and Jacchia-Roberts produce nearly identical results to CIRA 1972.

The correlation of the Jacchia 1971 empirical model is lower than any of the correlations produced by the various combinations of POE estimated density. This result is expected as these densities possess corrections which should improve the correlation. HASDM outperforms the densities estimated using both the MSISE 1990 model and the NRLMSISE 2000 model, and produces similar correlation to those of the Jacchia family of models. However, the best correlation from the POE estimated density is superior to that of HASDM.

Table 3.2: Root Mean Square Values Time Averaged over all Solution Periods for CHAMP. *The columns represent the baseline model used in calculating POE derived densities. RMS for HASDM and the Jacchia 1971 empirical model are included. Yellow (light gray) highlighting indicates the best value for the baseline model. Orange (darker gray) indicates the best value of all possible combinations. Units of RMS are kg/m^3*10^{-12}.*

		A_p Avg	$F_{10.7}$ Avg	HASDM	Jacchia 1971
		43.3	101.8	0.647	1.074
BC-Density Half-Lives	CIRA 1972	Jacchia 1971	Jacchia-Roberts	MSISE 1990	NRLMSISE 2000
1.8-1.8	0.678	0.674	0.675	0.948	0.949
18-1.8	0.782	0.771	0.773	0.960	0.963
180-1.8	0.900	0.895	0.897	1.003	1.002
1.8-18	0.623	0.628	0.627	0.957	0.952
18-18	0.654	0.648	0.649	0.955	0.953
180-18	0.782	0.764	0.768	1.036	1.033
1.8-180	0.625	0.632	0.630	0.948	0.953
18-180	0.657	0.653	0.654	0.966	0.972
180-180	0.801	0.770	0.777	1.144	1.145

Table 3.2 displays the RMS values comparing the POE derived densities for CHAMP to the accelerometer derived densities averaged over all solution periods. Units are in 10^{-12} kg/m^3. A lower RMS value indicates better agreement in magnitude than a higher

value. Again, the same general trends are seen. RMS results are again superior for the best POE estimated density combinations to both HASDM and the Jacchia 1971 model. For RMS, a density correlated half-life of 180 minutes is superior for the MSISE 1990 and NRLMSISE 2000 baseline models.

Table 3.3: Zero Delay Cross Correlation Coefficients Time Averaged over all Solution Periods for GRACE-A. *The columns represent the baseline model used in calculating POE derived densities. Correlation with HASDM and the Jacchia 1971 empirical model are included. Yellow (light gray) highlighting indicates the best value for the baseline model. Orange (darker gray) indicates the best value of all possible combinations.*

		A_p Avg	$F_{10.7}$ Avg	HASDM	Jacchia 1971
		43.3	101.5	0.841	0.790
BC-Density Half-Lives	CIRA 1972	Jacchia 1971	Jacchia-Roberts	MSISE 1990	NRLMSISE 2000
1.8-1.8	0.819	0.820	0.818	0.802	0.800
18-1.8	0.824	0.824	0.823	0.805	0.804
180-1.8	0.821	0.821	0.820	0.808	0.807
1.8-18	0.834	0.834	0.832	0.809	0.809
18-18	0.833	0.834	0.832	0.809	0.808
180-18	0.832	0.832	0.831	0.811	0.810
1.8-180	0.850	0.850	0.849	0.825	0.823
18-180	0.846	0.846	0.846	0.821	0.820
180-180	0.830	0.830	0.830	0.810	0.809

Table 3.3 shows the zero delay cross correlation coefficients averaged over all time periods for GRACE-A. For GRACE, a density correlated half-life of 180 minutes and a ballistic coefficient of 1.8 minutes give the best correlations for all baseline atmospheric models. Once again, the Jacchia-based models slightly outperform models from the MSIS family. In this case, Jacchia 1971 as baseline yields the best results, though nearly identical to those produced by CIRA 1972 and Jacchia-Roberts. As with CHAMP, the POE estimated densities outperform the Jacchia 1971 model in all cases, and outperform HASDM for most cases for both CC and RMS. In this case, using Jacchia-Roberts as baseline produces slightly better RMS results than the other Jacchia models. Table 3.4 below displays RMS results for

GRACE averaged over all time periods. Note that the RMS values are much lower than the RMS values for CHAMP. This results from lower densities encountered by the GRACE satellites due to their higher altitude. The same trends are seen here as with CC for GRACE.

Table 3.4: Root Mean Square Values Time Averaged over all Solution Periods for GRACE-A. *The columns represent the baseline model used in calculating POE derived densities. RMS for HASDM and the Jacchia 1971 empirical model are included. Yellow (light gray) highlighting indicates the best value for the baseline model. Orange (darker gray) indicates the best value of all possible combinations. Units of RMS are kg/m^3*10^{-12}.*

		A_p Avg	$F_{10.7}$ Avg	HASDM	Jacchia 1971
		43.3	101.8	0.133	0.248
BC-Density Half-Lives	CIRA 1972	Jacchia 1971	Jacchia-Roberts	MSISE 1990	NRLMSISE 2000
1.8-1.8	0.145	0.145	0.143	0.235	0.237
18-1.8	0.161	0.161	0.159	0.233	0.235
180-1.8	0.195	0.196	0.195	0.239	0.242
1.8-18	0.127	0.127	0.125	0.232	0.234
18-18	0.132	0.133	0.130	0.233	0.235
180-18	0.166	0.166	0.164	0.255	0.257
1.8-180	0.125	0.125	0.123	0.229	0.231
18-180	0.131	0.131	0.128	0.233	0.235
180-180	0.174	0.174	0.171	0.280	0.283

3.2 Comparison of Results Binned According to Solar and Geomagnetic Activity Levels

In the previous section, results are considered from the perspective of an overall average of all time periods examined. To better understand the effects of varying levels of solar and geomagnetic activity, results are divided into bins in this section. The classifications for these bins were defined earlier, and are repeated here:

- Solar Activity Level Bins (units of SFU)
  - Low Solar Flux for $F_{10.7} < 75$
  - Moderate Solar Flux for $75 \leq F_{10.7} < 150$
  - Elevated Solar Flux for $150 \leq F_{10.7} < 190$

- High Solar Flux for $F_{10.7} \geq 75$

- Geomagnetic Activity Level Bins (units of gamma)
  - Quiet Geomagnetic for $A_p \leq 10$
  - Moderate Geomagnetic for $10 < A_p < 50$
  - Active Geomagnetic for $A_p \geq 50$

Once again, results are examined with varying baseline atmospheric density model, ballistic coefficient correlated half-life, and density correlated half-life. Cross correlation and RMS are calculated for the POE estimated densities versus the accelerometer derived densities. These are then sorted into the corresponding solar and geomagnetic activity level bins and averaged for both CHAMP and GRACE-A. Finally, days which are representative of certain bins are examined in further detail.

3.3 Effects of Solar Activity on Results

Identification of the best combinations of baseline atmospheric density model and density and ballistic coefficient half-lives as a function of solar activity is presented in this section. Solar activity is separated into four bins and both CHAMP and GRACE-A are examined.

3.3.1 Low Solar Activity Bin

During periods of low solar activity, atmospheric density variations are generally small and there are few large-scale changes. Atmospheric density is easiest to model when solar activity is low. Extremely low solar activity is also difficult to model, however. Table 3.5 shows cross correlation results for CHAMP during periods of low solar activity, and Table 3.6 shows RMS results for CHAMP during periods of low solar activity. For this set of data, correlations are very good. The Jacchia models as baseline produce better results than

HASDM for the best cases, and are again superior to the MSIS models. Using MSISE 1990 and NRLMSISE 2000 as baseline models with corrections produces better results than the Jacchia 1971 empirical model for the majority of cases, and better than HASDM for the best cases. The best combination of ballistic coefficient correlated half-life and density correlated half-life are 1.8 minutes and 180 minutes, respectively. The best baseline atmospheric model is CIRA 1972. The same trends are seen with RMS for CHAMP in the low solar activity bin.

Table 3.5: Zero Delay Cross Correlation Coefficients Time Averaged over Low Solar Activity Periods for CHAMP. *The columns represent the baseline model used in calculating POE derived densities. Correlation with HASDM and the Jacchia 1971 empirical model are included. Yellow (light gray) highlighting indicates the best value for the baseline model. Orange (darker gray) indicates the best value of all possible combinations.*

		A_p Avg	$F_{10.7}$ Avg	HASDM	Jacchia 1971
		7.8	71.2	0.922	0.915
BC-Density Half-Lives	CIRA 1972	Jacchia 1971	Jacchia-Roberts	MSISE 1990	NRLMSISE 2000
1.8-1.8	0.913	0.911	0.910	0.907	0.908
18-1.8	0.921	0.921	0.921	0.915	0.915
180-1.8	0.921	0.921	0.921	0.917	0.917
1.8-18	0.921	0.920	0.920	0.914	0.915
18-18	0.922	0.921	0.921	0.914	0.915
180-18	0.917	0.917	0.917	0.910	0.911
1.8-180	0.928	0.928	0.928	0.920	0.921
18-180	0.926	0.926	0.926	0.917	0.919
180-180	0.908	0.907	0.907	0.901	0.903

Table 3.6: Root Mean Square Values Time Averaged over Low Solar Activity Periods for CHAMP. *The columns represent the baseline model used in calculating POE derived densities. RMS for HASDM and the Jacchia 1971 empirical model are included. Yellow (light gray) highlighting indicates the best value for the baseline model. Orange (darker gray) indicates the best value of all possible combinations. Units of RMS are* kg/m^3*10^{-12}.

		A_p Avg	$F_{10.7}$ Avg	HASDM	Jacchia 1971
		7.8	71.2	0.267	0.602
BC-Density Half-Lives	CIRA 1972	Jacchia 1971	Jacchia-Roberts	MSISE 1990	NRLMSISE 2000
1.8-1.8	0.336	0.323	0.325	0.370	0.370
18-1.8	0.421	0.403	0.404	0.452	0.452
180-1.8	0.521	0.513	0.513	0.540	0.539
1.8-18	0.284	0.278	0.280	0.320	0.317
18-18	0.305	0.288	0.290	0.348	0.347
180-18	0.423	0.401	0.402	0.469	0.468
1.8-180	0.264	0.263	0.264	0.298	0.295
18-180	0.276	0.265	0.267	0.317	0.315
180-180	0.398	0.367	0.369	0.450	0.451

Table 3.7 displays correlations for GRACE-A during periods of low solar activity, and Table 3.8 displays the corresponding RMS values. Once again, the Jacchia-based models were superior to the MSIS-based models when used as baseline, with extremely close results within each set. The best cross correlation and RMS values result from the Jacchia 1971 model as baseline, 1.8 minutes for ballistic coefficient half-life, and 180 minutes for density half-life.

Table 3.7: Zero Delay Cross Correlation Coefficients Time Averaged over Low Solar Activity Periods for GRACE-A. *The columns represent the baseline model used in calculating POE derived densities. Correlation with HASDM and the Jacchia 1971 empirical model are included. Yellow (light gray) highlighting indicates the best value for the baseline model. Orange (darker gray) indicates the best value of all possible combinations.*

		A_p Avg	$F_{10.7}$ Avg	HASDM	Jacchia 1971
		7.8	71.2	0.768	0.769
BC-Density Half-Lives	CIRA 1972	Jacchia 1971	Jacchia-Roberts	MSISE 1990	NRLMSISE 2000
1.8-1.8	0.730	0.731	0.727	0.723	0.723
18-1.8	0.753	0.753	0.751	0.742	0.744
180-1.8	0.769	0.769	0.769	0.763	0.764
1.8-18	0.720	0.721	0.716	0.706	0.712
18-18	0.725	0.727	0.722	0.712	0.717
180-18	0.748	0.749	0.746	0.740	0.743
1.8-180	0.766	0.766	0.765	0.751	0.755
18-180	0.764	0.764	0.762	0.749	0.753
180-180	0.755	0.755	0.753	0.744	0.748

Table 3.8: Root Mean Square Values Time Averaged over Low Solar Activity Periods for GRACE-A. *The columns represent the baseline model used in calculating POE derived densities. RMS for HASDM and the Jacchia 1971 empirical model are included. Yellow (light gray) highlighting indicates the best value for the baseline model. Orange (darker gray) indicates the best value of all possible combinations. Units of RMS are* $kg/m^3 * 10^{-12}$.

		A_p Avg	$F_{10.7}$ Avg	HASDM	Jacchia 1971
		7.8	71.2	0.030	0.070
BC-Density Half-Lives	CIRA 1972	Jacchia 1971	Jacchia-Roberts	MSISE 1990	NRLMSISE 2000
1.8-1.8	0.044	0.044	0.043	0.047	0.047
18-1.8	0.048	0.048	0.048	0.051	0.051
180-1.8	0.060	0.060	0.060	0.062	0.062
1.8-18	0.034	0.034	0.033	0.038	0.037
18-18	0.035	0.036	0.035	0.039	0.039
180-18	0.046	0.046	0.045	0.049	0.049
1.8-180	0.030	0.030	0.029	0.034	0.033
18-180	0.031	0.031	0.030	0.035	0.034
180-180	0.043	0.043	0.042	0.046	0.046

3.3.2 Moderate Solar Activity Bin

The majority of days examined fall in the moderate solar activity bin. Table 3.9 shows cross correlation values for CHAMP during periods of moderate solar activity, and Table 3.10 shows RMS values for these periods. These tables show that a ballistic coefficient correlated half-life of 1.8 minutes is again optimal. However, a density correlated half-life of 18 minutes is superior to 180 minutes during moderate solar activity for CHAMP. The best combinations of POE derived densities outperform HASDM, and nearly all combinations outperform the Jacchia 1971 empirical model. The best results use CIRA 1972 as the baseline model, though correlations are nearly identical to Jacchia 1971 and Jacchia-Roberts.

Table 3.11 and Table 3.12 are the moderate solar activity CC and RMS averages, respectively, for the GRACE-A satellite. Here again the best combination is 1.8 minutes for ballistic coefficient half-life and 180 minutes for density half-life. Jacchia family models produce nearly identical results, and are superior to MSIS family models yet again.

Table 3.9: Zero Delay Cross Correlation Coefficients Time Averaged over Moderate Solar Activity Periods for CHAMP. *The columns represent the baseline model used in calculating POE derived densities. Correlation with HASDM and the Jacchia 1971 empirical model are included. Yellow (light gray) highlighting indicates the best value for the baseline model. Orange (darker gray) indicates the best value of all possible combinations.*

		A_p Avg	$F_{10.7}$ Avg	HASDM	Jacchia 1971
		57.8	114.3	0.845	0.771
BC-Density Half-Lives	CIRA 1972	Jacchia 1971	Jacchia-Roberts	MSISE 1990	NRLMSISE 2000
1.8-1.8	0.855	0.854	0.854	0.820	0.821
18-1.8	0.839	0.838	0.838	0.812	0.812
180-1.8	0.827	0.826	0.826	0.806	0.807
1.8-18	0.868	0.868	0.867	0.827	0.830
18-18	0.861	0.861	0.861	0.823	0.825
180-18	0.847	0.846	0.846	0.813	0.816
1.8-180	0.860	0.860	0.860	0.824	0.823
18-180	0.850	0.850	0.850	0.816	0.815
180-180	0.832	0.832	0.832	0.805	0.805

Table 3.10: Root Mean Square Values Time Averaged over Moderate Solar Activity Periods for CHAMP. *The columns represent the baseline model used in calculating POE derived densities. RMS for HASDM and the Jacchia 1971 empirical model are included. Yellow (light gray) highlighting indicates the best value for the baseline model. Orange (darker gray) indicates the best value of all possible combinations. Units of RMS are kg/m^3*10^{-12}.*

		A_p Avg	$F_{10.7}$ Avg	HASDM	Jacchia 1971
		57.8	114.3	0.802	1.267
BC-Density Half-Lives	CIRA 1972	Jacchia 1971	Jacchia-Roberts	MSISE 1990	NRLMSISE 2000
1.8-1.8	0.818	0.818	0.818	1.185	1.185
18-1.8	0.930	0.921	0.924	1.167	1.172
180-1.8	1.055	1.051	1.053	1.192	1.192
1.8-18	0.761	0.772	0.769	1.218	1.211
18-18	0.796	0.795	0.796	1.204	1.200
180-18	0.929	0.912	0.918	1.268	1.264
1.8-180	0.772	0.783	0.780	1.214	1.222
18-180	0.813	0.811	0.812	1.231	1.240
180-180	0.966	0.934	0.943	1.427	1.429

Table 3.11: Zero Delay Cross Correlation Coefficients Time Averaged over Moderate Solar Activity Periods for GRACE-A. *The columns represent the baseline model used in calculating POE derived densities. Correlation with HASDM and the Jacchia 1971 empirical model are included. Yellow (light gray) highlighting indicates the best value for the baseline model. Orange (darker gray) indicates the best value of all possible combinations.*

		A_p Avg	$F_{10.7}$ Avg	HASDM	Jacchia 1971
		57.8	114.3	0.870	0.798
BC-Density Half-Lives	CIRA 1972	Jacchia 1971	Jacchia-Roberts	MSISE 1990	NRLMSISE 2000
1.8-1.8	0.855	0.855	0.854	0.834	0.831
18-1.8	0.852	0.852	0.852	0.831	0.828
180-1.8	0.841	0.841	0.841	0.826	0.824
1.8-18	0.879	0.879	0.879	0.850	0.847
18-18	0.876	0.876	0.876	0.848	0.845
180-18	0.865	0.865	0.865	0.840	0.837
1.8-180	0.883	0.883	0.883	0.854	0.850
18-180	0.879	0.879	0.879	0.850	0.846
180-180	0.860	0.860	0.860	0.836	0.833

Table 3.12: Root Mean Square Values Time Averaged over Moderate Solar Activity Periods for GRACE-A. *The columns represent the baseline model used in calculating POE derived densities. RMS for HASDM and the Jacchia 1971 empirical model are included. Yellow (light gray) highlighting indicates the best value for the baseline model. Orange (darker gray) indicates the best value of all possible combinations. Units of RMS are* kg/m^3*10^{-12}.

		A_p Avg	$F_{10.7}$ Avg	HASDM	Jacchia 1971
		57.8	114.3	0.173	0.318
BC-Density Half-Lives	CIRA 1972	Jacchia 1971	Jacchia-Roberts	MSISE 1990	NRLMSISE 2000
1.8-1.8	0.184	0.185	0.182	0.310	0.312
18-1.8	0.205	0.205	0.203	0.306	0.309
180-1.8	0.249	0.249	0.248	0.310	0.313
1.8-18	0.164	0.164	0.161	0.310	0.312
18-18	0.171	0.171	0.168	0.310	0.312
180-18	0.214	0.214	0.212	0.336	0.340
1.8-180	0.163	0.163	0.160	0.307	0.310
18-180	0.170	0.171	0.167	0.311	0.315
180-180	0.226	0.226	0.223	0.373	0.377

3.3.3 Elevated and High Solar Activity Bins

Unfortunately, due to an extended solar minimum period which produced very low levels of solar activity in 2008 and 2009, no data is available for the GRACE satellites which fall into the elevated or high solar activity level bins. Elevated and high solar activity level data is available for CHAMP. However, since results are being compared between the same time periods for CHAMP and GRACE, this data is not used in this work. The best results for CHAMP during this elevated solar activity periods were produced from using a Jacchia family baseline model with a half-life combination of 1.8 minutes for ballistic coefficient and 18 minutes for density, respectively. During periods of high activity, the same combination of half-lives producing the best results held true.

3.3.4 Summary of the Solar Activity Bins

Examining the cross correlation coefficients and root mean square values obtained through the comparison of POE derived densities and accelerometer derived densities, the effects of the Sun's output are evident. For CHAMP, as solar activity increases, CC values decrease and RMS values increase. For GRACE, RMS values worsen also as solar activity increases. However, cross correlation coefficients actually improve for GRACE as solar activity moves from low to moderate. This may be due to the very low densities encountered during low solar activity for GRACE, causing more difficulty in modeling. For GRACE, a ballistic coefficient correlated half-life of 1.8 minutes and a density correlated half-life of 180 minutes produce the best results regardless of solar activity level. For CHAMP, a ballistic coefficient correlated half-life of 1.8 minutes and a density correlated half-life of 180 minutes produce the best results at low solar activity levels, while at moderate solar activity level a density correlated half-life of 18 minutes is superior. For both CHAMP and GRACE at both low and moderate solar activity levels, a Jacchia model as baseline produces the best results.

3.4 Effect of Geomagnetic Activity on Results

Identification of the best combinations of baseline atmospheric density model and density and ballistic coefficient half-lives as a function of geomagnetic activity is presented in this section. Geomagnetic activity is separated into three bins and both CHAMP and GRACE-A are examined.

3.4.1 Quiet Geomagnetic Activity Bin

Geomagnetic activity has a profound impact on upper atmospheric density as well. Historically, the majority of days fall within the quiet geomagnetic activity bin. Theoretically, quiet geomagnetic activity should produce less density variability.

Accordingly, density should be easier to model during these periods. Table 3.13 shows the cross correlation values obtained for the CHAMP satellite during periods of quiet geomagnetic activity, and Table 3.14 contains RMS values for the same periods. For CHAMP, CIRA 1972 as baseline model, as well as ballistic coefficient and density half-lives of 1.8 and 180 minutes, respectively, produces the best results.

Table 3.13: Zero Delay Cross Correlation Coefficients Time Averaged over Quiet Geomagnetic Activity Periods for CHAMP. *The columns represent the baseline model used in calculating POE derived densities. Correlation with HASDM and the Jacchia 1971 empirical model are included. Yellow (light gray) highlighting indicates the best value for the baseline model. Orange (darker gray) indicates the best value of all possible combinations.*

		A_p Avg	$F_{10.7}$ Avg	HASDM	Jacchia 1971
		5.8	81.6	0.931	0.921
BC-Density Half-Lives	CIRA 1972	Jacchia 1971	Jacchia-Roberts	MSISE 1990	NRLMSISE 2000
1.8-1.8	0.925	0.924	0.923	0.916	0.918
18-1.8	0.929	0.930	0.929	0.922	0.923
180-1.8	0.928	0.928	0.928	0.923	0.923
1.8-18	0.931	0.930	0.930	0.920	0.922
18-18	0.931	0.931	0.930	0.920	0.922
180-18	0.924	0.925	0.924	0.915	0.917
1.8-180	0.936	0.936	0.936	0.926	0.927
18-180	0.933	0.934	0.933	0.923	0.924
180-180	0.916	0.916	0.916	0.908	0.910

Table 3.14: Root Mean Square Values Time Averaged over Quiet Geomagnetic Activity Periods for CHAMP. *The columns represent the baseline model used in calculating POE derived densities. RMS for HASDM and the Jacchia 1971 empirical model are included. Yellow (light gray) highlighting indicates the best value for the baseline model. Orange (darker gray) indicates the best value of all possible combinations. Units of RMS are* kg/m^3*10^{-12}.

		A_p Avg	$F_{10.7}$ Avg	HASDM	Jacchia 1971
		5.8	81.6	0.274	0.499
BC-Density Half-Lives	CIRA 1972	Jacchia 1971	Jacchia-Roberts	MSISE 1990	NRLMSISE 2000
1.8-1.8	0.316	0.316	0.315	0.350	0.348
18-1.8	0.372	0.368	0.366	0.394	0.395
180-1.8	0.436	0.434	0.432	0.449	0.449
1.8-18	0.285	0.290	0.289	0.327	0.319
18-18	0.297	0.296	0.294	0.339	0.335
180-18	0.371	0.362	0.360	0.413	0.411
1.8-180	0.272	0.278	0.278	0.314	0.306
18-180	0.280	0.280	0.279	0.326	0.321
180-180	0.368	0.351	0.350	0.428	0.425

Table 3.15 and Table 3.16 contain the same information for GRACE-A during periods of quiet geomagnetic activity. For GRACE during these periods, the combination of 1.8 minutes for BC half-life and 180 minutes for density half-life produces the best results for RMS. For cross correlation, however, a combination of 180 minutes and 1.8 minutes for BC and density correlated half-lives is best, which is a departure from the results seen thus far. Important to note is the fact that the cross correlations with a 180 minute ballistic coefficient half-life and 1.8 minute density half-life differ very little from the usual best combination of 1.8 and 180 minutes. Again, a Jacchia family model as baseline is best for GRACE for quiet geomagnetic activity periods.

Table 3.15: Zero Delay Cross Correlation Coefficients Time Averaged over Quiet Geomagnetic Activity Periods for GRACE-A. *The columns represent the baseline model used in calculating POE derived densities. Correlation with HASDM and the Jacchia 1971 empirical model are included. Yellow (light gray) highlighting indicates the best value for the baseline model. Orange (darker gray) indicates the best value of all possible combinations.*

		A_p Avg	$F_{10.7}$ Avg	HASDM	Jacchia 1971
		5.8	81.6	0.799	0.801
BC-Density Half-Lives	CIRA 1972	Jacchia 1971	Jacchia-Roberts	MSISE 1990	NRLMSISE 2000
1.8-1.8	0.793	0.794	0.792	0.774	0.780
18-1.8	0.798	0.798	0.797	0.783	0.788
180-1.8	0.804	0.805	0.804	0.798	0.800
1.8-18	0.776	0.778	0.773	0.756	0.764
18-18	0.779	0.781	0.777	0.760	0.768
180-18	0.794	0.794	0.792	0.782	0.786
1.8-180	0.803	0.803	0.802	0.788	0.792
18-180	0.801	0.801	0.800	0.787	0.791
180-180	0.795	0.795	0.794	0.784	0.788

Table 3.16: Root Mean Square Values Time Averaged over Quiet Geomagnetic Activity Periods for GRACE-A. *The columns represent the baseline model used in calculating POE derived densities. RMS for HASDM and the Jacchia 1971 empirical model are included. Yellow (light gray) highlighting indicates the best value for the baseline model. Orange (darker gray) indicates the best value of all possible combinations. Units of RMS are* kg/m^3*10^{-12}.

		A_p Avg	$F_{10.7}$ Avg	HASDM	Jacchia 1971
		5.8	81.6	0.041	0.055
BC-Density Half-Lives	CIRA 1972	Jacchia 1971	Jacchia-Roberts	MSISE 1990	NRLMSISE 2000
1.8-1.8	0.046	0.047	0.045	0.050	0.049
18-1.8	0.047	0.047	0.046	0.050	0.050
180-1.8	0.051	0.052	0.051	0.054	0.053
1.8-18	0.041	0.041	0.039	0.046	0.045
18-18	0.041	0.042	0.040	0.046	0.046
180-18	0.051	0.051	0.050	0.054	0.054
1.8-180	0.038	0.039	0.037	0.043	0.042
18-180	0.039	0.040	0.038	0.044	0.043
180-180	0.055	0.056	0.054	0.059	0.058

3.4.2 Moderate Geomagnetic Activity Bin

A large number of days fall into the moderate geomagnetic activity level bin as well. Once again, CC and RMS are examined for days with moderate geomagnetic activity for both

CHAMP and GRACE-A. Table 3.17 contains CC values for CHAMP, and Table 3.18 contains RMS values. The same combination of CIRA 1972, BC half-life of 1.8 minutes and density half-life of 180 minutes produce the best results. Table 3.19 and Table 3.20 contain the same information for GRACE. HASDM correlations are superior to the best results from the POE method for GRACE during these periods. The same half-lives produce the best results, with a best baseline atmospheric density model of Jacchia 1971 for CC and Jacchia-Roberts for RMS.

Table 3.17: Zero Delay Cross Correlation Coefficients Time Averaged over Moderate Geomagnetic Activity Periods for CHAMP. *The columns represent the baseline model used in calculating POE derived densities. Correlation with HASDM and the Jacchia 1971 empirical model are included. Yellow (light gray) highlighting indicates the best value for the baseline model. Orange (darker gray) indicates the best value of all possible combinations.*

		A_p Avg	$F_{10.7}$ Avg	HASDM	Jacchia 1971
		15.6	103.0	0.938	0.920
BC-Density Half-Lives	CIRA 1972	Jacchia 1971	Jacchia-Roberts	MSISE 1990	NRLMSISE 2000
1.8-1.8	0.935	0.932	0.933	0.924	0.925
18-1.8	0.936	0.935	0.935	0.926	0.926
180-1.8	0.933	0.932	0.933	0.925	0.926
1.8-18	0.940	0.939	0.940	0.926	0.928
18-18	0.939	0.937	0.938	0.925	0.927
180-18	0.930	0.930	0.930	0.917	0.919
1.8-180	0.945	0.944	0.945	0.929	0.932
18-180	0.941	0.941	0.941	0.927	0.929
180-180	0.925	0.924	0.925	0.915	0.915

Table 3.18: Root Mean Square Values Time Averaged over Moderate Geomagnetic Activity Periods for CHAMP. *The columns represent the baseline model used in calculating POE derived densities. RMS for HASDM and the Jacchia 1971 empirical model are included. Yellow (light gray) highlighting indicates the best value for the baseline model. Orange (darker gray) indicates the best value of all possible combinations. Units of RMS are* kg/m^3*10^{-12}.

		A_p Avg	$F_{10.7}$ Avg	HASDM	Jacchia 1971
		15.6	103.0	0.427	0.831
BC-Density Half-Lives	CIRA 1972	Jacchia 1971	Jacchia-Roberts	MSISE 1990	NRLMSISE 2000
1.8-1.8	0.487	0.477	0.478	0.731	0.646
18-1.8	0.588	0.567	0.573	0.739	0.693
180-1.8	0.708	0.697	0.700	0.783	0.764
1.8-18	0.436	0.438	0.434	0.741	0.629
18-18	0.467	0.452	0.454	0.741	0.650
180-18	0.609	0.580	0.588	0.838	0.773
1.8-180	0.418	0.424	0.418	0.733	0.615
18-180	0.442	0.430	0.430	0.749	0.643
180-180	0.614	0.567	0.578	0.951	0.853

Table 3.19: Zero Delay Cross Correlation Coefficients Time Averaged over Moderate Geomagnetic Activity Periods for GRACE-A. *The columns represent the baseline model used in calculating POE derived densities. Correlation with HASDM and the Jacchia 1971 empirical model are included. Yellow (light gray) highlighting indicates the best value for the baseline model. Orange (darker gray) indicates the best value of all possible combinations.*

		A_p Avg	$F_{10.7}$ Avg	HASDM	Jacchia 1971
		15.6	103.0	0.917	0.887
BC-Density Half-Lives	CIRA 1972	Jacchia 1971	Jacchia-Roberts	MSISE 1990	NRLMSISE 2000
1.8-1.8	0.864	0.864	0.861	0.869	0.861
18-1.8	0.888	0.888	0.886	0.881	0.878
180-1.8	0.898	0.898	0.897	0.889	0.888
1.8-18	0.883	0.883	0.882	0.875	0.873
18-18	0.885	0.885	0.883	0.875	0.873
180-18	0.884	0.884	0.883	0.873	0.872
1.8-180	0.912	0.912	0.912	0.893	0.896
18-180	0.910	0.910	0.909	0.890	0.892
180-180	0.887	0.887	0.886	0.872	0.872

Table 3.20: Root Mean Square Values Time Averaged over Moderate Geomagnetic Activity Periods for GRACE-A. *The columns represent the baseline model used in calculating POE derived densities. RMS for HASDM and the Jacchia 1971 empirical model are included. Yellow (light gray) highlighting indicates the best value for the baseline model. Orange (darker gray) indicates the best value of all possible combinations. Units of RMS are* kg/m^3*10^{-12}.

		A_p Avg	$F_{10.7}$ Avg	HASDM	Jacchia 1971
		15.6	103.0	0.082	0.167
BC-Density Half-Lives	CIRA 1972	Jacchia 1971	Jacchia-Roberts	MSISE 1990	NRLMSISE 2000
1.8-1.8	0.100	0.100	0.097	0.153	0.136
18-1.8	0.111	0.112	0.109	0.154	0.141
180-1.8	0.139	0.139	0.138	0.164	0.157
1.8-18	0.084	0.085	0.081	0.147	0.126
18-18	0.089	0.089	0.086	0.149	0.129
180-18	0.120	0.121	0.118	0.172	0.157
1.8-180	0.079	0.080	0.076	0.144	0.123
18-180	0.084	0.085	0.081	0.148	0.127
180-180	0.127	0.128	0.123	0.191	0.171

3.4.3 Active Geomagnetic Activity Bin

Lastly, time periods falling into the active geomagnetic bin are examined. Days in the active bin are very rare. Table 3.21 contains CC values for CHAMP during these periods, and Table 3.22 contains RMS values. Here the best combination of BC and density half-life is 1.8 minutes and 18 minutes. Note again the superiority of the Jacchia-based atmospheric models as baseline.

Table 3.21: Zero Delay Cross Correlation Coefficients Time Averaged over Active Geomagnetic Activity Periods for CHAMP. *The columns represent the baseline model used in calculating POE derived densities. Correlation with HASDM and the Jacchia 1971 empirical model are included. Yellow (light gray) highlighting indicates the best value for the baseline model. Orange (darker gray) indicates the best value of all possible combinations.*

		A_p Avg	$F_{10.7}$ Avg	HASDM	Jacchia 1971
		84.7	114.9	0.783	0.677
BC-Density Half-Lives	CIRA 1972	Jacchia 1971	Jacchia-Roberts	MSISE 1990	NRLMSISE 2000
1.8-1.8	0.799	0.799	0.798	0.751	0.751
18-1.8	0.776	0.775	0.775	0.739	0.739
180-1.8	0.758	0.757	0.757	0.730	0.732
1.8-18	0.818	0.818	0.818	0.764	0.766
18-18	0.809	0.809	0.808	0.758	0.759
180-18	0.792	0.791	0.791	0.747	0.751
1.8-180	0.804	0.805	0.804	0.757	0.754
18-180	0.791	0.791	0.791	0.746	0.743
180-180	0.772	0.771	0.771	0.734	0.734

Table 3.22: Root Mean Square Values Time Averaged over Active Geomagnetic Activity Periods for CHAMP. *The columns represent the baseline model used in calculating POE derived densities. RMS for HASDM and the Jacchia 1971 empirical model are included. Yellow (light gray) highlighting indicates the best value for the baseline model. Orange (darker gray) indicates the best value of all possible combinations. Units of RMS are* $kg/m^3 * 10^{-12}$.

		A_p Avg	$F_{10.7}$ Avg	HASDM	Jacchia 1971
		84.7	114.9	1.027	1.607
BC-Density Half-Lives	CIRA 1972	Jacchia 1971	Jacchia-Roberts	MSISE 1990	NRLMSISE 2000
1.8-1.8	1.035	1.032	1.034	1.481	1.532
18-1.8	1.173	1.162	1.167	1.472	1.505
180-1.8	1.327	1.323	1.326	1.507	1.517
1.8-18	0.961	0.968	0.968	1.512	1.568
18-18	1.004	1.001	1.004	1.499	1.548
180-18	1.162	1.144	1.150	1.575	1.607
1.8-180	0.984	0.994	0.993	1.504	1.588
18-180	1.038	1.035	1.037	1.527	1.604
180-180	1.204	1.172	1.182	1.743	1.804

For GRACE-A, Table 3.23 displays cross correlation results and Table 3.24 displays RMS results during periods of active geomagnetism. For CC results Jacchia 1971 as baseline

atmospheric model, BC half-life of 1.8 minutes and density half-life of 180 minutes produce the best results.

Table 3.23: Zero Delay Cross Correlation Coefficients Time Averaged over Active Geomagnetic Activity Periods for GRACE-A. *The columns represent the baseline model used in calculating POE derived densities. Correlation with HASDM and the Jacchia 1971 empirical model are included. Yellow (light gray) highlighting indicates the best value for the baseline model. Orange (darker gray) indicates the best value of all possible combinations.*

		A_p Avg	$F_{10.7}$ Avg	HASDM	Jacchia 1971
		84.7	114.9	0.825	0.725
BC-Density Half-Lives	CIRA 1972	Jacchia 1971	Jacchia-Roberts	MSISE 1990	NRLMSISE 2000
1.8-1.8	0.811	0.811	0.811	0.783	0.778
18-1.8	0.804	0.805	0.804	0.776	0.772
180-1.8	0.787	0.787	0.786	0.767	0.764
1.8-18	0.843	0.843	0.843	0.807	0.801
18-18	0.839	0.840	0.839	0.803	0.798
180-18	0.827	0.827	0.827	0.795	0.790
1.8-180	0.845	0.845	0.845	0.809	0.802
18-180	0.839	0.840	0.839	0.804	0.797
180-180	0.821	0.821	0.821	0.792	0.786

Table 3.24: Root Mean Square Values Time Averaged over Active Geomagnetic Activity Periods for GRACE-A. *The columns represent the baseline model used in calculating POE derived densities. RMS for HASDM and the Jacchia 1971 empirical model are included. Yellow (light gray) highlighting indicates the best value for the baseline model. Orange (darker gray) indicates the best value of all possible combinations. Units of RMS are* kg/m^3*10^{-12}.

		A_p Avg	$F_{10.7}$ Avg	HASDM	Jacchia 1971
		84.7	114.9	0.223	0.423
BC-Density Half-Lives	CIRA 1972	Jacchia 1971	Jacchia-Roberts	MSISE 1990	NRLMSISE 2000
1.8-1.8	0.237	0.236	0.235	0.406	0.420
18-1.8	0.265	0.265	0.263	0.402	0.414
180-1.8	0.324	0.324	0.324	0.407	0.417
1.8-18	0.209	0.209	0.207	0.407	0.422
18-18	0.218	0.218	0.216	0.406	0.422
180-18	0.270	0.270	0.268	0.436	0.451
1.8-180	0.209	0.209	0.207	0.403	0.421
18-180	0.219	0.219	0.216	0.408	0.426
180-180	0.280	0.280	0.278	0.480	0.498

3.4.4 Summary of the Geomagnetic Activity Bins

While increased geomagnetic activity would seem to imply a decrease in cross correlation coefficients and an increase in RMS values, that trend is not clearly seen in these results. However, some conclusions are clear. A ballistic coefficient correlated half-life of 1.8 minutes consistently produces the highest correlations and the lowest RMS values. The best density correlated half-life decreases from 180 minutes to 18 minutes as geomagnetic activity increases for CHAMP. The same trend is seen in GRACE RMS results. For GRACE CC results, a combination of 1.8 minutes and 180 minutes for BC and density half-lives is best at all geomagnetic activity levels. Finally, the Jacchia family models again prove superior for use as the baseline atmospheric density model.

3.5 Representative Days for the Solar and Geomagnetic Activity Bins

Four days representative of the conditions experienced by the CHAMP and GRACE satellites are presented. Days were selected that covered as wide a range of solar and geomagnetic activity levels as possible. The days selected are August 3, 2006, December 22, 2006, March 13, 2005, and September 12, 2005. Low solar and quiet geomagnetic activity level periods are represented by August 3, 2006. December 22 of the same year was a day of low solar and moderate geomagnetic activity. March 13, 2005 falls into the moderate bins for both solar and geomagnetic activity, and September 12, 2005 covers the moderate solar and active geomagnetic levels.

3.5.1 August 3, 2006 Covering Low Solar and Quiet Geomagnetic Activity

On August 3, 2006 conditions were very quiet. An A_p of 5 and an $F_{10.7}$ of 71.3 were recorded for this time period. Table 3.25 summarizes the CC and RMS results obtained for this day for CHAMP and GRACE-A with the ballistic coefficient correlated half-life/density correlated half-life combination/baseline atmospheric model in parentheses. Note that the best values achieved for this day did not agree with the averages for results in the corresponding activity level bins. However, the best results available did not differ significantly from average best combination results in the same activity level bins. Figure 3.1 shows the POE estimated density (solid line) using a ballistic coefficient correlated half-life of 1.8 minutes and a density correlated half-life of 180 minutes for CHAMP and GRACE-A for a fourteen hour span starting from 10 AM UTC on August 3, 2006. In addition, the accelerometer derived density is shown (dotted line), as well as densities obtained from the Jacchia 1971 empirical model (dashed line). For CHAMP, the Jacchia 1971 model actually matches the accelerometer more closely for this day. For GRACE, the POE estimated

density matches the accelerometer much better, as the Jacchia 1971 model overestimates the density during this time.

Table 3.25: Summary of Cross Correlation Coefficients and Root Mean Square Values for August 3, 2006. *Inputs to POE Method are shown in parentheses with Ballistic Coefficient Half-life/Density Coefficient Half-life/Baseline Density Model.*

	CC	**RMS (kg/m^3*10^{-12})**
CHAMP		
HASDM	0.960	0.220
Jacchia 1971	0.972	0.274
Overall Best POE Result with Inputs	0.972 (180/1.8/C72)	0.235 (18/1.8/J71)
POE Result Shown in Plot with Inputs	0.929 (1.8/180/J71)	0.291 (1.8/180/J71)
GRACE-A		
HASDM	0.848	0.033
Jacchia 1971	0.873	0.038
Overall Best POE Result with Inputs	0.874 (180/1.8/C72)	0.025 (1.8/180/MSISE90)
POE Result Shown in Plot with Inputs	0.870 (1.8/180/J71)	0.026 (1.8/180/J71)

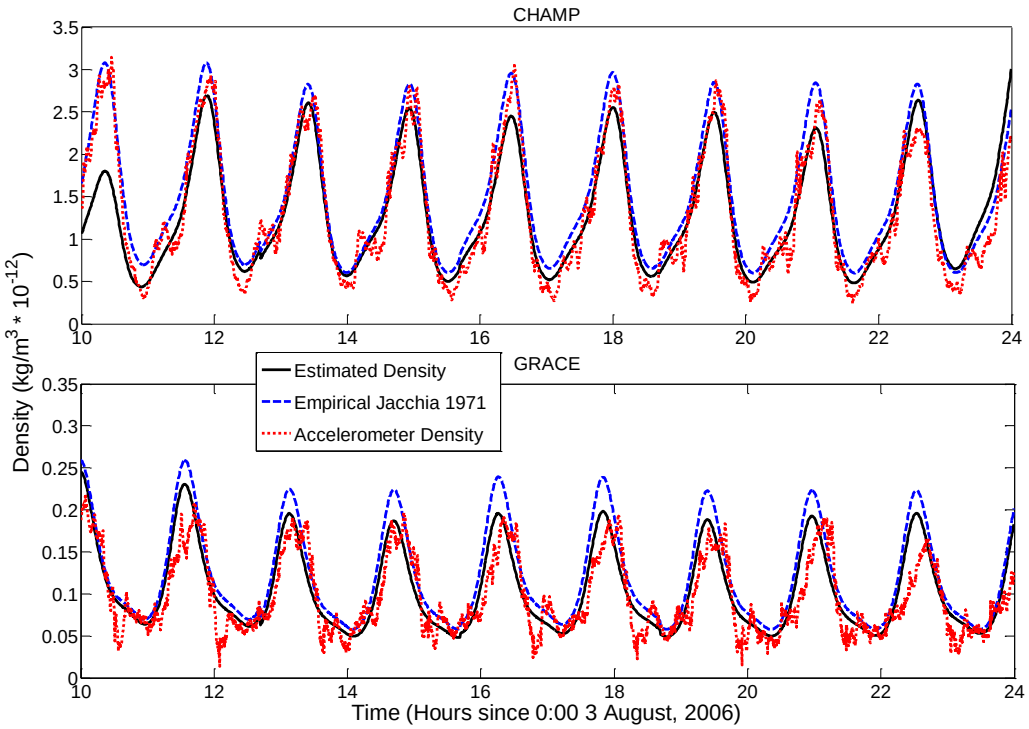

Figure 3.1: POE Estimated Density, Jacchia 1971 Model Density and Accelerometer Density of CHAMP and GRACE-A Satellites for August 3, 2006. *Ballistic coefficient and density correlated half-lives are 1.8 and 180 minutes, respectively. The baseline atmospheric model is Jacchia 1971.*

3.5.2 December 22, 2006 Covering Low Solar and Moderate Geomagnetic Activity

December 22, 2006 featured low solar activity and moderate geomagnetic activity, with an A_p of 18 and an $F_{10.7}$ of 73.2. Table 3.26 summarizes the CC and RMS results obtained for this day for CHAMP and GRACE-A. Once again, the best values achieved for this day did not always agree with the averages for results in the corresponding activity level bins, but results were very similar. Figure 3.2 shows the densities for CHAMP and GRACE-A on this particular day. For both CHAMP and GRACE on this day, the POE estimated density matches much more closely with the accelerometer in magnitude compared to the Jacchia 1971 model, as reflected in the RMS results. The trends are also matched more closely, as reflected in the CC values. However, note that shorter period secondary peaks observed by the accelerometer are not characterized by the POE method or the Jacchia model.

Table 3.26: Summary of Cross Correlation Coefficients and Root Mean Square Values for December 22, 2006. *Inputs to POE Method are shown in parentheses with Ballistic Coefficient Half-life/Density Coefficient Half-life/Baseline Density Model.*

	CC	**RMS (kg/m^3*10^{-12})**
CHAMP		
HASDM	0.909	0.411
Jacchia 1971	0.901	1.15
Overall Best POE Result with Inputs	0.927 (18/18/J-R)	0.374 (1.8/180/J-R)
POE Result Shown in Plot with Inputs	0.921 (1.8/180/J71)	0.376 (1.8/180/J71)
GRACE-A		
HASDM	0.846	0.960
Jacchia 1971	0.811	0.972
Overall Best POE Result with Inputs	0.834(180/1.8/C72)	0.044 (1.8/180/J71)
POE Result Shown in Plot with Inputs	0.830 (1.8/180/J71)	0.044 (1.8/180/J71)

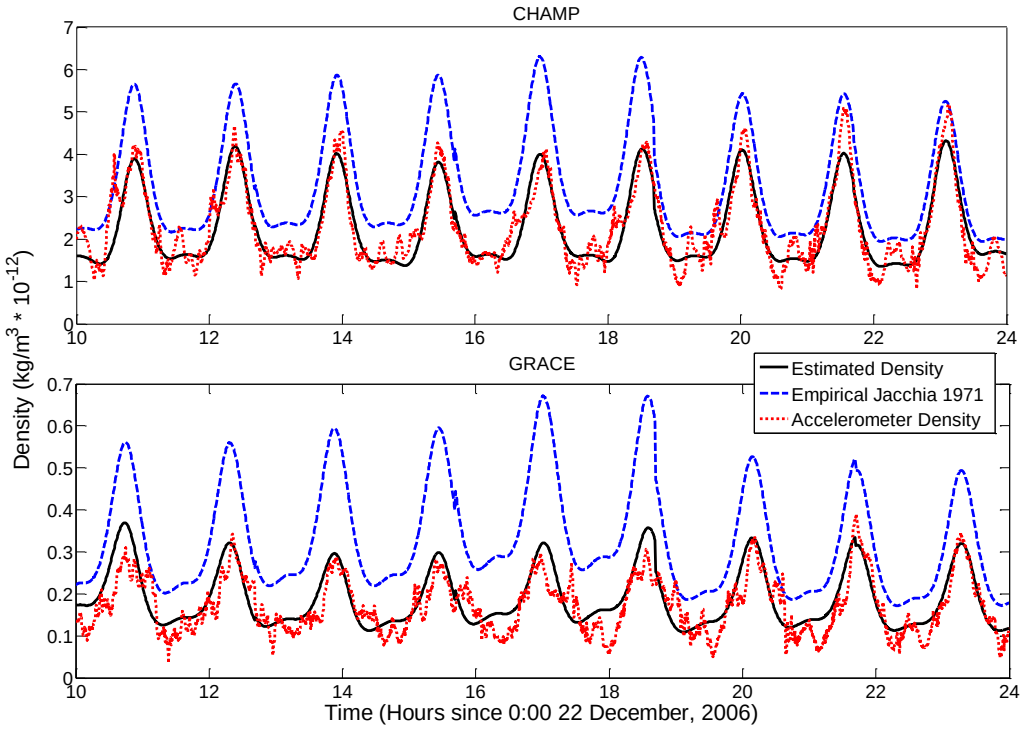

Figure 3.2: POE Estimated Density, Jacchia 1971 Model Density and Accelerometer Density of CHAMP and GRACE-A Satellites for December 22, 2006. *Ballistic coefficient and density correlated half-lives are 1.8 and 180 minutes, respectively. The baseline atmospheric model is Jacchia 1971.*

3.5.3 March 13, 2005 Covering Moderate Solar and Moderate Geomagnetic Activity

March 13, 2005 was a day of both moderate solar and geomagnetic activity. An A_p of 19 and an $F_{10.7}$ of 113.8 were recorded. Table 3.27 tabulates CC and RMS values for CHAMP and GRACE-A. Here HASDM, the Jacchia 1971 empirical, and the POE densities all produced very similar results for CHAMP. For GRACE-A, the RMS values were actually better using the Jacchia 1971 model than HASDM and all but one case of POE densities. Figure 3.3 shows the densities for CHAMP and GRACE-A for a fourteen hour span starting from 10 AM UTC on March 13, 2005. On this day, the Jacchia 1971 empirical model consistently underestimated the CHAMP accelerometer density, while the POE CHAMP density matched the accelerometer well. For GRACE-A however, the estimated density

usually overestimated the accelerometer density while the Jacchia 1971 matched fairly closely.

Table 3.27: Summary of Cross Correlation Coefficients and Root Mean Square Values for March 13, 2005. *Inputs to POE Method are shown in parentheses with Ballistic Coefficient Half-life/Density Coefficient Half-life/Baseline Density Model.*

	CC	**RMS (kg/m^3*10^{-12})**
CHAMP		
HASDM	0.976	0.378
Jacchia 1971	0.973	0.695
Overall Best POE Result with Inputs	0.977(18/1.8/J71)	0.371 (1.8/180/C72)
POE Result Shown in Plot with Inputs	0.976 (1.8/180/J71)	0.373 (1.8/180/J71)
GRACE-A		
HASDM	0.949	0.103
Jacchia 1971	0.955	0.054
Overall Best POE Result with Inputs	0.962(180/1.8/J-R)	0.053(180/1.8/J71)
POE Result Shown in Plot with Inputs	0.962 (1.8/180/J71)	0.087(1.8/180/J71)

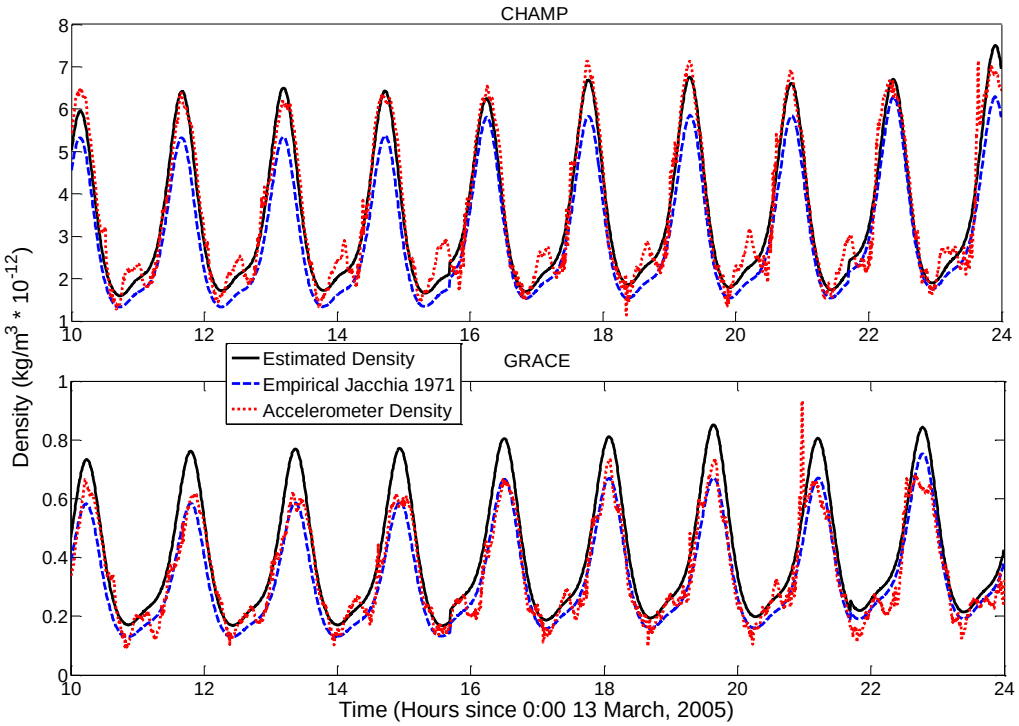

Figure 3.3: POE Estimated Density, Jacchia 1971 Model Density and Accelerometer Density of CHAMP and GRACE-A Satellites for March 13, 2005. *Ballistic coefficient and density correlated half-lives are 1.8 and 180 minutes, respectively. The baseline atmospheric model is Jacchia 1971.*

3.5.4 September 12, 2005 Covering Moderate Solar and Active Geomagnetic Activity

September 12, 2005 was among the most active days available for examination, with an A_p of 75 and an $F_{10.7}$ of 118.0. Table 3.28 contains a summary of the RMS and CC information for this day. CC values were worse for CHAMP than GRACE-A. Note that RMS values are worse for CHAMP and GRACE compared with the other days examined, as the variability is greater. Figure 3.4 shows the densities for CHAMP and GRACE-A on this day. Clearly visible is the increased variability of the accelerometer density for both CHAMP and GRACE. For both satellites, the POE derived densities match the accelerometer more closely than the Jacchia 1971 model.

Table 3.28: Summary of Cross Correlation Coefficients and Root Mean Square Values for September 12, 2005. *Inputs to POE Method are shown in parentheses with Ballistic Coefficient Half-life/Density Coefficient Half-life/Baseline Density Model.*

	CC	**RMS (kg/m^3*10^{-12})**
CHAMP		
HASDM	0.782	0.951
Jacchia 1971	0.606	1.64
Overall Best POE Result with Inputs	0.796(18/18/J71)	0.921 (18/18/J71)
POE Result Shown in Plot with Inputs	0.772 (1.8/180/J71)	0.987 (1.8/180/J71)
GRACE-A		
HASDM	0.909	0.153
Jacchia 1971	0.901	0.484
Overall Best POE Result with Inputs	0.917(18/180/C72)	0.144 (1.8/18/J-R)
POE Result Shown in Plot with Inputs	0.913(1.8/180/J71)	0.153(1.8/180/J71)

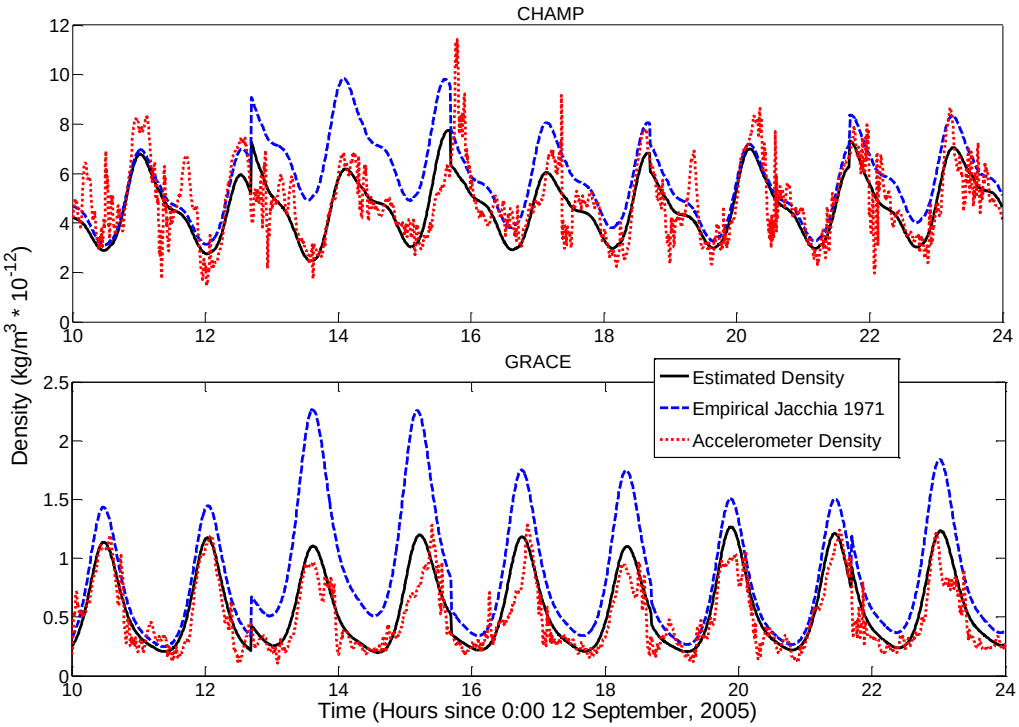

Figure 3.4: POE Estimated Density, Jacchia 1971 Model Density and Accelerometer Density of CHAMP and GRACE-A Satellites for September 12, 2005. *Ballistic coefficient and density correlated half-lives are 1.8 and 180 minutes, respectively. The baseline atmospheric model is Jacchia 1971.*

3.6 Chapter Summary

Cross correlation coefficients and root mean square values are calculated by comparing densities obtained from various methods. The Jacchia 1971 empirical model, HASDM, and forty-five combinations of POE derived densities are compared to densities obtained from the onboard accelerometers of the CHAMP and GRACE-A satellites. All of the time periods examined are sorted into four solar activity level bins and three geomagnetic activity bins. However, data for the GRACE satellites is only available during periods of the two lower levels of solar activity. Table 3.29 displays the combination of ballistic coefficient correlated half-life, density correlated half-life, and baseline atmospheric density model which produces the best results of cross correlation for CHAMP for all available solar and

geomagnetic activity levels. Table 3.30 displays the same information for the best RMS values for CHAMP. Table 3.31 displays this information for GRACE-A for cross correlation coefficients, and Table 3.32 shows the information for GRACE-A RMS values.

Table 3.29: Best Combinations for CHAMP POE Density Correlation to Accelerometer Density by Activity Levels

Bin	Best Density Half-Life (min)	Best BC Half-Life (min)	Best Atmospheric Model	Best Cross Correlation
Quiet Geomagnetic	180	1.8	CIRA 1972	0.936
Moderate Geomagnetic	180	1.8	CIRA 1972	0.945
Active Geomagnetic	18	1.8	Jacchia 1971	0.818
Low Solar	180	1.8	CIRA 1972	0.928
Moderate Solar	18	1.8	CIRA 1972	0.868

Table 3.30: Best Combinations for CHAMP POE Density and Accelerometer Density Root Mean Square by Activity Levels

Bin	Best Density Half-Life (min)	Best BC Half-Life (min)	Best Atmospheric Model	Best RMS Value (kg/m^3*10^{-12})
Quiet Geomagnetic	180	1.8	CIRA 1972	0.272
Moderate Geomagnetic	180	1.8	CIRA 1972	0.418
Active Geomagnetic	18	1.8	CIRA 1972	0.961
Low Solar	180	1.8	CIRA 1972	0.264
Moderate Solar	18	1.8	CIRA 1972	0.761

Table 3.31: Best Combinations for GRACE-A POE Density Correlation to Accelerometer Density by Activity Levels

Bin	Best Density Half-Life (min)	Best BC Half-Life (min)	Best Atmospheric Model	Best Cross Correlation
Quiet Geomagnetic	1.8	180	Jacchia 1971	0.805
Moderate Geomagnetic	180	1.8	Jacchia 1971	0.912
Active Geomagnetic	180	1.8	Jacchia 1971	0.845
Low Solar	180	1.8	Jacchia 1971	0.766
Moderate Solar	180	1.8	Jacchia-Roberts	0.883

Table 3.32: Best Combinations for GRACE-A POE Density and Accelerometer Density Root Mean Square by Activity Levels

Bin	Best Density Half-Life (min)	Best BC Half-Life (min)	Best Atmospheric Model	Best RMS Value (kg/m^3*10^{-12})
Quiet Geomagnetic	180	1.8	Jacchia-Roberts	0.037
Moderate Geomagnetic	180	1.8	Jacchia-Roberts	0.076
Active Geomagnetic	18	1.8	Jacchia-Roberts	0.207
Low Solar	180	1.8	Jacchia-Roberts	0.029
Moderate Solar	180	1.8	Jacchia-Roberts	0.160

From these tables, it can be surmised that a Jacchia-family model is the optimal model to use as baseline. Jacchia 1971 is chosen for further examination in this work. A ballistic coefficient correlated half-life of 1.8 minutes is nearly always superior to other values. A density correlated half-life of 180 minutes is usually the best for both CHAMP and GRACE. For higher activity levels 18 minutes is the superior density correlated half-life for CHAMP.

From examining four dates with differing levels of solar and geomagnetic activity levels, the ability of the POE derived density method to accurately and precisely characterize

density variations experienced by these satellites is clearly seen. However, this method is unable to model higher frequency variations visible in the accelerometer derived densities. In general, as solar and geomagnetic activity levels increase CC and RMS values worsen for both CHAMP and GRACE.

4 EXAMINATION OF RESULTS DURING EXTENDED SOLAR MINIMUM PERIOD FOR CHAMP AND GRACE SATELLITES

In 2008 and 2009, behavior of the Sun was different than previous cycles observed. Lower solar activity was recorded than should have occurred as activity should have been increasing according to the 11-year cycle. All data available for this period fell into the low solar activity bin. Some of the data examined occurred during periods of moderate geomagnetic activity, and some occurred during periods of quiet geomagnetic activity. Data examined for this period includes February 1-4 and March 10-13 of 2008, and February 1-4 and July 10-13 of 2009.

4.1 Overall Results for Extended Solar Minimum

Results for 2008 and 2009 are averaged overall as was performed in the previous chapter. Table 4.1 displays the cross correlation coefficients obtained for CHAMP during 2008 and 2009. The combination of half-lives producing the best correlations is 1.8 minutes and 180 minutes for ballistic coefficient correlated half-life and density correlated half-life, respectively. The best correlation is produced using CIRA 1972 as the baseline atmospheric density model. Correlation between the accelerometer derived density and HASDM density are not given as HASDM densities are not currently available for 2009. The best correlations are superior to the Jacchia 1971 model. Note that the best correlations during 2008 and 2009 for CHAMP are superior to the overall averages of results during the previous time periods examined from 2004 through 2007. Table 4.2 displays the overall root mean square values during these periods. The same combination of half-lives produces the best results with a baseline model of Jacchia 1971. The POE method again outperforms the Jacchia 1971

empirical model for RMS values. In addition, RMS values are lower than those overall values from 2004 through 2007, resulting from the lower densities encountered.

Table 4.1: Zero Delay Cross Correlation Coefficients Time Averaged over all Solution Periods During Extended Solar Minimum for CHAMP. *The columns represent the baseline model used in calculating POE derived densities. Correlation with the Jacchia 1971 empirical model is included. Yellow (light gray) highlighting indicates the best value for the baseline model. Orange (darker gray) indicates the best value of all possible combinations.*

			A_p Avg	$F_{10.7}$ Avg	Jacchia 1971
			11.9	69.8	0.856
BC-Density Half-Lives	CIRA 1972	Jacchia 1971	Jacchia-Roberts	MSISE 1990	NRLMSISE 2000
1.8-1.8	0.835	0.826	0.820	0.828	0.829
18-1.8	0.866	0.866	0.864	0.857	0.857
180-1.8	0.866	0.866	0.865	0.860	0.860
1.8-18	0.876	0.871	0.867	0.864	0.864
18-18	0.873	0.869	0.864	0.860	0.860
180-18	0.867	0.866	0.863	0.854	0.854
1.8-180	0.889	0.887	0.887	0.879	0.880
18-180	0.880	0.879	0.878	0.871	0.873
180-180	0.846	0.843	0.840	0.842	0.843

Table 4.2: Root Mean Square Values Time Averaged over all Solution Periods During Extended Solar Minimum for CHAMP. *The columns represent the baseline model used in calculating POE derived densities. RMS for the Jacchia 1971 empirical model is included. Yellow (light gray) highlighting indicates the best value for the baseline model. Orange (darker gray) indicates the best value of all possible combinations. Units of RMS are* kg/m^3*10^{-12}.

			A_p Avg	$F_{10.7}$ Avg	Jacchia 1971
			11.9	69.8	0.831
BC-Density Half-Lives	CIRA 1972	Jacchia 1971	Jacchia-Roberts	MSISE 1990	NRLMSISE 2000
1.8-1.8	0.786	0.709	0.687	0.865	0.855
18-1.8	1.265	1.196	1.172	1.335	1.328
180-1.8	1.705	1.683	1.675	1.747	1.744
1.8-18	0.507	0.476	0.481	0.589	0.580
18-18	0.651	0.570	0.549	0.754	0.743
180-18	1.217	1.148	1.122	1.317	1.309
1.8-180	0.452	0.444	0.459	0.511	0.502
18-180	0.516	0.463	0.459	0.595	0.585
180-180	0.905	0.801	0.762	1.025	1.018

Table 4.3 displays cross correlation between the GRACE-A accelerometer and the POE combinations as well as the Jacchia 1971 model for the same days examined for CHAMP. For GRACE, the Jacchia 1971 model outperforms all POE derived densities. The best POE derived density correlation is produced for a baseline model of Jacchia 1971 with a BC half-life of 180 minutes and a density half-life of 1.8 minutes. Correlations are considerably worse than the overall averages obtained for 2004-2007. However, the small sample size may overemphasize days with poor correlations. Table 4.4 displays RMS values for GRACE-A in 2008 and 2009. Here the lowest RMS results when both half-lives are 1.8 minutes and the Jacchia-Roberts model is used as the baseline. For RMS, the POE method outperforms the Jacchia 1971 model. Overall RMS results are slightly better for the 2008-2009 dates than those of 2004-2007. However, density values are usually much lower during these periods of very low solar activity, which likely causes the very low RMS values.

Table 4.3: Zero Delay Cross Correlation Coefficients Time Averaged over all Solution Periods During Extended Solar Minimum for GRACE-A. *The columns represent the baseline model used in calculating POE derived densities. Correlation with the Jacchia 1971 empirical model is included. Yellow (light gray) highlighting indicates the best value for the baseline model. Orange (darker gray) indicates the best value of all possible combinations.*

			A_p Avg	$F_{10.7}$ Avg	Jacchia 1971
			11.9	69.8	0.804
BC-Density Half-Lives	CIRA 1972	Jacchia 1971	Jacchia-Roberts	MSISE 1990	NRLMSISE 2000
1.8-1.8	0.446	0.450	0.440	0.501	0.484
18-1.8	0.494	0.496	0.490	0.527	0.513
180-1.8	0.719	0.720	0.720	0.718	0.715
1.8-18	0.457	0.459	0.453	0.483	0.472
18-18	0.461	0.463	0.457	0.485	0.475
180-18	0.518	0.520	0.516	0.535	0.528
1.8-180	0.563	0.564	0.562	0.561	0.560
18-180	0.563	0.564	0.562	0.564	0.562
180-180	0.551	0.552	0.550	0.556	0.555

Table 4.4: Root Mean Square Values Time Averaged over all Solution Periods During Extended Solar Minimum for GRACE-A. *The columns represent the baseline model used in calculating POE derived densities. RMS for the Jacchia 1971 empirical model is included. Yellow (light gray) highlighting indicates the best value for the baseline model. Orange (darker gray) indicates the best value of all possible combinations. Units of RMS are kg/m^3*10^{-12}.*

			A_p Avg	$F_{10.7}$ Avg	Jacchia 1971
			11.9	69.8	0.150
BC-Density Half-Lives	CIRA 1972	Jacchia 1971	Jacchia-Roberts	MSISE 1990	NRLMSISE 2000
1.8-1.8	0.116	0.116	0.116	0.124	0.122
18-1.8	0.121	0.121	0.120	0.127	0.126
180-1.8	0.137	0.137	0.136	0.142	0.141
1.8-18	0.138	0.138	0.137	0.152	0.149
18-18	0.140	0.140	0.139	0.154	0.151
180-18	0.170	0.170	0.168	0.182	0.179
1.8-180	0.135	0.135	0.133	0.152	0.148
18-180	0.131	0.131	0.130	0.148	0.144
180-180	0.140	0.140	0.138	0.157	0.153

4.2 Effect of Geomagnetic Activity on Results

All periods examined for this part of the study in 2008 and 2009 fall into the low solar activity bin, so data will be binned according to geomagnetic activity. No data falls in the active geomagnetic bin. Cross correlation and RMS results will be examined for both quiet and moderate geomagnetic activity. The results may be skewed by the small sample size for 2008 and 2009. All of the July 2009 data fall in the quiet geomagnetic activity bin, and this is where the most unusual results are seen. Hence, conclusions drawn for the quiet activity bin may not hold true once more data is examined.

4.2.1 Quiet Geomagnetic Activity Bin

Roughly half of the dates examined during 2008-2009 fell into the quiet geomagnetic activity bin, including all the data from July 10-13, 2009. Table 4.5 displays the cross correlations with the CHAMP accelerometer for the Jacchia 1971 model and the POE derived densities. Here an unusual combination of 180 minutes for ballistic coefficient correlated

half-life, 1.8 minutes for density correlated half-life, and a baseline model of Jacchia 1971 produce the best correlation. Table 4.6 shows RMS values for CHAMP during periods of quiet geomagnetic activity during 2008-2009. Here the most common combination of half-lives again produces the best result: 1.8 minutes for ballistic coefficient and 180 minutes for density. However, rather than a Jacchia family model, MSISE 1990 as the baseline model produces the lowest RMS.

Table 4.5: Zero Delay Cross Correlation Coefficients Time Averaged over Quiet Geomagnetic Activity Periods for CHAMP. *The columns represent the baseline model used in calculating POE derived densities. Correlation with the Jacchia 1971 empirical model is included. Yellow (light gray) highlighting indicates the best value for the baseline model. Orange (darker gray) indicates the best value of all possible combinations.*

			A_p Avg	$F_{10.7}$ Avg	Jacchia 1971
			5.7	68.9	0.940
BC-Density Half-Lives	CIRA 1972	Jacchia 1971	Jacchia-Roberts	MSISE 1990	NRLMSISE 2000
1.8-1.8	0.835	0.832	0.832	0.843	0.841
18-1.8	0.927	0.927	0.927	0.925	0.925
180-1.8	0.943	0.943	0.943	0.942	0.943
1.8-18	0.855	0.857	0.857	0.862	0.863
18-18	0.858	0.859	0.858	0.867	0.868
180-18	0.921	0.922	0.922	0.923	0.924
1.8-180	0.882	0.883	0.883	0.883	0.883
18-180	0.873	0.874	0.874	0.876	0.877
180-180	0.864	0.862	0.861	0.871	0.871

Table 4.6: Root Mean Square Values Time Averaged over Quiet Geomagnetic Activity Periods for CHAMP. *The columns represent the baseline model used in calculating POE derived densities. RMS for the Jacchia 1971 empirical model is included. Yellow (light gray) highlighting indicates the best value for the baseline model. Orange (darker gray) indicates the best value of all possible combinations. Units of RMS are* $kg/m^3 * 10^{-12}$.

			A_p Avg	$F_{10.7}$ Avg	Jacchia 1971
			5.7	68.9	2.77
BC-Density Half-Lives	CIRA 1972	Jacchia 1971	Jacchia-Roberts	MSISE 1990	NRLMSISE 2000
1.8-1.8	1.004	0.959	0.944	1.066	1.067
18-1.8	1.616	1.572	1.556	1.697	1.685
180-1.8	2.357	2.352	2.350	2.392	2.387
1.8-18	0.804	0.800	0.805	0.818	0.827
18-18	0.870	0.834	0.825	0.924	0.920
180-18	1.523	1.486	1.470	1.614	1.607
1.8-180	0.738	0.760	0.774	0.733	0.749
18-180	0.753	0.748	0.752	0.769	0.774
180-180	1.014	0.953	0.930	1.107	1.099

Table 4.7 presents cross correlation coefficients for the GRACE-A satellite during times of quiet geomagnetic activity. Very poor cross correlations are seen here relative to periods of quiet geomagnetic activity for GRACE between 2004 and 2007. The best correlation results from a baseline model of Jacchia-Roberts, a BC half-life of 180 minutes, and a density half-life of 1.8 minutes. All correlations fall short of those achieved by the Jacchia 1971 empirical model. Table 4.8 presents the root mean square values for the same time period for GRACE. Here RMS values are similar to those achieved by the Jacchia 1971 model. The lowest RMS results from using Jacchia-Roberts as the baseline model with 1.8 minutes for both half-lives.

Table 4.7: Zero Delay Cross Correlation Coefficients Time Averaged over Quiet Geomagnetic Activity Periods for GRACE-A. *The columns represent the baseline model used in calculating POE derived densities. Correlation with the Jacchia 1971 empirical model is included. Yellow (light gray) highlighting indicates the best value for the baseline model. Orange (darker gray) indicates the best value of all possible combinations.*

			A_p Avg	$F_{10.7}$ Avg	Jacchia 1971
			5.7	68.9	0.829
BC-Density Half-Lives	CIRA 1972	Jacchia 1971	Jacchia-Roberts	MSISE 1990	NRLMSISE 2000
1.8-1.8	0.210	0.213	0.205	0.258	0.243
18-1.8	0.234	0.236	0.230	0.270	0.254
180-1.8	0.651	0.652	0.653	0.646	0.642
1.8-18	0.230	0.231	0.228	0.255	0.246
18-18	0.228	0.229	0.226	0.249	0.241
180-18	0.300	0.301	0.299	0.315	0.309
1.8-180	0.349	0.350	0.349	0.352	0.350
18-180	0.348	0.349	0.348	0.351	0.350
180-180	0.334	0.335	0.334	0.339	0.338

Table 4.8: Root Mean Square Values Time Averaged over Quiet Geomagnetic Activity Periods for GRACE-A. *The columns represent the baseline model used in calculating POE derived densities. RMS for the Jacchia 1971 empirical model is included. Yellow (light gray) highlighting indicates the best value for the baseline model. Orange (darker gray) indicates the best value of all possible combinations. Units of RMS are* $kg/m^3 * 10^{-12}$.

			A_p Avg	$F_{10.7}$ Avg	Jacchia 1971
			5.7	68.9	0.176
BC-Density Half-Lives	CIRA 1972	Jacchia 1971	Jacchia-Roberts	MSISE 1990	NRLMSISE 2000
1.8-1.8	0.171	0.171	0.171	0.175	0.175
18-1.8	0.173	0.173	0.173	0.173	0.174
180-1.8	0.175	0.175	0.175	0.178	0.178
1.8-18	0.231	0.231	0.229	0.247	0.245
18-18	0.233	0.233	0.231	0.248	0.246
180-18	0.280	0.280	0.278	0.292	0.289
1.8-180	0.236	0.236	0.234	0.257	0.253
18-180	0.227	0.227	0.225	0.246	0.243
180-180	0.227	0.227	0.225	0.243	0.241

4.2.2 Moderate Geomagnetic Activity Bin

The rest of the results in the 2008 and 2009 period fall into the moderate geomagnetic activity level bin. Table 4.9 shows correlations for CHAMP during these periods. Again CHAMP results for POE density estimation surpass the Jacchia 1971 model. The best correlation results from a half-life combination of 1.8 minutes and 180 minutes for ballistic coefficient and density, respectively. CIRA 1972 as the baseline atmospheric model produces this result. The increased geomagnetic activity has decreased correlations from the quiet geomagnetic periods. RMS values for CHAMP are displayed in Table 4.10. The lowest RMS results from the same inputs as for cross correlation. Almost all RMS results are superior to those produced by the Jacchia 1971 model.

Table 4.9: Zero Delay Cross Correlation Coefficients Time Averaged over Moderate Geomagnetic Activity Periods for CHAMP. *The columns represent the baseline model used in calculating POE derived densities. Correlation with the Jacchia 1971 empirical model is included. Yellow (light gray) highlighting indicates the best value for the baseline model. Orange (darker gray) indicates the best value of all possible combinations.*

			A_p Avg	$F_{10.7}$ Avg	Jacchia 1971
			16.2	70.4	0.850
BC-Density Half-Lives	CIRA 1972	Jacchia 1971	Jacchia-Roberts	MSISE 1990	NRLMSISE 2000
1.8-1.8	0.863	0.855	0.849	0.851	0.851
18-1.8	0.868	0.868	0.866	0.857	0.857
180-1.8	0.862	0.862	0.861	0.855	0.855
1.8-18	0.883	0.878	0.874	0.866	0.866
18-18	0.880	0.876	0.872	0.862	0.862
180-18	0.865	0.864	0.861	0.850	0.850
1.8-180	0.891	0.889	0.888	0.877	0.879
18-180	0.884	0.883	0.883	0.871	0.873
180-180	0.854	0.851	0.849	0.845	0.846

Table 4.10: Root Mean Square Values Time Averaged over Moderate Geomagnetic Activity Periods for CHAMP. *The columns represent the baseline model used in calculating POE derived densities. RMS for the Jacchia 1971 empirical model is included. Yellow (light gray) highlighting indicates the best value for the baseline model. Orange (darker gray) indicates the best value of all possible combinations. Units of RMS are* kg/m^3*10^{-12}.

			A_p Avg	$F_{10.7}$ Avg	Jacchia 1971
			16.2	70.4	1.36
BC-Density Half-Lives	CIRA 1972	Jacchia 1971	Jacchia-Roberts	MSISE 1990	NRLMSISE 2000
1.8-1.8	0.635	0.577	0.568	0.735	0.714
18-1.8	0.908	0.844	0.824	0.996	0.981
180-1.8	1.158	1.133	1.124	1.216	1.209
1.8-18	0.492	0.481	0.496	0.593	0.570
18-18	0.572	0.511	0.504	0.697	0.673
180-18	0.892	0.822	0.800	1.017	0.999
1.8-180	0.464	0.467	0.487	0.554	0.530
18-180	0.510	0.468	0.471	0.622	0.596
180-180	0.795	0.690	0.660	0.942	0.917

Table 4.11 displays cross correlations achieved during periods of moderate geomagnetic activity in 2008-2009 for GRACE-A. These correlations are actually superior to those in the quiet geomagnetic activity bin, though all POE derived density correlations are worse than the Jacchia 1971 empirical model. With the exception of periods which exhibit extremely low correlations, most of the data in the moderate activity bin produce results in accordance with those seen during 2004-2007. The best half-life combination is 180 minutes for BC and 1.8 minutes for density, as was the case in the quiet bin. This time the best baseline model is MSISE 1990. RMS values for the same time periods for GRACE are shown in Table 4.12. RMS values are superior to the Jacchia 1971 model, with the best result coming from the typical 1.8 minutes (BC), 180 minutes (density), and Jacchia-Roberts as baseline model.

Table 4.11: Zero Delay Cross Correlation Coefficients Time Averaged over Moderate Geomagnetic Activity Periods for GRACE-A. *The columns represent the baseline model used in calculating POE derived densities. Correlation with the Jacchia 1971 empirical model is included. Yellow (light gray) highlighting indicates the best value for the baseline model. Orange (darker gray) indicates the best value of all possible combinations.*

			A_p Avg	$F_{10.7}$ Avg	Jacchia 1971
			16.2	70.4	0.783
BC-Density Half-Lives	CIRA 1972	Jacchia 1971	Jacchia-Roberts	MSISE 1990	NRLMSISE 2000
1.8-1.8	0.641	0.646	0.633	0.702	0.683
18-1.8	0.709	0.711	0.704	0.738	0.728
180-1.8	0.776	0.776	0.775	0.777	0.775
1.8-18	0.644	0.646	0.638	0.670	0.658
18-18	0.653	0.656	0.648	0.679	0.667
180-18	0.699	0.701	0.696	0.716	0.710
1.8-180	0.739	0.740	0.738	0.735	0.733
18-180	0.741	0.741	0.739	0.739	0.737
180-180	0.730	0.731	0.728	0.736	0.734

Table 4.12: Root Mean Square Values Time Averaged over Moderate Geomagnetic Activity Periods for GRACE-A. *The columns represent the baseline model used in calculating POE derived densities. RMS for the Jacchia 1971 empirical model is included. Yellow (light gray) highlighting indicates the best value for the baseline model. Orange (darker gray) indicates the best value of all possible combinations. Units of RMS are* $kg/m^3 * 10^{-12}$.

			A_p Avg	$F_{10.7}$ Avg	Jacchia 1971
			16.2	70.4	0.129
BC-Density Half-Lives	CIRA 1972	Jacchia 1971	Jacchia-Roberts	MSISE 1990	NRLMSISE 2000
1.8-1.8	0.071	0.071	0.070	0.082	0.079
18-1.8	0.078	0.079	0.078	0.090	0.087
180-1.8	0.105	0.105	0.104	0.111	0.110
1.8-18	0.061	0.062	0.061	0.073	0.070
18-18	0.063	0.064	0.062	0.076	0.072
180-18	0.078	0.079	0.077	0.091	0.088
1.8-180	0.051	0.051	0.050	0.066	0.062
18-180	0.052	0.052	0.051	0.067	0.062
180-180	0.068	0.069	0.067	0.086	0.081

4.3 Representative Days for the Solar and Geomagnetic Activity Bins

All days feature low solar activity and either quiet or moderate geomagnetic activity. Three days will be examined. The first is a day of low solar and quiet geomagnetic activity, February 1, 2009. The second is a day of low solar and moderate geomagnetic activity, March 11, 2008. Finally, July 11, 2009, which features unusual results, will be studied.

4.3.1 February 1, 2009 Covering Low Solar and Quiet Geomagnetic Activity

February 1, 2009 was a day of very low activity, with an A_p of 3 and an $F_{10.7}$ of 69.5. Table 4.13 summarizes the CC and RMS results for this time span for CHAMP and GRACE-A with the ballistic coefficient correlated half-life/density correlated half-life combination/baseline atmospheric model in parentheses. The cross correlation for the Jacchia 1971 empirical model was better for GRACE-A than all the POE combinations. However, RMS was much better for the POE densities. Figure 4.1 shows the densities for a fourteen hour span starting from 10 AM UTC on February 1, 2009. Shown are the accelerometer derived density, the POE derived density, and the Jacchia 1971 empirical model density. The POE density is obtained using the Jacchia 1971 baseline model, 1.8 minute ballistic coefficient correlated half-life, and 180 minute density correlated half-life.

Table 4.13: Summary of Cross Correlation Coefficients and Root Mean Square Values for February 1, 2009. *Inputs to POE Method are shown in parentheses with Ballistic Coefficient Half-life/Density Coefficient Half-life/Baseline Density Model.*

	CC	**RMS (kg/m^3*10^{-12})**
CHAMP		
HASDM	N/A	N/A
Jacchia 1971	0.951	2.83
Overall Best POE Result with Inputs	0.954 (180/1.8/NRLM00)	0.385 (1.8/180/J71)
POE Result Shown in Plot with Inputs	0.948 (1.8/180/J71)	0.385 (1.8/180/J71)
GRACE-A		
HASDM	N/A	N/A
Jacchia 1971	0.942	0.164
Overall Best POE Result with Inputs	0.914 (180/1.8/J71)	0.046 (180/180/J-R)
POE Result Shown in Plot with Inputs	0.692 (1.8/180/J71)	0.049 (1.8/180/J71)

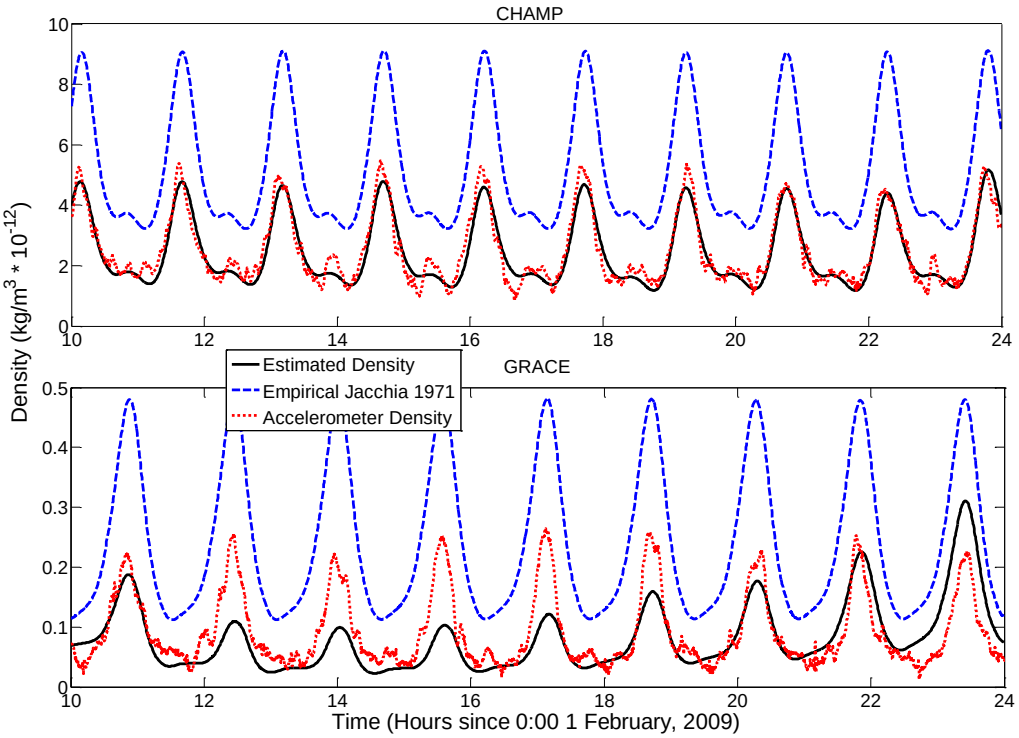

Figure 4.1: POE Estimated Density, Jacchia 1971 Model Density and Accelerometer Density of CHAMP and GRACE-A Satellites for February 1, 2009. *Ballistic coefficient and density correlated half-lives are 1.8 and 180 minutes, respectively. The baseline atmospheric model is Jacchia 1971.*

4.3.2 March 11, 2008 Covering Low Solar and Moderate Geomagnetic Activity

On March 11, 2008 an A_p of 15 and an $F_{10.7}$ of 70.2 were recorded, placing it in the low solar and moderate geomagnetic activity bins. Table 4.14 summarizes the cross correlation and RMS information. Correlations are worse for CHAMP for this period than February 1, 2009. As is usually the case, the POE method outperforms the Jacchia 1971 model and HASDM for both CC and RMS. For this day the GRACE-A satellite correlations are superior for the POE method, and the lowest RMS value matches that obtained for HASDM. Figure 4.2 shows the densities for this day. The Jacchia 1971 model clearly overestimates the accelerometer density for both satellites, especially GRACE-A.

Table 4.14: Summary of Cross Correlation Coefficients and Root Mean Square Values for March 11, 2008. *Inputs to POE Method are shown in parentheses with Ballistic Coefficient Half-life/Density Coefficient Half-life/Baseline Density Model.*

	CC	**RMS (kg/m^3*10^{-12})**
CHAMP		
HASDM	0.792	0.500
Jacchia 1971	0.780	1.27
Overall Best POE Result with Inputs	0.833 (1.8/180/J71)	0.461 (1.8/180/C72)
POE Result Shown in Plot with Inputs	0.832 (1.8/180/J71)	0.465 (1.8/180/J71)
GRACE-A		
HASDM	0.885	0.037
Jacchia 1971	0.876	0.167
Overall Best POE Result with Inputs	0.910 (1.8/180/J71)	0.037 (1.8/180/J-R)
POE Result Shown in Plot with Inputs	0.910 (1.8/180/J71)	0.039 (1.8/180/J71)

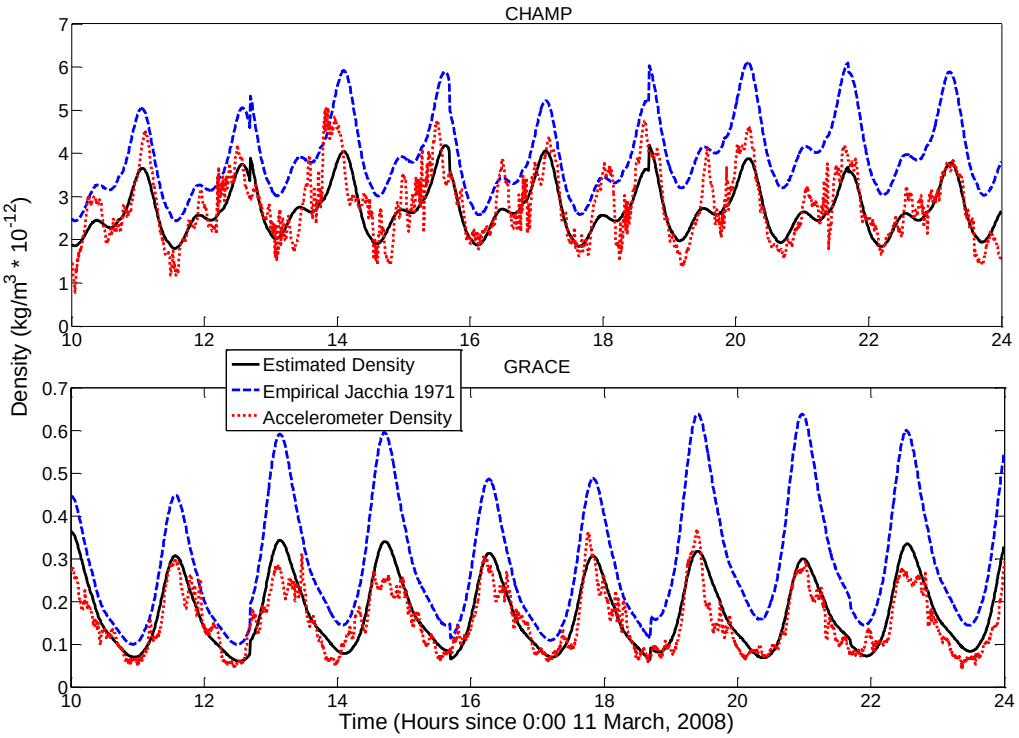

Figure 4.2: POE Estimated Density, Jacchia 1971 Model Density and Accelerometer Density of CHAMP and GRACE-A Satellites for March 11, 2008. *Ballistic coefficient and density correlated half-lives are 1.8 and 180 minutes, respectively. The baseline atmospheric model is Jacchia 1971.*

4.3.3 July 11, 2009 Covering Low Solar and Quiet Geomagnetic Activity

The last day examined July 11, 2009 featured an A_p of 3 and an $F_{10.7}$ of 68.2, placing it in the low solar and quiet geomagnetic bins. CHAMP densities produced results similar to other time periods, with the best POE results outperforming the Jacchia 1971 empirical model for both CC and RMS. CC and RMS results are tabulated in Table 4.15 below. The POE method for GRACE-A, however, produced some anomalous results. Negative densities resulted for some half-life combinations. The reason for impossible negative densities may be a result of extremely low densities. For such densities, the solar radiation pressure may become lumped into density corrections, producing a correction which yields negative density. This requires further investigation. The densities for CHAMP and GRACE-A on July 11, 2009 are plotted in Figure 4.3. The usual BC/Density half-life combination of 1.8

minutes/180 minutes is shown by the black solid line. The negative densities are evident for GRACE-A on this day. In addition, the density producing best correlation resulting from a BC/Density half-life combination of 180 minutes/1.8 minutes is shown by the green dashed line.

Table 4.15: Summary of Cross Correlation Coefficients and Root Mean Square Values for July 11, 2009. *Inputs to POE Method are shown in parentheses with Ballistic Coefficient Half-life/Density Coefficient Half-life/Baseline Density Model.*

	CC	**RMS (kg/m^3*10^{-12})**
CHAMP		
HASDM	N/A	N/A
Jacchia 1971	0.946	3.33
Overall Best POE Result with Inputs	0.950 (180/1.8/J-R)	0.721 (1.8/180/J71)
POE Result Shown in Plot with Inputs	0.884 (1.8/180/J71)	0.721 (1.8/180/J71)
GRACE-A		
HASDM	N/A	N/A
Jacchia 1971	0.870	0.213
Overall Best POE Result with Inputs	0.667 (180/1.8/J71)	0.265 (1.8/1.8/J-R)
POE Result Usually Shown in Plot with Inputs	-0.035(1.8/180/J71)	0.385 (1.8/180/J71)

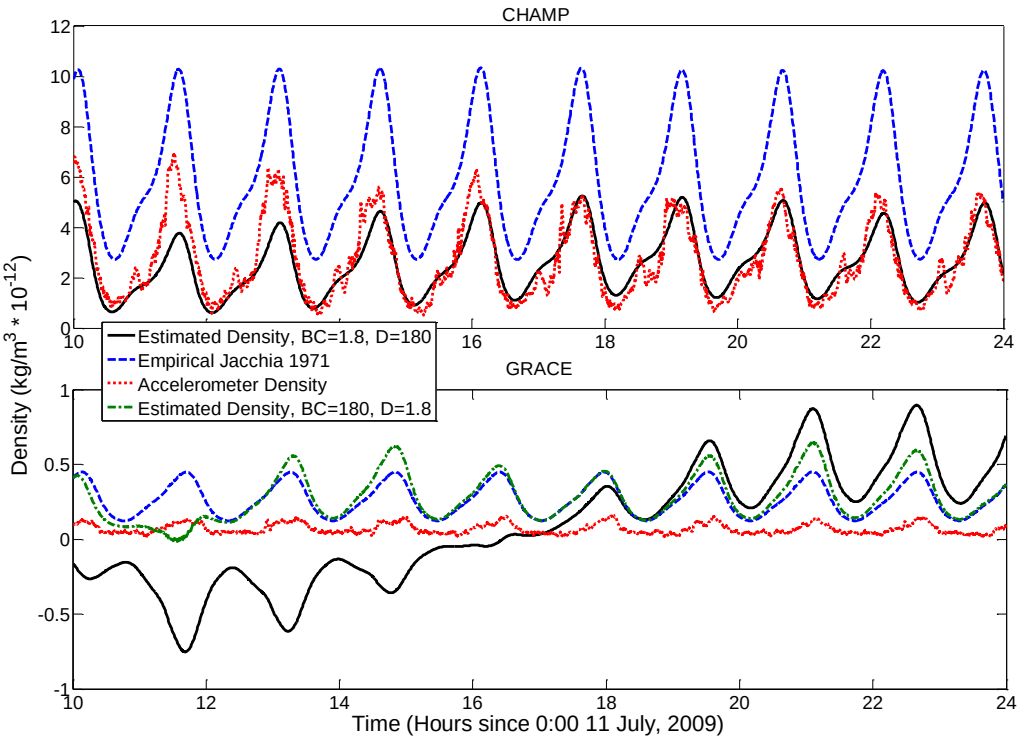

Figure 4.3: POE Estimated Density, Jacchia 1971 Model Density and Accelerometer Density of CHAMP and GRACE-A Satellites for July 11, 2009. *Black solid line using ballistic coefficient and density correlated half-lives of 1.8 and 180 minutes, respectively. Dashed green line using ballistic coefficient and density correlated half-lives of 180 and 1.8 minutes, respectively. The baseline atmospheric model for both POE Estimated Densities is Jacchia 1971.*

4.4 Chapter Summary

The majority of time periods examined in 2008 and 2009 produced results similar to those obtained from 2004-2007. A Jacchia-family model usually yielded the best results. For CHAMP a half-life combination of 1.8 minutes for BC half-life and 180 minutes for density half-life usually produced the best results for both CC and RMS. For GRACE-A however, a deviation from this trend was seen. Some anomalous results in July 2009 produced negative densities and negative correlations. These time periods need further analysis. Performing a long-term look at data in 2008 and 2009, such as the one performed for 2005-2006 in the next chapter, may be very helpful to understanding atypical results.

5 EXAMINATION OF POOR RESULTS FOR PARTICULAR TIME PERIODS

For the overall averages of the solutions, CHAMP and GRACE-A possess fairly similar cross correlation coefficients. CHAMP cross correlation coefficients are slightly better than those of GRACE-A in most cases, but not significantly. However, beginning in late October of 2005, the correlation between POE derived densities for GRACE-A and the densities derived from its onboard accelerometer began to worsen significantly. A solution of densities preceding this period will be examined, in addition to time spans during this period of poor correlations for GRACE. A long-term look at cross correlation coefficients surrounding this period for CHAMP and GRACE-A is also performed.

5.1 Examination of October 23, 2005

October 23, 2005 featured quiet geomagnetic activity with an A_p of 4 and low solar activity with an $F_{10.7}$ of 74.2. Cross correlation and RMS for CHAMP were better than the overall average values. For GRACE-A, the values were similar to the overall averages. The cross correlation coefficients and root mean square values for this day are summarized in Table 5.1 below. Figure 5.1 shows the accelerometer derived density, the density obtained from the Jacchia 1971 model, and the POE derived density for both CHAMP and GRACE-A using Jacchia 1971 as the baseline model with BC and density half-lives of 1.8 minutes and 180 minutes, respectively. October 23 was one of the final time periods in which densities compared favorably with densities derived from the onboard accelerometer of GRACE-A.

Table 5.1: Summary of Cross Correlation Coefficients and Root Mean Square Values for October 23, 2005. *Inputs to POE Method are shown in parentheses with Ballistic Coefficient Half-life/Density Coefficient Half-life/Baseline Density Model.*

	CC	**RMS (kg/m^3*10^{-12})**
CHAMP		
HASDM	0.944	0.259
Jacchia 1971	0.923	0.276
Overall Best POE Result with Inputs	0.938 (1.8/1.8/ C72)	0.242 (1.8/180/MSISE90)
POE Result Shown in Plot with Inputs	0.927 (1.8/180/J71)	0.319 (1.8/180/J71)
GRACE-A		
HASDM	0.690	0.039
Jacchia 1971	0.800	0.064
Overall Best POE Result with Inputs	0.841(1.8/180/J71)	0.031 (1.8/180/MSISE90)
POE Result Shown in Plot with Inputs	0.841(1.8/180/J71)	0.038(1.8/180/J71)

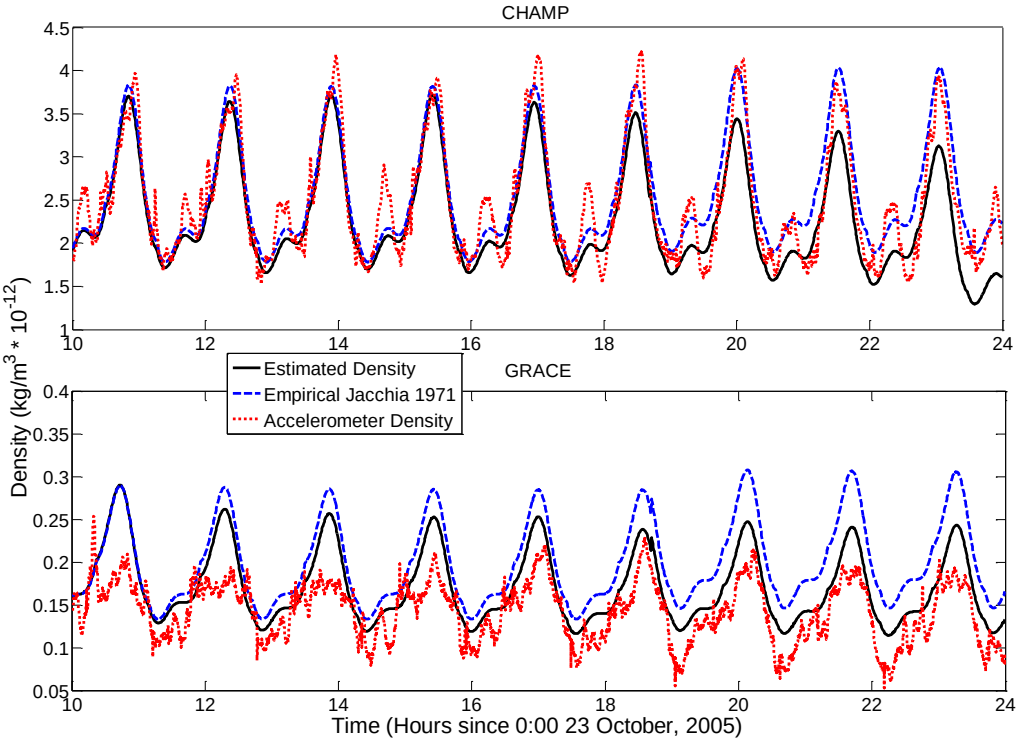

Figure 5.1: POE Estimated Density, Jacchia 1971 Model Density and Accelerometer Density of CHAMP and GRACE-A Satellites for October 23, 2005. *Ballistic coefficient and density correlated half-lives are 1.8 and 180 minutes, respectively. The baseline atmospheric model is Jacchia 1971.*

5.2 Examination of October 26, 2005

An A_p of 11 and an $F_{10.7}$ of 72.0 put October 26, 2005 in the low solar activity and moderate geomagnetic activity bin. This was the first day with notably worse correlations and RMS values for GRACE-A. Once again the CHAMP CC and RMS values compare favorably with the accelerometer and are superior to their overall averages. GRACE RMS values are still consistent with other days of low solar and quiet geomagnetic activity. However, GRACE CC values drop substantially, as shown in Table 5.2. The POE method outperforms both HASDM and the Jacchia 1971 model for both CHAMP and GRACE-A. Figure 5.2 shows the three densities for CHAMP and GRACE-A on this day as in the

previous day. Note the more rapid changes in density shown in the accelerometer for GRACE-A in this plot, as well as the tendency of the Jacchia 1971 model to overestimate the accelerometer density, particularly near the end of the fourteen hour time span.

Table 5.2: Summary of Cross Correlation Coefficients and Root Mean Square Values for October 26, 2005. *Inputs to POE Method are shown in parentheses with Ballistic Coefficient Half-life/Density Coefficient Half-life/Baseline Density Model.*

	CC	**RMS (kg/m^3*10^{-12})**
CHAMP		
HASDM	0.913	0.317
Jacchia 1971	0.864	0.821
Overall Best POE Result with Inputs	0.922 (1.8/18/C72)	0.299 (1.8/18/C72)
POE Result Shown in Plot with Inputs	0.921 (1.8/180/J71)	0.356 (1.8/180/J71)
GRACE-A		
HASDM	0.503	0.059
Jacchia 1971	0.429	0.148
Overall Best POE Result with Inputs	0.630(18/180/J-R)	0.044 (1.8/180/J-R)
POE Result Shown in Plot with Inputs	0.607(1.8/180/J71)	0.047 (1.8/180/J71)

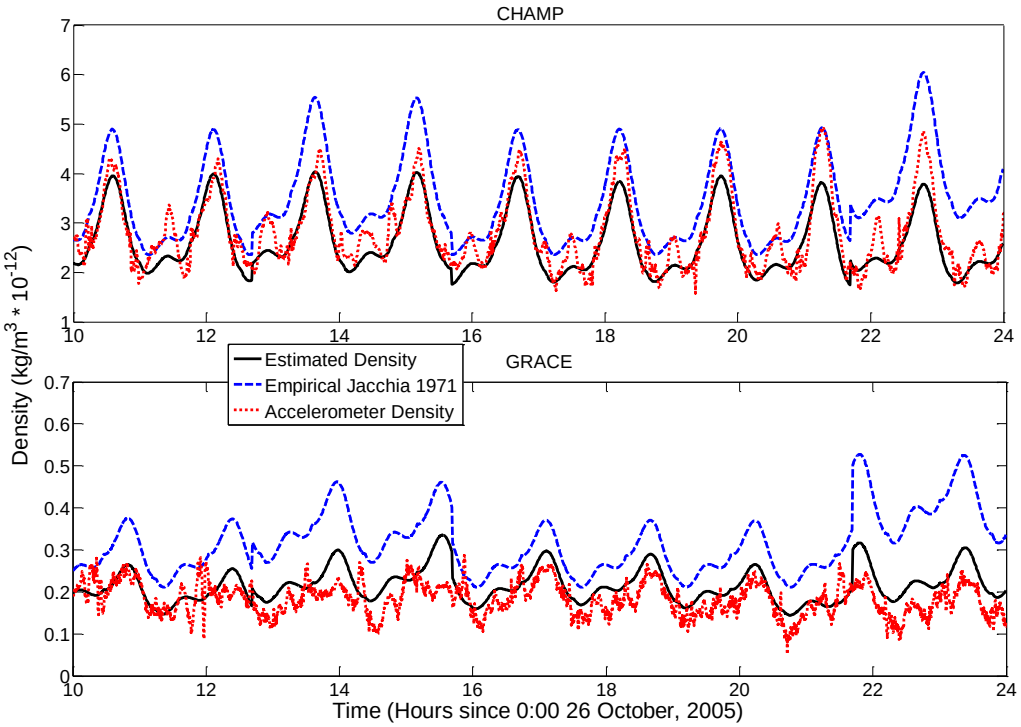

Figure 5.2: POE Estimated Density, Jacchia 1971 Model Density and Accelerometer Density of CHAMP and GRACE-A Satellites for October 26, 2005. *Ballistic coefficient and density correlated half-lives are 1.8 and 180 minutes, respectively. The baseline atmospheric model is Jacchia 1971.*

5.3 Examination of October 27, 2005

October 27, 2005 featured the same A_p and $F_{10.7}$ as the previous day, putting it in the low solar and moderate geomagnetic activity bins as well. Figure 5.3 displays accelerometer density, POE density, and Jacchia 1971 density for CHAMP and GRACE-A on this particular day. Here again, CHAMP cross correlation coefficients and RMS values are consistent with days of similar activity and superior to the overall averages. Cross correlations for the POE method, HASDM, and the Jacchia 1971 empirical model are even worse than the previous day for GRACE. RMS values obtained for the POE densities as well as HASDM are consistent with days of similar activity, but the Jacchia 1971 empirical model RMS is fairly poor as seen in the plot. Table 5.3 summarizes these findings.

Table 5.3: Summary of Cross Correlation Coefficients and Root Mean Square Values for October 27, 2005. *Inputs to POE Method are shown in parentheses with Ballistic Coefficient Half-life/Density Coefficient Half-life/Baseline Density Model.*

	CC	**RMS (kg/m^3*10^{-12})**
CHAMP		
HASDM	0.924	0.280
Jacchia 1971	0.746	0.982
Overall Best POE Result with Inputs	0.931 (1.8/180/J71)	0.278 (1.8/180/C72)
POE Result Shown in Plot with Inputs	0.931 (1.8/180/J71)	0.312 (1.8/180/J71)
GRACE-A		
HASDM	0.395	0.044
Jacchia 1971	0.171	0.146
Overall Best POE Result with Inputs	0.465 (1.8/180/J71)	0.041 (1.8/180/J-R)
POE Result Shown in Plot with Inputs	0.465 (1.8/180/J71)	0.043 (1.8/180/J71)

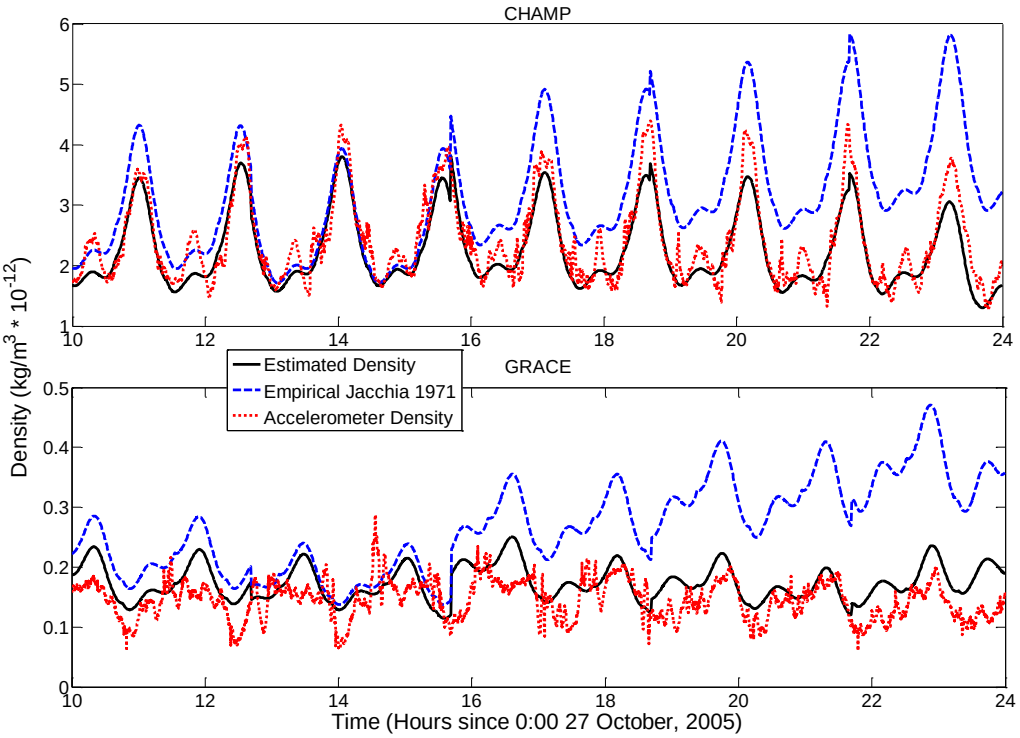

Figure 5.3: POE Estimated Density, Jacchia 1971 Model Density and Accelerometer Density of CHAMP and GRACE-A Satellites for October 27, 2005. *Ballistic coefficient and density correlated half-lives are 1.8 and 180 minutes, respectively. The baseline atmospheric model is Jacchia 1971.*

5.4 Examination of November 2, 2005

November 2, 2005 was a day of moderate solar and moderate geomagnetic activity, with an A_p of 24 and an $F_{10.7}$ of 78. Only GRACE-A is examined for this day. Table 5.4 shows the cross correlation coefficients and RMS values for this day. Figure 5.4 shows the accelerometer density, Jacchia 1971 model density, and POE density using the same combination of BC half-life, density half-life, and baseline model as the previous plots. It is apparent that the accelerometer is observing very rapid changes in density that the Jacchia 1971 empirical model, HASDM, and the POE method are incapable of observing. This is the cause of such poor correlation values. The magnitudes of the density obtained by the accelerometer do not differ greatly from the other methods used to obtain density which

results in RMS values which are consistent with other time periods of similar activity. Again, the best POE methods outperform both HASDM and the Jacchia 1971 model.

Table 5.4: Summary of Cross Correlation Coefficients and Root Mean Square Values for GRACE-A Satellite for November 2, 2005. *Inputs to POE Method are shown in parentheses with Ballistic Coefficient Half-life/Density Coefficient Half-life/Baseline Density Model.*

	CC	RMS (kg/m^3*10^{-12})
HASDM	0.360	0.051
Jacchia 1971	0.055	0.058
Overall Best POE Result with Inputs	0.319 (1.8/180/J-R)	0.042 (1.8/180/MSISE90)
POE Result Shown in Plot with Inputs	0.314 (1.8/180/J71)	0.050 (1.8/180/J71)

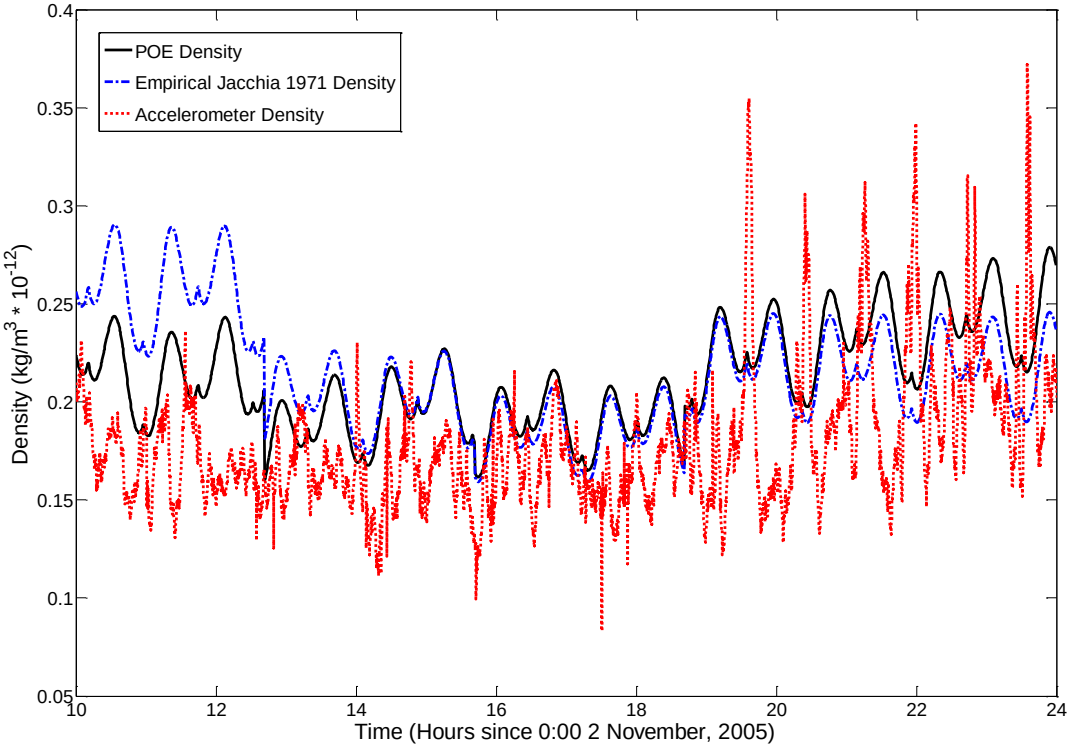

Figure 5.4: POE Estimated Density, Jacchia 1971 Model Density and Accelerometer Density of GRACE-A Satellite for November 2, 2005. *Ballistic coefficient and density correlated half-lives are 1.8 and 180 minutes, respectively. The baseline atmospheric model is Jacchia 1971.*

5.5 Examination of Cross Correlation for August 2005 through February 2006

Due to the unusually poor cross correlation results observed for the GRACE-A satellite during October and November of 2005, an extended period of time is examined beginning in August 2005 and extending through the beginning of 2006. Each consecutive fourteen hour interval for which POE data is available is used to create a plot of cross correlation versus time. Figure 5.5 shows this information. The red (solid) line connects points representing the cross correlations obtained using the POE method with a baseline model of CIRA 1972, a ballistic coefficient correlated half-life of 180 minutes, and a density correlated half-life of 1.8 minutes. The black (dotted) line connects points representing the cross correlations obtained using HASDM. The gap at the beginning of 2006 is due to accelerometer derived density data discontinuity. This graph displays the precipitous drop in cross correlation coefficients for GRACE-A beginning in late October. The next two months these correlations are recovering but are still poor. Around the beginning of 2006 the correlation values return to the 0.9 range. As seen in Figure 5.5, the POE estimated density and the HASDM density exhibit very similar trends in correlation over the time period examined. At times HASDM is superior, and at other the density estimated using the POE density with the given inputs is superior. However, in nearly all cases examined, at least one of the forty-five combinations of baseline atmospheric model and half-lives produce results superior to HASDM.

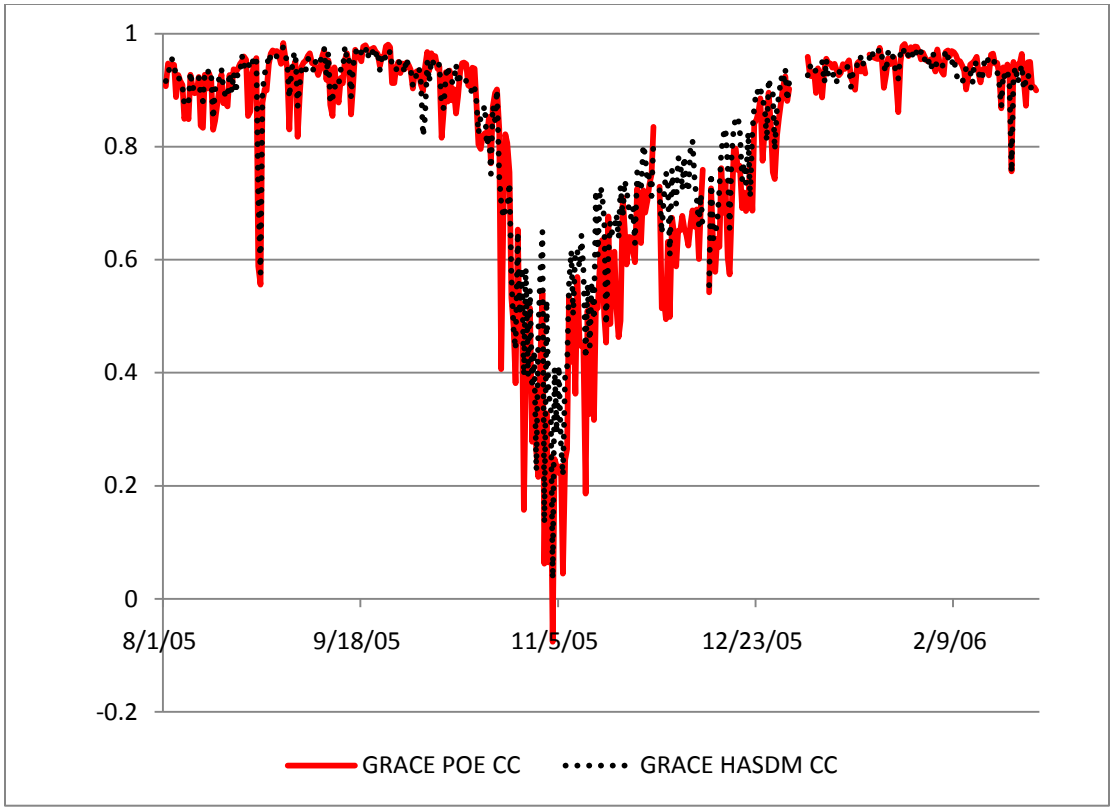

Figure 5.5: Cross Correlation of Accelerometer Density with POE Density and HASDM Density for GRACE-A Satellite between August 1, 2005 and February 28, 2006. *Ballistic coefficient and density correlated half-lives are 180 and 1.8 minutes, respectively. The baseline atmospheric model is CIRA 1972.*

Figure 5.6 shows correlations found for GRACE using POE estimated density and HASDM, in addition to those found for CHAMP during the same time period. Again, a baseline model of CIRA 1972, a ballistic coefficient correlated half-life of 180 minutes, and a density correlated half-life of 1.8 minutes are used, though this is the opposite of the usual best combination. The red (darker) dots represent the correlations for the GRACE-A POE density, while the black (darker) crosses represent the correlations for the HASDM density. The yellow (lighter) dots represent the correlations for the CHAMP POE density, while the blue (lighter) crosses represent the correlations for CHAMP HASDM density. CHAMP also

displays a period of worsened correlations in early 2006 as shown in this figure. Further research must be performed to discover the cause of these anomalously poor results.

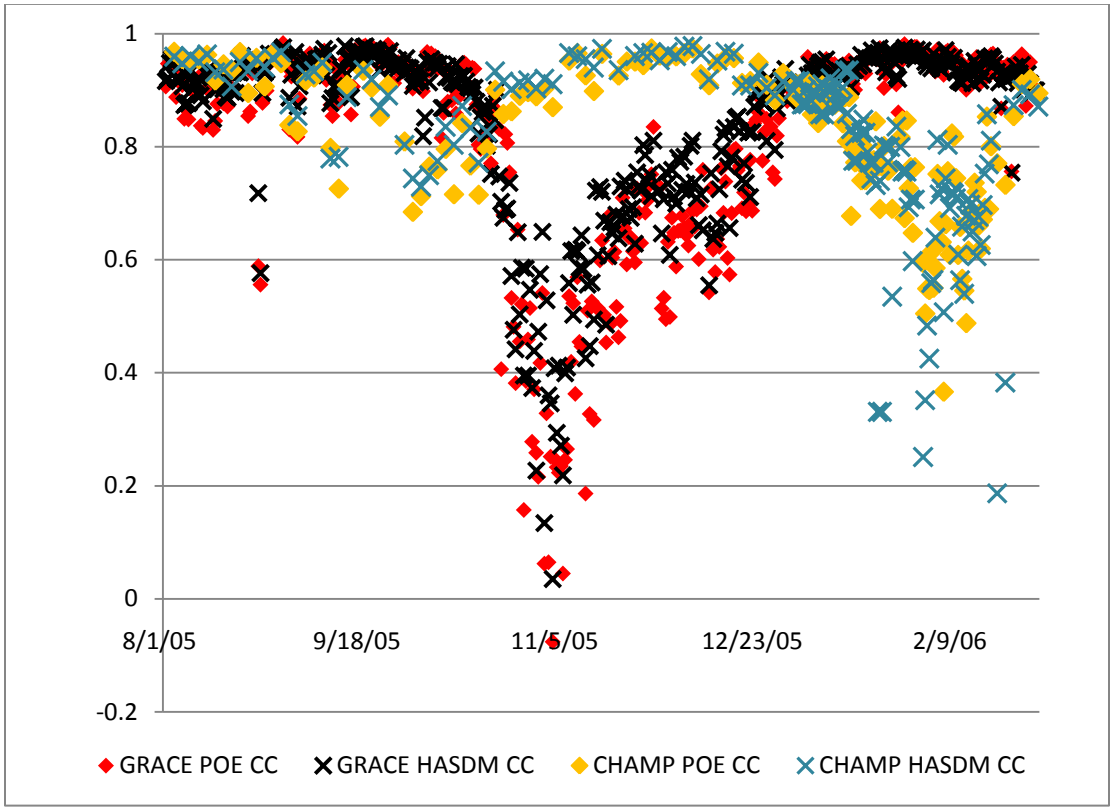

Figure 5.6: Cross Correlation of Accelerometer Density with POE Density and HASDM Density for CHAMP and GRACE-A Satellites between August 1, 2005 and February 28, 2006. *Ballistic coefficient and density correlated half-lives are 180 and 1.8 minutes, respectively. The baseline atmospheric model is CIRA 1972.*

5.6 Chapter Summary

Upon analysis of dates in late 2005, very low cross correlations were observed for the GRACE-A satellite. By performing POE density analysis on each consecutive fourteen hour time span from August 1, 2005 to February 28, 2006 for the combination of a ballistic coefficient correlated half-life of 180 minutes, a density correlated half-life of 1.8 minutes, and baseline model of CIRA 1972, the extent of these poor results was determined. By looking at specific days in this range, the inability of the POE method or HASDM to match

very short-term changes in density observed by the accelerometer becomes apparent. The reason for such rapid changes, which are not seen in most other time periods examined, is currently unknown. The GRACE-A and GRACE-B satellites performed a switch maneuver in December 2005, however, this does not account for anomalous correlations beginning in late October. GRACE-B began performing maneuvers on December 3, 2005, and its last maneuver was January 11, 2006. GRACE-A only recorded a 180° yaw maneuver on December 11, 2005 (Ref. 61). Another possible cause of the poor correlations could be error introduced into the estimates by solar radiation pressure. If rays from the Sun are aligned along the direction of motion of the satellite, radiation pressure may be mischaracterized as pressure due to drag. However, analysis of the β angle between the satellite and the Sun revealed no time correlation with the poor results. Further research must be performed to determine the cause of these rapid changes in density observed for GRACE-A during late 2005.

6 COMPARISON OF GRACE-A AND GRACE-B

The twin GRACE satellites fly in formation. Initially GRACE-B trailed GRACE-A by approximately 200 km. A switch maneuver was performed in December 2005. After January 2006, GRACE-A trailed GRACE-B by approximately 160 km. The two satellites theoretically will experience very little difference in atmospheric density as they orbit the Earth. POE data is used to generate density values over representative time periods already examined, in this case for both GRACE-A and GRACE-B. Comparison of the densities obtained for both satellites is performed in this section.

6.1 Examination of August 3, 2006

As previously discussed, August 3, 2006 was a day of low solar activity and quiet geomagnetic activity. Figure 6.1 below shows the accelerometer derived density, as well as the POE derived density using Jacchia 1971 as the baseline atmospheric model, a ballistic coefficient correlated half-life of 1.8 minutes, and a density correlated half-life of 180 minutes. Since the accelerometer derived densities are obtained using measurements from the onboard accelerometer of GRACE-A, these results are examined qualitatively. This figure shows that the GRACE-B estimated density is nearly identical to the GRACE-A estimated density. The GRACE-B density however, is slightly lower in magnitude than the GRACE-A density at the peaks. Note that the densities are very low for this period.

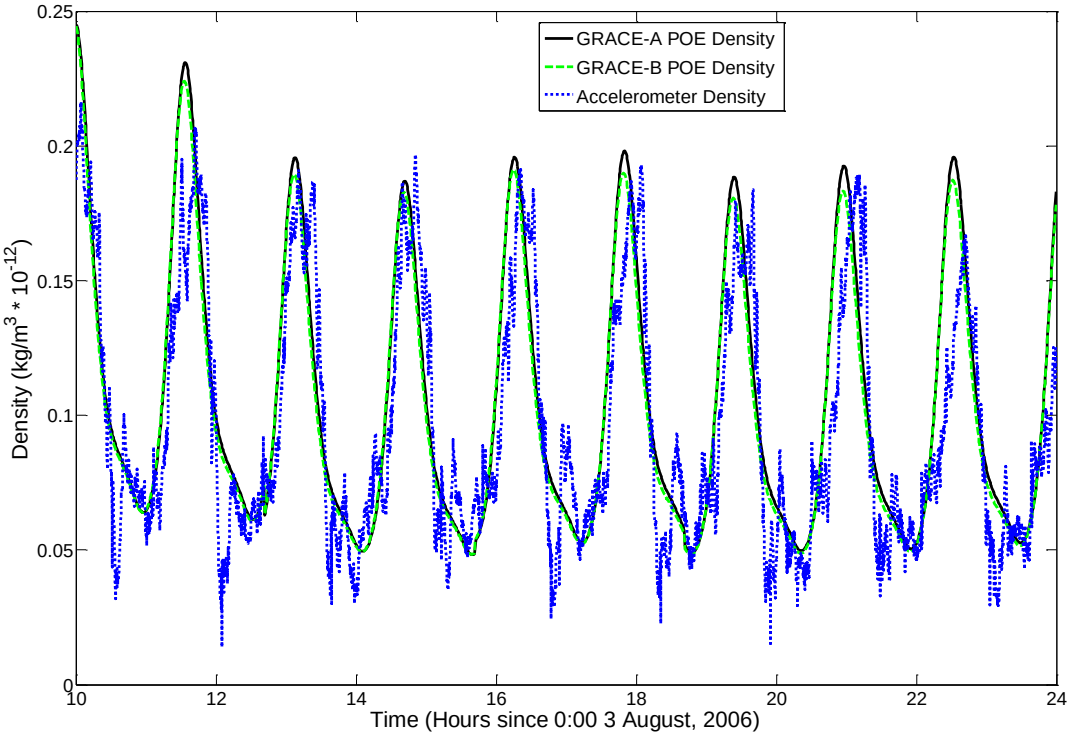

Figure 6.1: POE Estimated Density for GRACE-A (solid black line), POE Estimated Density for GRACE-B (dashed green line) and GRACE-A Accelerometer Density (dotted blue line) for August 3, 2006. *Ballistic coefficient and density correlated half-lives are 1.8 and 180 minutes, respectively. The baseline atmospheric model is Jacchia 1971.*

6.2 Examination of December 22, 2006

December 22, 2006 featured low solar activity and moderate geomagnetic activity. Figure 6.2 shows the accelerometer derived density as well as the densities obtained for GRACE-A and GRACE-B again using Jacchia 1971 as baseline and BC and density half-lives of 1.8 minutes and 180 minutes, respectively. Note that the accelerometer density is much more variable for this day than for the previous day examined. As might be expected the densities obtained using the POE method for GRACE-A and GRACE-B differ more than the previous day examined. Again, the trends in the densities for these satellites are nearly identical. The magnitudes differ at the peaks somewhat noticeably at the first and last density peaks.

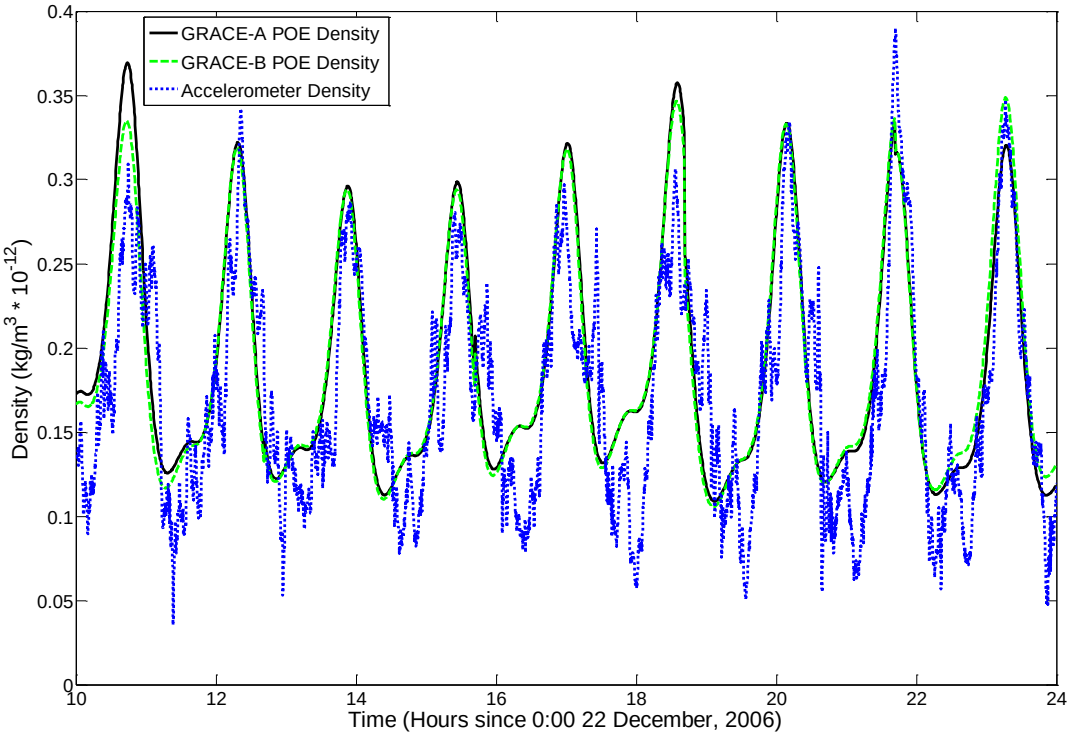

Figure 6.2: POE Estimated Density for GRACE-A (solid black line), POE Estimated Density for GRACE-B (dashed green line) and GRACE-A Accelerometer Density (dotted blue line) for December 22, 2006. *Ballistic coefficient and density correlated half-lives are 1.8 and 180 minutes, respectively. The baseline atmospheric model is Jacchia 1971.*

6.3 Examination of March 13, 2005

The level of solar activity was moderate and the geomagnetic activity was moderate on March 13, 2005. Figure 6.3 shows the accelerometer derived density, as well as the POE derived densities for GRACE-A and GRACE-B using the same baseline atmospheric model and Gauss-Markov half-lives as the previous plots. For this time period, the GRACE-A POE density and the GRACE-B density are very close in magnitude. Both GRACE-A and GRACE-B overestimate the density compared to the accelerometer. Densities for this day are roughly double the magnitude of densities on December 22, 2006.

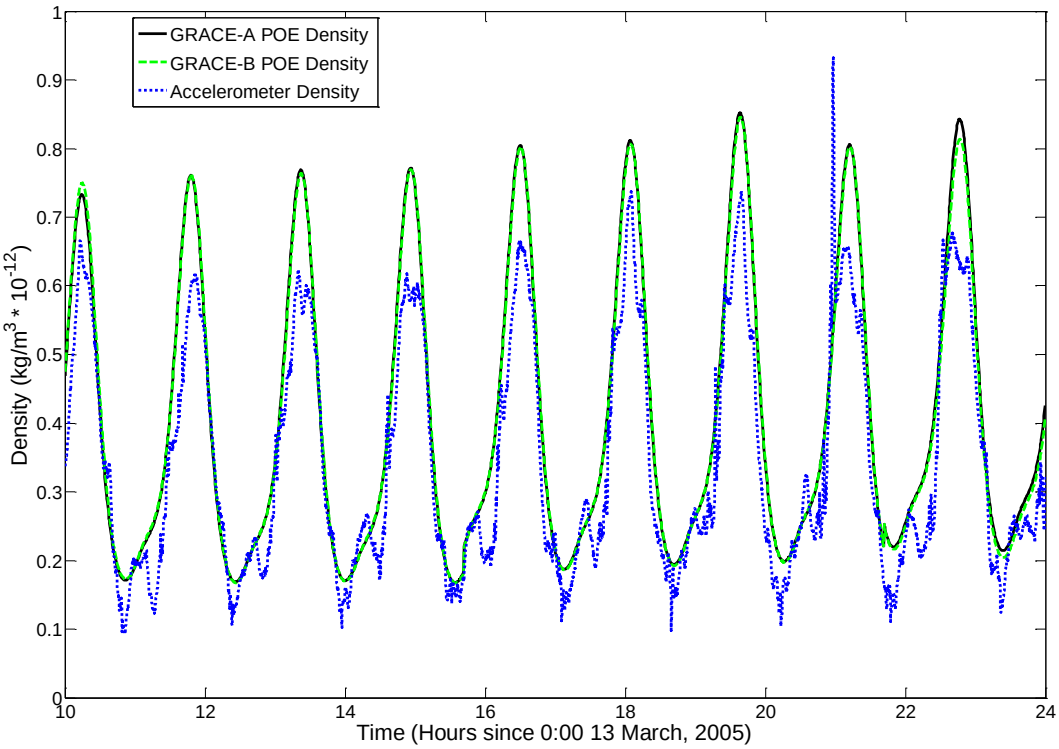

Figure 6.3: POE Estimated Density for GRACE-A (solid black line), POE Estimated Density for GRACE-B (dashed green line) and GRACE-A Accelerometer Density (dotted blue line) for March 13, 2005. *Ballistic coefficient and density correlated half-lives are 1.8 and 180 minutes, respectively. The baseline atmospheric model is Jacchia 1971.*

6.4 Examination of September 12, 2005

As previously examined, the day of September 12, 2005 was one of moderate solar and active geomagnetic activity. Figure 6.4 shows the same information as the other plots for this day. On this day, the magnitude of the densities is the largest of all of the days examined. Both GRACE-A and GRACE-B POE derived densities match very well with the accelerometer density on this day, and yet again the GRACE-A and GRACE-B densities are very close to one another.

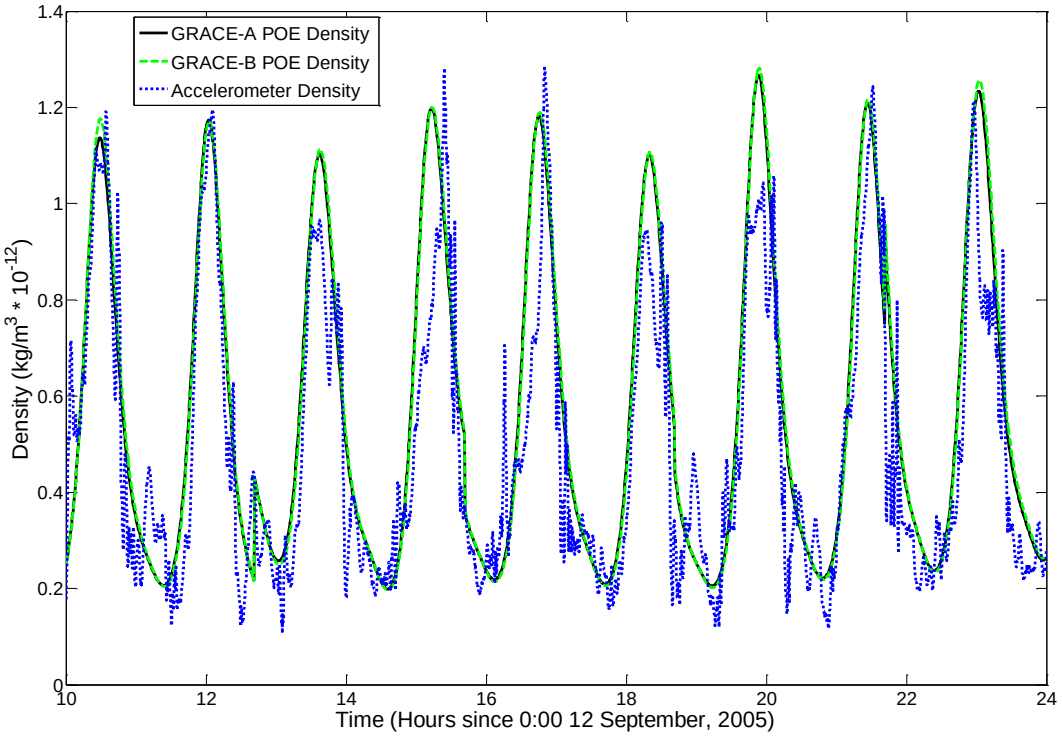

Figure 6.4: POE Estimated Density for GRACE-A (solid black line), POE Estimated Density for GRACE-B (dashed green line) and GRACE-A Accelerometer Density (dotted blue line) for September 12, 2005. *Ballistic coefficient and density correlated half-lives are 1.8 and 180 minutes, respectively. The baseline atmospheric model is Jacchia 1971.*

6.5 Examination of October 26, 2005

Lastly, October 26, 2005 is examined. This is during the time period where GRACE results produced very poor cross correlation coefficients with the accelerometer densities. This day featured low solar activity and moderate geomagnetic activity. Figure 6.5 shows the densities obtained from GRACE-A and GRACE-B using the baseline atmospheric model of Jacchia 1971 and half-lives of 1.8 minutes for BC and 180 minutes for density. The accelerometer derived density is shown as well. No real difference between GRACE-A and GRACE-B can be seen during this period as both the trends and the magnitudes of the densities are nearly indistinguishable.

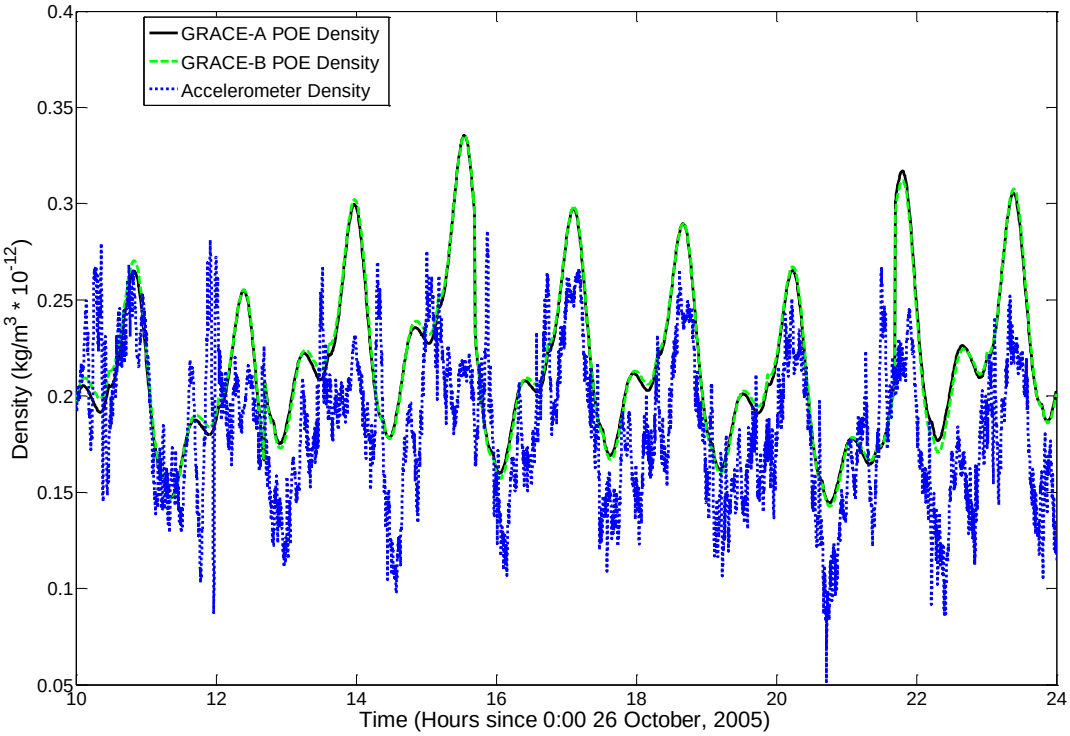

Figure 6.5: POE Estimated Density for GRACE-A (solid black line), POE Estimated Density for GRACE-B (dashed green line) and GRACE-A Accelerometer Density (dotted blue line) for October 26, 2005. *Ballistic coefficient and density correlated half-lives are 1.8 and 180 minutes, respectively. The baseline atmospheric model is Jacchia 1971.*

6.6 Chapter Summary

For all days examined regardless of solar and geomagnetic activity levels, the trends seen in the density profiles estimated using GRACE-A POE data were nearly identical to the trends seen in the density profiles obtained from the GRACE-B data. In addition, very small differences were seen in the magnitudes of densities obtained using these two satellites for the majority of the periods examined. A few of the peaks differed somewhat in magnitude, most noticeably at the beginning and end of the fourteen hour span on December 22, 2006. Even for a time period which featured very poor correlation with the accelerometer, GRACE-A and GRACE-B did not differ significantly. These comparisons suggest that the POE method is producing consistent results.

7 SUMMARY, CONCLUSIONS, AND FUTURE WORK

7.1 Summary

Current models of Earth's atmosphere are inadequate in modeling most variations in atmospheric density, particularly in the thermosphere and exosphere. These variations significantly affect bodies orbiting the Earth. Drag on satellites, which is directly proportional to atmospheric density, is one of the largest uncertainties in orbit determination and prediction. Increased levels of solar or geomagnetic activity only serve to make modeling atmospheric density variability more difficult.

In this research, precision orbit ephemerides are used to generate corrections to existing atmospheric density models through the use of an optimal orbit determination process. These corrections yield more accurate density information, which in turn improves drag calculations on orbiting bodies. More accurate density estimates improves orbit determination and prediction as well as providing insight into density variations in the upper atmosphere.

Densities derived using the precision orbit ephemerides are compared to densities derived from onboard accelerometers of the CHAMP and GRACE-A satellites. The densities are compared for trends in the variations, using cross correlation coefficients, and are compared for magnitude using root mean square analysis. Precision orbit data is taken from many time periods spanning 2004-2009 covering all possible solar and geomagnetic conditions. Results are binned according to solar and geomagnetic activity levels.

A sequential Kalman filter and smoother scheme is used to generate corrections to a baseline atmospheric density model using precision orbit data from the CHAMP and GRACE satellites as measurements. The program to analyze the data, Orbit Determination Toolkit (ODTK), has five different baseline atmospheric models available. They are the CIRA 1972,

Jacchia 1971, Jacchia-Roberts, MSISE 1990, and NRLMSISE 2000 models. Two inputs which can be specified, called the ballistic coefficient correlated half-life and density half-life, are each varied among the values of 1.8, 18, and 180 minutes. These half-lives determine the extent to which a previous estimate of a correction affects the current correction. Baseline density model and the half-lives are varied producing forty-five different sets of results for each time period examined. The densities obtained are compared to densities derived by Sean Bruinsma from the onboard accelerometers of CHAMP and GRACE. Densities obtained using the High Accuracy Satellite Drag Model (HASDM) are also compared to the accelerometer density during the same time periods as the POE derived densities.

ODTK also calculates residuals for each time period examined using the filtering and smoothing process in the orbit determination scheme. These residuals are the difference between the measured and estimated positions at each time step. The residuals are used to check the accuracy of a particular orbit determination solution. Position and velocity consistency test graphs are also output by ODTK to ensure the orbit determination process is producing reasonable results. Finally, the McReynolds' filter-smoother consistency test is an internal check on the validity of estimates output by the filter and smoother.

Cross correlation coefficients between density solutions and the accelerometer derived density are calculated. In addition, the correlations of the Jacchia 1971 empirical model and HASDM with the accelerometer density are calculated for the purpose of comparison. These correlation coefficients indicate how well density variations observed by the accelerometer are matched by these methods. Another measure of comparison between the density data sets is root mean square values. These RMS values indicate how well the magnitudes of two data sets match. Cross correlation and RMS values are calculated for all

time periods examined for CHAMP and GRACE-A. They are then given as overall averages as well as averages according to solar and geomagnetic activity level bins. Particular days corresponding to a range of solar and geomagnetic activity levels are examined.

Data is separated into a separate set of averages for the extended solar minimum occurring in 2008 and 2009. Cross correlation and RMS values are again calculated as overall averages for this data, as well as sorting data into solar and geomagnetic activity level bins, although all days fall into the low solar activity level bin, and either the quiet or moderate geomagnetic activity level bins. This is performed for both the CHAMP and GRACE-A satellites. Again, representative days of the available bins are examined in further detail.

A period of time beginning in late October 2005 and extending to early 2006 that produced unusually low cross correlation coefficients for GRACE was examined. Days before as well as during the range of poor results are inspected in greater detail. A long-term look at cross correlation coefficients for CHAMP and GRACE-A is performed by calculating CC values for each fourteen hour time span with precision orbit data available from August 2005 through February 2006.

Finally, precision orbit data for GRACE-B is used to generate density solutions for GRACE-B during multiple time periods. Density estimates from GRACE-A and GRACE-B are qualitatively compared to the GRACE-A accelerometer derived densities during periods from a range of solar and geomagnetic activity levels, as well as during a period which featured very low cross correlation coefficients for GRACE-A. Densities produced during concurrent time period for GRACE-A and GRACE-B were very similar as is expected for twin satellites flying in relatively close proximity.

7.2 Conclusions

As a result of this research, the following conclusions can be drawn.

1. Atmospheric density models based on the Jacchia lineage nearly always produce superior results to those of the MSIS-based models when used as the baseline model.
2. Results from the Jacchia-based models differ very little from one another, and results from the MSIS-based models differ very little from each other.
3. The POE derived density produced by the best combination of half-lives and baseline model nearly always outperforms both HASDM and the Jacchia 1971 empirical model for both CHAMP and GRACE for CC and RMS.
4. HASDM correlations and RMS values are usually superior to the Jacchia 1971 empirical model.
5. The overall best ballistic coefficient correlated half-life for CHAMP and GRACE between 2004 and 2007 is 1.8 minutes.
6. Between 2004 and 2007 for CHAMP, the overall best correlations and RMS values are produced using a baseline atmospheric model of CIRA 1972 and density correlated half-life of 18 minutes.
7. Between 2004 and 2007 for GRACE, the overall best correlations and RMS values are produced using a density correlated half-life of 180 minutes.
8. Between 2004 and 2007, the best density half-life for CHAMP during periods of quiet geomagnetic activity, moderate geomagnetic activity, and low solar activity is 180 minutes.
9. Between 2004 and 2007, the best density half-life for CHAMP during periods of active geomagnetic activity and moderate solar activity is 18 minutes.

10. Between 2004 and 2007, the best correlations for GRACE are produced using a BC half-life of 1.8 minutes and a density half-life of 180 minutes for all bins of solar and geomagnetic activity with the exception of the quiet geomagnetic activity bin.
11. For the quiet geomagnetic activity bin, a BC half-life of 180 minutes and density half-life of 1.8 minutes produces the best correlations between 2004 and 2007 for GRACE, although results with other combinations are very similar.
12. The best RMS results for GRACE between 2004 and 2007 use a BC half-life of 1.8 minutes for all levels of activity, and use a density half-life of 180 minutes for all levels of solar and geomagnetic activity with the exception of active geomagnetic activity, which uses a density half-life of 18 minutes, though 18 and 180 minutes for density half-life produce nearly identical results.
13. In general, as solar and geomagnetic activity levels increase, CC and RMS results worsen for CHAMP.
14. For GRACE, no clear trend is seen in correlation as solar and geomagnetic activity levels increase, but RMS values increase as solar and geomagnetic activity increase.
15. For 2008 and 2009, different combinations usually produce superior results; however, the limited amount of data must be considered.
16. All data in 2008 and 2009 is in the low solar activity bin, and either the quiet or moderate geomagnetic activity bin.
17. For CHAMP in 2008 and 2009, the best results are produced using a Jacchia-family model, a BC half-life of 1.8 minutes, and a density half-life of 180 minutes.

18. For GRACE in 2008 and 2009, the best cross correlation results are produced using a Jacchia-family model, a BC half-life of 180 minutes, and a density half-life of 1.8 minutes.
19. For GRACE in 2008 and 2009, the best RMS results are produced using a Jacchia-family model, a BC half-life of 1.8 minutes, and a density half-life of 1.8 minutes.
20. From late October 2005 through the end of 2005, low correlations are produced for GRACE-A.
21. These unusually low correlations are experienced by HASDM and the Jacchia 1971 empirical model as well.
22. Plots of time periods during this period reveal the inability of the POE method to characterize shorter period variations in density observed by the accelerometer.
23. POE derived densities produced using orbit data for the GRACE-B satellite are nearly identical to those of GRACE-A during concurrent time periods.
24. GRACE-B densities match those of GRACE-A very well both in the variations and the magnitudes.
25. GRACE-A and GRACE-B densities match for periods examined for various levels of solar and geomagnetic activity as well as for a period in which POE density for GRACE-A produces low correlation with the accelerometer density.

Densities obtained by generating corrections to existing atmospheric models were nearly always superior to the empirical models as well as HASDM. Though the best combination of half-lives was somewhat a function of solar and geomagnetic activity level, the best ballistic coefficient correlated half-life was nearly always 1.8 minutes for both satellites. The best density half-life is nearly always 180 minutes for GRACE. For CHAMP

the best density half-life is 180 minutes for lower levels of activity and 18 minutes for higher levels of activity.

Very low levels of solar activity seem to cause difficulty in estimating density variations, specifically for GRACE, as evidenced in 2008 and 2009. Poor results in 2005 for GRACE appear to be due to the short term variations in the accelerometer density. Unfortunately, the POE method appears incapable of characterizing the very short term density variations observed by the accelerometer. This is likely a shortcoming of the quality of the inputs for solar and geomagnetic activity into the atmospheric models. Shorter update times on solar and geomagnetic activity would likely increase the temporal resolution of density solutions, possibly improving correlation with the accelerometer density to some degree. The POE method produces nearly identical results for GRACE-A and GRACE-B, as expected.

7.3 Future Work

7.3.1 Examination of Additional Days

A much larger number of days should be examined from 2008 and 2009. Currently a very small sampling of data is used in examining this period. Creating a long-term look at cross correlation and RMS such as the one created for late 2005 would be very helpful in understanding the nature of poor results during this period. Additionally, estimating density for all periods where precision orbit data is available should eventually be performed for both CHAMP and the GRACE satellites.

7.3.2 Examining the Significance of Precision Orbit Data

Precision orbit data used as measurements in the orbit determination scheme are taken from GFZ. This data is prefiltered. Using the raw, unfiltered data should be performed to ensure that this filtering process is not significantly affecting the density estimates produced. In addition, examination of longer continuous time periods for solutions should be examined. This requires stitching together the precision orbit data where the files overlap for two hours to create longer sets of data which can be used in the orbit determination scheme.

7.3.3 Examination of Additional Density and Ballistic Coefficient Correlated Half-Lives

In this study, only three values of density and ballistic coefficient correlated half-lives are examined, 1.8, 18, and 180 minutes. Half-lives are separated by an order of magnitude. Because 18 minutes sometimes yielded better results and 180 minutes yielded better results at other times, examination of intermediate values may be useful. Using smaller increments of values may be very insightful. Future work might examine half-lives varying in 1 minute increments. Another possibility would be varying by even divisions, i.e., 0.18 minutes, 0.36 minutes, etc. for those up to 1.8 minutes, and 3.6 minutes, 5.4 minutes, etc. between 1.8 and 18 minutes. Similarly, values between 18 and 180 minutes would be 36 minutes, 54 minutes, etc.

7.3.4 Using the Jacchia-Bowman 2008 Atmospheric Model as a Baseline Model

Currently, ODTK supports the five baseline atmospheric density models previously mentioned. These models use 3-hourly a_p and $F_{10.7}$ values. Solar and geomagnetic activity measurements are now available with higher temporal resolution. The Jacchia-Bowman 2008

model is able to utilize this data, suggesting it would produce improved baseline density estimates for variations caused by changes in solar and geomagnetic activity. Implementing the Jacchia-Bowman 2008 model into ODTK would likely improve estimates obtained via the POE method.

7.3.5 Additional Satellites with Precision Orbit Ephemerides

Processing additional satellites with available precision orbit ephemerides would be of interest. More data should be processed for TerraSAR-X as well as the TanDEM-X satellite. Though most additional satellites do not possess accelerometers, estimating density through orbit determination would be very valuable for any satellites with the ability to provide sufficiently accurate position and velocity data. Other possibilities include Jason-1, ICESat, or other Earth-observing satellites. Additional satellites at a greater range of altitudes and inclinations will improve spatial resolution of atmospheric density estimates.

REFERENCES

1. S. Bruinsma and R. Biancale, "Total Density Retrieval with STAR," *First CHAMP Mission Results for Gravity, Magnetic and Atmospheric Studies*, eds. C. Reigber, H. Luhr, P. Schwintzer, Springer, Berlin, 2003, pp. 192-199.
2. S. Bruinsma and R. Biancale, "Total Densities Derived from Accelerometer Data," *Journal of Spacecraft and Rockets*, Vol. 40, No. 2, March-April 2003, pp. 230-236.
3. S. Bruinsma, S. D. Tamagnan and R. Biancale, "Atmospheric Densities Derived from CHAMP/STAR Accelerometer Observations," *Planetary and Space Science*, Vol. 52, 2004, pp. 297-312.
4. R. S. Nerem, J. M. Forbes, E. K. Sutton, and S. Bruinsma, "Atmospheric Density Measurements Derived from CHAMP/STAR Accelerometer Data," *Advances in the Astronautical Sciences*, Vol. 116, AAS 03-621, Univelt, 2003, pp. 1879-1898.
5. M. F. Storz, B. R. Bowman, Major J. I. Branson, S. J. Casali, and W. K. Tobiska, "High Accuracy Satellite Drag Model (HASDM)," *Advances in Space Research*, Vol. 36, Issue 12, 2005, pp. 2497-2505.
6. D. A. Vallado, *Fundamentals of Astrodynamics and Applications*, Microcosm Press, El Segundo, CA, 3rd Edition, 2007, Chap. 8, App. B.
7. A. C. Tribble, *The Space Environment: Implications for Spacecraft Design*, Princeton University Press, Princeton, New Jersey, 2003.
8. C. A. McLaughlin, "Upper Atmospheric Phenomena and Satellite Drag," *Advances in the Astronautical Sciences*, Vol. 123, AAS 05-315, Univelt, 2005, pp. 989-996.
9. J. K. Hargreaves, *The Solar-Terrestrial Environment*, Cambridge University Press, Cambridge, 1992.
10. C. Sabol and K. K. Luu, "Atmospheric Density Dynamics and the Motion of Satellites," *AMOS Technical Conference*, Wailea, HI, September 2002.
11. D. H. Hathaway and L. Rightmire, "Variations in the Sun's Meridional Flow over a Solar Cycle," *Science*, v.327, No. 5971, pp.1350-1352, 2010.
12. L. G. Jacchia, *Revised Static Models for the Thermosphere and Exosphere with Empirical Temperature Profiles*, SAO Special Report No. 332, Smithsonian Institution Astrophysical Observatory, Cambridge, MA, 1971.
13. C. E. Roberts, Jr., "An Analytic Model for Upper Atmosphere Densities Based upon Jacchia's 1970 Models," *Celestial Mechanics*, Vol. 4, Issue 3-4, December 1971, pp. 368-377.
14. COSPAR Working Group IV, *COSPAR International Reference Atmosphere*, Akademie-Verlag, Berlin, 1972.
15. A. E. Hedin, "Extension of the MSIS Thermosphere Model into the Middle and Lower Atmosphere," *Journal of Geophysical Research*, Vol. 96, 1991, pp. 1159-1172.
16. J.M. Picone, A. E. Hedin, D. P. Drob, "NRLMSISE-00 Empirical Model of the Atmosphere: Statistical Comparisons and Scientific Issues," *Journal of Geophysical Research*, Vol. 107, No. A12, 2002.
17. B. R. Bowman, W. K. Tobiska, F. A. Marcos, C. Y. Huang, C. S. Lin, W. J. Burke, "A New Empirical Thermospheric Density Model JB2008 Using New Solar and Geomagnetic Indices," AIAA 2008-6438, AIAA/AAS Astrodynamics Specialist Conference, Honolulu, HI, August 2008.

18. National Geophysical Data Center, *Solar Indices Bulletin*, Boulder, CO: National Geophysical Data Center, http://www.ngdc.noaa.gov/ and ftp://ftp.ngdc.noaa.gov/STP/SOLAR_DATA/SOLAR_RADIO/FLUX.
19. National Geophysical Data Center, *Solar Indices Bulletin*, Boulder, CO: National Geophysical Data Center, http://www.ngdc.noaa.gov/ and ftp://ftp.ngdc.noaa.gov/STP/GEOMAGNETIC_DATA/INDICES/KP_AP/.
20. M. F. Storz, B. R. Bowman, Major J. I. Branson, S. J. Casali, and W. K. Tobiska, "High Accuracy Satellite Drag Model (HASDM)," *Advances in Space Research*, Vol. 36, Issue 12, 2005, pp. 2497-2505.
21. B. Bowman, "The Semiannual Thermospheric Density Variation from 1970 to 2002 Between 200-1100 km," *Advances in the Astronautical Sciences*, Vol. 119, AAS 04-174, Univelt, 2004, pp. 1135-1154.
22. V. S. Yurasov, A. I. Nazarenko, P. J. Cefola, and K. T. Alfriend, "Results and Issues of Atmospheric Density Correction," *Journal of the Astronautical Sciences*, Vol. 52, No. 3, July-September 2004, pp. 281-300.
23. P. J. Cefola, R. J. Proulx, A. I. Nazarenko, and V. S. Yurasov, "Atmospheric Density Correction Using Two Line Element Sets as the Observation Data," *Advances in the Astronautical Sciences*, Vol. 116, AAS 03-626, Univelt, 2003, pp. 1953-1978.
24. V. S. Yurasov, A. I. Nazarenko, K. T. Alfriend, and P. J. Cefola, "Reentry Time Prediction Using Atmospheric Density Corrections," *Journal of Guidance, Control, and Dynamics*, Vol. 31, No. 2, March-April 2008, pp. 282-289.
25. M. P. Wilkins, C. A. Sabol, P. J. Cefola, and K. T. Alfriend, "Improving Dynamic Calibration of the Atmosphere," *Advances in the Astronautical Sciences*, Vol. 127, AAS 07-185, Univelt, 2007, pp. 1257-1272.
26. M. P. Wilkins, C. A. Sabol, P. J. Cefola, and K. T. Alfriend, "Practical Challenges in Implementing Atmospheric Density Corrections to the NRLMSISE-00 Model," *Advances in the Astronautical Sciences*, Vol. 124, AAS 06-170, Univelt 2006, pp. 1113-1130.
27. M. P. Wilkins, C. A. Sabol, P. J. Cefola, and K. T. Alfriend, "Validation and Application of Corrections to the NRLMSISE-00 Atmospheric Density Model," *Advances in the Astronautical Sciences*, Vol. 127, AAS 07-189, Univelt, 2007, pp. 1285-1304.
28. S. R. Mance, C. A. McLaughlin, F. G. Lemoine, D. D. Rowlands, and P. J. Cefola, "GEOSAT Follow-On Precision Orbit Improvement Through Drag Model Update," *Advances in the Astronautical Sciences*, Vol. 134, AAS 09-105, Univelt, 2009, pp. 43-62.
29. E. Doornbos, H. Klinkrad, and P. Visser, "Use of Two-Line Element Data for Thermosphere Neutral Density Model Calibration," *Advances in Space Research*, Vol. 41, 2008, pp. 1115-1122.
30. C. A. McLaughlin and B. S. Bieber, "Neutral Density Determined from CHAMP Precision Orbits," *Advances in the Astronautical Sciences*, Vol. 129, AAS 07-260, Univelt, 2008, pp. 167-186.
31. E. A. Rhoden, J. M. Forbes, and F. A. Marcos, "The Influence of Geomagnetic and Solar Variability on Lower Thermospheric Density," *Journal of Atmospheric and Solar-Terrestrial Physics*, Vol. 62, 2000, pp. 999-1013.
32. R. Konig and K. H. Neumayer, "Thermospheric Events in CHAMP Precise Orbit Determination," *First CHAMP Mission Results for Gravity, Magnetic and*

Atmospheric Studies, eds. C. Reigber, H. Luhr, P. Schwintzer, Springer, Berlin, 2003, pp. 112-119.
33. K. Schlegel, H. Luhr, J. P. St. Maurice, G. Crowley, and C. Hackert, "Thermospheric Density Structures over the Polar Regions Observed with CHAMP," *Annales Geophysicae*, Vol. 23, 2005, pp. 1659-1672.
34. E. K. Sutton, R. S. Nerem, and J. M. Forbes, "Global Thermospheric Neutral Density and Wind Response to the Severe 2003 Geomagnetic Storms from CHAMP Accelerometer Data," *Journal of Geophysical Research*, Vol. 110, 2005.
35. J. M. Forbes, G. Lu, S. Bruinsma, S. Nerem, and X. Zhang, "Thermospheric Density Variations Due to the 15-24 April 2002 Solar Events from CHAMP/STAR Accelerometer Measurements," *Journal of Geophysical Research*, Vol. 110, 2005, pp. 1-9.
36. E. K. Sutton, J. M. Forbes, R. S. Nerem, and T. N. Woods, "Neutral Density Response to the Solar Flares of October and November, 2003," *Geophysical Research Letters*, Vol. 33, 2006.
37. S. Bruinsma, J. M. Forbes, R. S. Nerem, and X. Zhang, "Thermospheric Density Response to the 20-21 November 2003 Solar and Geomagnetic Storm from CHAMP and GRACE Accelerometer Data," *Journal of Geophysical Research*, Vol. 111, No. AO6303, 2006, pp. 1-14.
38. S. L. Bruinsma and J. M. Forbes, "Storm-Time Equatorial Density Enhancements Observed by CHAMP and GRACE," *Journal of Spacecraft and Rockets*, Vol. 44, No. 6, 2007, pp. 1154-1159.
39. E. K. Sutton, R. S. Nerem, and J. M. Forbes, "Density and Winds in the Thermosphere Deduced from Accelerometer Data," *Journal of Spacecraft and Rockets*, Vol. 44, No. 6, 2007, pp. 1210-1219.
40. B. D. Tapley, J. C. Ries, S. Bettadpur, and M. Cheng, "Neutral Density Measurements for the Gravity Recovery and Climate Experiment Accelerometers," *Journal of Spacecraft and Rockets*, Vol. 44, No. 6, 2007, pp. 1220-1225.
41. S. L. Bruinsma and J. M. Forbes, "Medium- to Large-Scale Density Variability as Observed by CHAMP," *Space Weather*, Vol. 6, S08002, doi:10.1029/2008SW000411, 2008.
42. S. L. Bruinsma and J. M. Forbes, "Properties of Traveling Atmospheric Disturbances (TADs) Inferred from CHAMP Accelerometer Observations," *Advances in Space Research*, Vol. 43, 2009, pp. 369-376.
43. Y. L. Zhou, S. Y. Ma, H. Lühr, C. Xiong, and C. Reigber, "An Empirical Relation to Correct Storm-Time Thermospheric Mass Density Modeled by NRLMSISE-00 with CHAMP Satellite Air Drag Data," *Advances in Space Research*, Vol. 43, 2009, pp. 819-828.
44. E. Doornbos, H. Klinkrad, and P. Visser, "Atmospheric Density Calibration Using Satellite Drag Observations," *Advances in Space Research*, Vol. 36, 2005, pp. 515-521.
45. J. van den Ijssel, P. Visser, and R. Haagmans, "Determination of Non-Conservative Accelerations from Orbit Analysis," *Earth Observation with CHAMP Results from Three Years in Orbit*, eds. C. Reigber, H. Luhr, P. Schwintzer, J. Wickert, Springer, Berlin, 2005, pp. 95-100.
46. J. van den IJssel and P. Visser, "Performance of GPS Accelerometry: CHAMP and GRACE," *Advances in Space Research*, Vol. 39, 2007, pp. 1597-1603.

47. J. van den IJssel and P. Visser, "Determination of Non-Gravitational Accelerations from GPS Satellite-to-Satellite Tracking of CHAMP," *Advances in Space Research*, Vol. 36, 2005, pp. 418-423.
48. O. Montenbruck, T. van Helleputte, R. Kroes, and E. Gill, "Reduced Dynamic Orbit Determination Using GPS Code and Carrier Measurements," *Aerospace Science and Technology*, Vol. 9, 2005, pp. 261-271.
49. P. Willis, F. Deleflie, F. Barlier, Y. E. Bar-Sever, and L. J. Romans, "Effects of Thermosphere Total Density Perturbations on LEO Orbits During Severe Geomagnetic Conditions (Oct-Nov 2003) Using DORIS and SLR Data," *Advances in Space Research*, Vol. 36, 2005, pp. 522-533.
50. C. A. McLaughlin, A. Hiatt, and B. S. Bieber, "Comparison of Total Density Derived from CHAMP Precision Orbits and CHAMP Accelerometer," *Advances in the Astronautical Sciences*, Vol. 130, AAS 08-177, Univelt, 2008, pp. 1193-1206.
51. C. A. McLaughlin, A. Hiatt, T. Lechtenberg, "Precision Orbit Derived Total Density," *Journal of Spacecraft and Rockets*, Vol. 48, No.1, January-February 2011, pp. 166-174.
52. A. Hiatt, C. A. McLaughlin, and T. Lechtenberg, "Deriving Density Estimates Using CHAMP Precision Orbit Data for Periods of High Solar Activity," *Advances in the Astronautical Sciences*, Vol. 134, AAS 09-104, Univelt, 2009, pp. 23-42.
53. A. Hiatt, "Deriving Atmospheric Density Estimates Using Satellite Precision Orbit Ephemerides," M.S. Thesis, University of Kansas, 2009.
54. T. Lechtenberg, "Derivation and Observability of Upper Atmospheric Density Variations Utilizing Precision Orbit Ephemerides," M.S. Thesis, University of Kansas, 2010.
55. C. A. McLaughlin, T. Lechtenberg, E. Fattig, "Estimating Density Using Precision Satellite Orbits From Multiple Satellites," AAS 10-307, *Kyle T. Alfriend Astrodynamics Symposium*, Monterey, CA, May, 2010.
56. E. Fattig, C. A. McLaughlin, T. Lechtenberg, "Comparison of Density Estimation for CHAMP and GRACE Satellites," AIAA 2010-7976, *2010 AIAA/AAS Astrodynamics Specialist Conference and Exhibit*, Toronto, ON, CA, August 2010.
57. B. D. Tapley, B. E. Schutz, and G. H. Born, *Statistical Orbit Determination*, Elsevier Academic Press, Amsterdam, 2004.
58. J. R. Wright, "Real-Time Estimation of Local Atmospheric Density," *Advances in the Astronautical Sciences*, Vol. 114, AAS 03-164, Univelt, 2003, pp. 927-950.
59. J. R. Wright and J. Woodburn, "Simultaneous Real-Time Estimation of Atmospheric Density and Ballistic Coefficient," *Advances in the Astronautical Sciences*, Vol. 119, AAS 04-175, Univelt, 2004, pp. 1155-1184.
60. National Aeronautics and Space Administration, "CHAMP," Last Accessed: March 2, 2011.
61. GRACE: Gravity Recovery and Climate Experiment: Center for Space Research, "GRACE Orbital Configuration," August 2, 2007, Last Accessed: April 12, 2011, http://www.csr.utexas.edu/grace/operations/configuration.html.
62. R. Konig, S. Zhu, C. Reigber, K. H. Neumayer, H. Meixner, R. Galas, G. Baustert, "CHAMP Rapid Orbit Determination for GPS Atmospheric Limb Sounding," *Advances in Space Research*, Vol. 30, No. 2, 2002, pp. 289-293.
63. G. Michalak, G. Baustert, R. Konig, C. Reigber, "CHAMP Rapid Science Orbit Determination: Status and Future Prospects," *First CHAMP Mission Results for*

Gravity, Magnetic and Atmospheric Studies, eds. C. Reigber, H. Luhr, P. Schwintzer, Springer, Berlin, 2003, pp. 98-103.

64. R. Konig, G. Michalak, K. H. Neumayer, S. Y. Zhu, H. Meixner, C. Reigber, "Recent Developments in CHAMP Orbit Determination at GFZ," *Earth Observation with CHAMP Results from Three Years in Orbit*, eds. C. Reigber, H. Luhr, P. Schwintzer, J. Wickert, Springer, Berlin, 2005, pp. 65-70.
65. R. Konig, G. Michalak, K. H. Neumayer, S. Zhu, "Remarks on CHAMP Orbit Products," *Observation of the Earth System from Space*, eds. J. Flury, R. Rummel, C. Reigber, M. Rothacher, G. Boedecker, U. Schreiber, Springer, Berlin, 2006, pp. 17-26.
66. O. Montenbruck and E. Gill, *Satellite Orbits: Models, Methods, and Applications*, Springer-Verlag, Berlin, 2001.
67. J. R. Wright, "Optimal Orbit Determination," *Advances in the Astronautical Sciences*, Vol. 112, AAS 02-192, Univelt, 2002, pp. 1123-1134, http://www.agi.com/downloads/support/productSupport/literature/pdfs/whitePapers/optimal_od.pdf.
68. Analytical Graphics, Inc., "Orbit Determination Tool Kit Help," *Orbit Determination Tool Kit*, Version 5.1.3.
69. J. R. Wright, "Orbit Determination Tool Kit Theorems and Algorithms," *Analytical Graphics, Inc.*, 2007.
70. B. Tapley, J. Ries, S. Bettadpur, D. Chambers, M. Cheng, F. Condi, B. Gunter, Z. Kang, P. Nagel, R. Pastor, T. Pekker, S. Poole, and F. Wang, "GGM02 - An Improved Earth Gravity Field Model from GRACE," *Journal of Geodesy*, Vol. 79, Issue 8, pp.467-478.
71. B. R. Bowman, F. A. Marcos, K. Moe, M. M. Moe, "Determination of Drag Coefficient Values for CHAMP and GRACE Satellites Using Orbit Drag Analysis," *Advances in the Astronautical Sciences*, Vol. 129, AAS 07-259, Univelt, 2008, pp. 147-166.
72. P. Bourke, "Cross Correlation," August 1996, Last Accessed: March 4, 2011, http://local.wasp.uwa.edu.au/~pbourke/miscellaneous/correlate/.